Performance of Wireless Networks with Directional Antennas

by

Ping-Cheng Yeh

A dissertation submitted in partial fulfillment
of the requirements for the degree of
Doctor of Philosophy
(Electrical Engineering: Systems)
in The University of Michigan
2005

Doctoral Committee:

Professor Wayne E. Stark, Chair
Professor Brian E. Gilchrist
Professor Andrew E. Yagle
Assistant Professor Achilleas Anastasopoulos
Assistant Professor Mingyan Liu
Associate Research Scientist Kurt Metzger

To my parents, my wife Joanna and our baby Justin.

ACKNOWLEDGEMENTS

I would like to express my deepest gratitude to my advisor Professor Wayne E. Stark for giving me the opportunity to join his research group. Without his guidance and support over the years, it would not have been possible for me to finish my doctoral work and to pursue my dream of teaching. I would also like to thank other committee members Professor Brian E. Gilchrist, Achilleas Anastasopoulos, and Mingyan Liu for their helpful suggestions and comments to my thesis.

I am very grateful to Professor Andrew E. Yagle whom I always respect as my mentor in teaching. I learned so much about teaching from the countless lectures I sat in as his GSI. Without his constant encouragement and inspiration, it would not be possible for a foreign GSI like me to develop and achieve some success, if any at all, in teaching.

I would like to thank Doctor Kurt Metzger who has taught me many lessons not only in DSP programming but also in the wisdoms of life. The most important lesson I learned from him is that we should never stop ourselves just because of the fear of failure. We should just do the work and learn from the result, whether good or bad.

Many thanks to my colleagues in the Wireless Communications Laboratory, Do-Sik Yoo, Hua Wang, Salam Zummo, Ali Yilmaz, and Kar-Peo Yar, for their true friendship as well as their advices and assistance over the years. I am also thankful to Chun-Ting Chou, Wei-Cheng Tian, Wen-Lung Huang, Wei-Chen Chien, Hao-Wei Chen, and all other friends in Ann Arbor for their cares for me and the great times we had together.

Finally, I would like to dedicate this thesis to my parents, my wife Joanna, and our baby Justin. Their unreserved support and love give me the strength to face the challenges in my life. I am especially grateful to Joanna for her continuous caring for me and bringing me the biggest joy of my life, our cute baby Justin (MoMo).

PREFACE

Directional antennas have been considered to be a promising technology that can improve user capacity and power efficiency for wireless networks. In this thesis, we analyze the performance of a wireless network using directional antennas with an antenna beam pattern of arbitrary shape under a realistic channel model which includes the effects of path loss, shadowing, and Rayleigh fading. The performance is analyzed for both slow fading and fast fading cases. The performance measure considered is the outage probability.

A mobile using directional antenna needs to know the direction of its communicating party to achieve good performance. However in reality, direction estimation is imperfect and the error affects the system performance. This effect is analyzed in this thesis. Other than direction estimation error, we also consider the effect of power control which is often used to combat the power loss in wireless environments. We analyze the system performance under power control and combine the analysis with a simulated annealing algorithm to find the optimal power control scheme for any given wireless network.

In order to generalize our outage probability analysis to wireless networks with different physical layers, we need to determine the threshold of signal-to-interference-noise ratio (SINR) for the outage probability computation according to the coding and modulation scheme used in the physical layer. Bit-interleaved coded modulation (BICM) and turbo codes are commonly used in wireless communications and their performance is analyzed in the thesis. This enables us to find the SINR threshold and thus compute the outage probability when BICM or turbo codes are used in the physical layer of a wireless network. Since bit-interleaved space-time (BI-ST) code is very effective in combating fading due to its time diversity and transmit diversity, we also generalize our

BICM performance analysis to analyze the performance of BI-ST coded systems under various fading distributions.

TABLE OF CONTENTS

DEDICATION ii

ACKNOWLEDGEMENTS iii

PREFACE iv

LIST OF FIGURES viii

CHAPTERS

1 Introduction **1**
- 1.1 Wireless Networks with Directional Antennas **2**
- 1.2 Bit-Interleaved Coded Modulation (BICM) **4**
- 1.3 Bit-Interleaved Space-Time (BI-ST) Coded Systems **5**
- 1.4 Error Floor Analysis of Turbo Codes **6**
- 1.5 Thesis Outline **6**

2 Wireless Networks with Directional Antennas **7**
- 2.1 Introduction **7**
- 2.2 Model Description **10**
- 2.3 Outage Probability of a Slow Faded Link **14**
  - 2.3.1 Simplified Beam Pattern **14**
  - 2.3.2 Arbitrary Beam Pattern and Array Interference Factor . . . **19**
  - 2.3.3 Numerical Examples **20**
- 2.4 Outage Probability of a Fast Faded Link **27**
  - 2.4.1 Outage Probability Analysis **27**
  - 2.4.2 Numerical Computation Concerns **29**
  - 2.4.3 Numerical Examples **31**
- 2.5 Effect of Direction Estimation Error **34**
  - 2.5.1 Outage Probability Analysis **34**
  - 2.5.2 Numerical Examples **35**
- 2.6 Power Control **39**
  - 2.6.1 Outage Probability under Discrete Power Control **40**
  - 2.6.2 Outage Probability under Continuous Power Control **42**
  - 2.6.3 Numerical Examples **43**
- 2.7 Application to System Design Optimization **45**
  - 2.7.1 Optimal Mobile Density for System Throughput **45**
  - 2.7.2 Optimal Code Rate for Link Throughput **50**

2.8 Conclusions . . . 51

3 Performance Analysis of Bit-Interleaved Coded Modulation (BICM) in Wireless Environments . . . 55
3.1 Introduction . . . 55
3.2 System Model . . . 57
3.3 The Union Bound . . . 59
3.4 Pairwise Error Probability . . . 63
3.4.1 AWGN . . . 63
3.4.2 Rayleigh Fading . . . 63
3.4.3 Rician Fading . . . 64
3.4.4 Nakagami Fading . . . 67
3.5 Conclusions . . . 69

4 Performance Analysis of Bit-Interleaved Space-Time (BI-ST) Coded Systems in Wireless Environment . . . 70
4.1 Introduction . . . 70
4.2 System Model . . . 72
4.3 The Union Bound . . . 74
4.4 Characteristic Function . . . 77
4.4.1 BI-STCM . . . 77
4.4.2 BI-STBC . . . 79
4.4.2.1 Rayleigh Fading . . . 80
4.4.2.2 Rician Fading . . . 80
4.4.2.3 Nakagami Fading . . . 80
4.5 Multiple-Receive Antennas . . . 80
4.6 Numerical Results . . . 81
4.7 Conclusions . . . 84

5 On the Error Floor Analysis of Turbo Codes: Weight Spectrum Estimation (WSE) Scheme . . . 85
5.1 Introduction . . . 85
5.2 Weight Spectrum of Turbo Code . . . 89
5.3 Error Floor Performance of Turbo Code . . . 90
5.4 Weight Spectrum Estimation . . . 91
5.4.1 Phase I: Single Error Event and Tail Error Event Search . . . 94
5.4.2 Phase II: Multiple Error Event Search . . . 98
5.4.3 Accuracy Analysis and Stopping Criterion of WSE . . . 100
5.5 Modified S-random Interleaver . . . 101
5.6 Numerical Examples . . . 103
5.7 Conclusions . . . 108

6 Conclusions and Future Research . . . 110
6.1 Summary of Contributions . . . 110
6.2 Future Research . . . 112

BIBLIOGRAPHY . . . 113

LIST OF FIGURES

Figure

2.1 Wireless network using directional antennas. **11**
2.2 Beam pattern $f(\theta)$. **12**
2.3 Channel between Tx and Rx. **12**
2.4 Simplified beam pattern. **14**
2.5 PER union bounds of (1, 33/37, 33/37) turbo code and bit-interleaved (1, 5/7) convolutional coded 64-QAM in AWGN channel **21**
2.6 Beam pattern 1 (generated by 6 antenna elements, AIF: 0.6569 at $\eta = 4$ and 0.5699 at $\eta = 2.7$). **22**
2.7 Beam pattern 2 (generated by 10 antenna elements, AIF: 0.5511 at $\eta = 4$ and 0.4545 at $\eta = 2.7$). **22**
2.8 Outage probability vs. average received SNR γ_c with (1, 33/37, 33/37) turbo code in an obstructed environment under slow fading, $\lambda_M = 20.0$ mobiles/km^2, $b = 1.5$ dB, $\sigma = 6$ dB, $\eta = 4$, $r_0 = 0.1$ km. **24**
2.9 Outage probability vs. average received SNR γ_c with (1, 5/7) convolutional coded 64-QAM in an obstructed environment under slow fading, $\lambda_M = 20.0$ mobiles/km^2, $b = 13.5$ dB, $\sigma = 6$ dB, $\eta = 4$, $r_0 = 0.1$ km. **24**
2.10 Outage probability vs. average received SNR γ_c with (1, 5/7) convolutional coded 64-QAM in an obstructed environment under slow fading with lower mobile density, $\lambda_M = 2.0$ mobiles/km^2, $b = 13.5$ dB, $\sigma = 6$ dB, $\eta = 4$, $r_0 = 0.1$ km. **25**
2.11 Outage probability vs. average received SNR γ_c with (1, 5/7) convolutional coded 64-QAM in an urban area under slow fading, $\lambda_M = 2.0$ mobiles/km^2, $b = 13.5$ dB, $\sigma = 6$ dB, $\eta = 2.7$, $r_0 = 0.1$ km. **25**
2.12 Outage probability vs. transmitted SNR γ_0 with (1, 5/7) convolutional coded 64-QAM in an urban area under slow fading, $\lambda_M = 20.0$ mobiles/km^2, $b = 13.5$ dB, $\sigma = 6$ dB, $\eta = 2.7$, $r_0 = 0.2$ km. **26**
2.13 PER union bounds of (1, 33/37, 33/37) turbo code and bit-interleaved (1, 5/7) convolutional coded 64-QAM under fast Rayleigh fading **32**
2.14 Outage probability vs. average received SNR γ_c with (1, 33/37, 33/37) turbo code in an obstructed environment under fast (and slow) fading, $\lambda_M = 20.0$ mobiles/km^2, $\sigma = 6$ dB, $\eta = 4$, $r_0 = 0.1$ km. **32**
2.15 Outage probability vs. average received SNR γ_c with (1, 5/7) convolutional coded 64-QAM in an obstructed environment under fast (and slow) fading, $\lambda_M = 20.0$ mobiles/km^2, $\sigma = 6$ dB, $\eta = 4$, $r_0 = 0.1$ km. **33**

2.16 Outage probability vs. γ_c with direction estimation error using beam pattern 1 (AIF = 0.6569) and (1, 5/7) convolutional coded 64-QAM in an obstructed environment under slow fading, $\lambda_M = 20.0$ mobiles/km^2, $b = 13.5$ dB, $\sigma = 6$ dB, $\eta = 4$, $p = 0.045$, $r_0 = 0.1$ km. **36**
2.17 Outage probability vs. γ_c with direction estimation error using beam pattern 2 (AIF = 0.5511) and (1, 5/7) convolutional coded 64-QAM in an obstructed environment under slow fading, $\lambda_M = 20.0$ mobiles/km^2, $b = 13.5$ dB, $\sigma = 6$ dB, $\eta = 4$, $p = 0.045$, $r_0 = 0.1$ km. **36**
2.18 Outage probability vs. γ_c with direction estimation error using beam pattern 1 (AIF = 0.5699) and (1, 5/7) convolutional coded 64-QAM in an urban area under slow fading, $\lambda_M = 20.0$ mobiles/km^2, $b = 13.5$ dB, $\sigma = 6$ dB, $\eta = 2.7$, $p = 0.045$, $r_0 = 0.1$ km. **37**
2.19 Outage probability vs. γ_c with direction estimation error using beam pattern 2 (AIF = 0.4545) and (1, 5/7) convolutional coded 64-QAM in an urban area under slow fading, $\lambda_M = 20.0$ mobiles/km^2, $b = 13.5$ dB, $\sigma = 6$ dB, $\eta = 2.7$, $p = 0.045$, $r_0 = 0.1$ km. **37**
2.20 Outage probability vs. δ_{max} with fixed γ_c using (1, 5/7) convolutional coded 64-QAM under slow fading, $\gamma_c = 30$ dB, $\lambda_M = 20.0$ mobiles/km^2, $b = 13.5$ dB, $\sigma = 6$ dB, $\eta = 2.7$, $p = 0.045$, $r_0 = 0.1$ km. **38**
2.21 Outage probability vs. γ_c using beam pattern 2 (AIF = 0.4545) and (1, 33/37, 33/37) turbo code with optimal power control in an urban area under slow fading, $\lambda_M = 20.0$ mobiles/km^2, $b = 1.5$ dB, $\sigma = 6$ dB, $\eta = 2.7$, $p = 0.045$, $r_0 = 0.1$ km. . . **44**
2.22 Outage probability vs. γ_c using beam pattern 2 (AIF = 0.4545) and (1, 5/7) convolutional coded 64-QAM with optimal power control in an urban area under slow fading, $\lambda_M = 20.0$ mobiles/km^2, $b = 13.5$ dB, $\sigma = 6$ dB, $\eta = 2.7$, $p = 0.045$, $r_0 = 0.1$ km. **44**
2.23 System throughput $S_1(b)$ vs. λ_M with $r_0 = c = 0.1$ km in an obstructed environment under slow fading, $\gamma_c = 25$ dB, $\sigma = 6$ dB, $\eta = 4$, $p = 0.9$. **47**
2.24 System throughput $S_1(b)$ vs. λ_M with $r_0 = c = 0.1$ km in an urban area under slow fading, $\gamma_c = 25$ dB, $\sigma = 6$ dB, $\eta = 2.7$, $p = 0.9$. **47**
2.25 System throughput $S_2(b)$ vs. λ_M with $r_{max} = 1$ km in an obstructed environment under slow fading, $\gamma_c = 25$ dB, $\sigma = 6$ dB, $\eta = 4$, $p = 0.9$. **49**
2.26 System throughput $S_2(b)$ vs. λ_M with $r_{max} = 1$ km in an obstructed environment under slow fading, $\gamma_c = 25$ dB, $\sigma = 6$ dB, $\eta = 2.7$, $p = 0.9$. **49**
2.27 System throughput $S_2(b)$ vs. λ_M with $r_{max} = \min\{100, 1 + 9/\lambda_M\}$ km in an obstructed environment under slow fading, $\gamma_c = 25$ dB, $\sigma = 6$ dB, $\eta = 4$, $p = 0.9$. **50**
2.28 Link throughput vs. code rate R under slow fading, $\gamma_c = 18$ dB, $\lambda = 20.0$ mobiles/km^2, $\sigma = 6$ dB, $\eta = 4$, $p = 0.045$, $r_0 = 0.1$ km. (a) $n = 20$, (b) $n = 50$, (c) $n = 100$, (d) $n = 500$ **52**
2.29 Link throughput vs. code rate R under slow fading, $\gamma_c = 18$ dB, $\lambda = 20.0$ mobiles/km^2, $\sigma = 6$ dB, $\eta = 2.7$, $p = 0.045$, $r_0 = 0.1$ km. (a) $n = 20$, (b) $n = 50$, (c) $n = 100$, (d) $n = 500$ **53**
3.1 Block diagram of a BICM system employing iterative detection and decoding. **58**
3.2 Bit error probability of BICM using a rate-$\frac{1}{2}$ (1,5/7) convolutional code and QAM signaling over an AWGN channel. **65**

3.3 Bit error probability of BICM using a rate-$\frac{1}{2}$ (1,5/7) convolutional code and QAM signaling over a Rayleigh fading channel. **65**
3.4 Bit error probability of BICM using a rate-$\frac{1}{2}$ (1,5/7) convolutional code and a 64-QAM signaling over Rician fading channels with different κ values. . **68**
3.5 Bit error probability of BICM using a rate-$\frac{1}{2}$ (1,5/7) convolutional code and a 64-QAM signaling over Nakagami fading channels with different fading parameters μ. **68**
4.1 Block diagram of the general BI-ST coded system. **73**
4.2 Bit error probability of convolutionally encoded BI-ST systems using $n_T = 2$ over a Rayleigh fading channel. **82**
4.3 Bit error probability of a convolutionally encoded BI-STCM using $n_T = 2$ over Rician fading channels with different κ values. **82**
4.4 Bit error probability of a convolutionally encoded BI-STBC using $n_T = 2$ over Rician fading channels with different κ values. **83**
4.5 Bit error probability of a convolutionally encoded BI-STBC using $n_T = 2$ over Nakagami fading channels with different μ values. **83**
5.1 Union Bound and the performance of turbo codes with all $K!$ possible interleavers **86**
5.2 A typical turbo encoder with two recursive systematic convolutional (RSC) constituent encoders. **89**
5.3 Typical trellis diagrams generated by the RSC constituent encoder. **93**
5.4 Flow chart of WSE algorithm. **95**
5.5 $(1, 33/37, 33/37)$ turbo code with interleaver #0, $S = 12$, $K = 1000$, and $R_c = 1/3$. **104**
5.6 $(1, 33/37, 33/37)$ turbo code with interleaver #1, $S = 12$, $K = 1000$, and $R_c = 1/3$. **104**
5.7 $(1, 5/7, 33/23)$ turbo code with interleaver #1, $S = 12$, $K = 1000$, and $R_c = 1/3$. . **105**
5.8 $(1, 5/7, 33/23)$ punctured turbo code with interleaver #1, $S = 12$, $K = 1000$, and $R_c = 1/2$. **105**
5.9 $(1, 5/7, 5/7)$ and $(1, 33/37, 33/37)$ turbo codes with $K = 4096$ and $R_c = 1/3$. . . . **107**
5.10 $(1, 5/7, 5/7, 5/7)$ multilevel turbo code with $K = 256$ and $R_c = 1/4$. **107**
5.11 Performance comparison of (1,33/37,33/37) turbo code with the original and the modified S-random interleaver (with $T = 60$), $S = 15$, $K = 1024$, and $R_c = 1/3$. . **108**

CHAPTER 1

Introduction

The demand for wireless communication has been growing rapidly in the past two decades. As multimedia technology evolves, more and more users require larger bandwidth to support high data rate services such as exchanging multimedia files over wireless networks. However, wireless spectrum is limited and thus strictly regulated for various wireless communication systems. Any wireless network can only operate using a finite bandwidth. As a result, the number of users that can be accommodated by a wireless network, usually denoted as the user capacity, is restricted unless some other technology is applied.

The user capacity of a wireless network is greatly affected by the interference generated by users. In a wireless network, when a mobile transmits signal to another mobile, it also causes interference to the other mobiles in the same network. In particular, most systems use omnidirectional antennas; while the receiving mobile is located in a particular direction from the transmitting mobile, the omnidirectional antenna transmits signal to all directions with the same amount of power. This makes the interference problem even worse. To achieve a certain communication quality, the interference experienced in each communication link can not be too big. The larger the number of active mobiles in the network, the larger the interference experienced by each mobile. The user capacity is again restricted in the wireless network. It is worth noting that since the power is wasted in the directions that are away from the receiving mobile, the other major drawback of omnidirectional antennas is the low power efficiency. This is a crucial problem since long battery life is desirable for modern mobile communications.

Recently, directional antennas have been considered to be a promising technology to

solve the user capacity and the power efficiency problems for wireless networks [1, 2]. To optimize the system performance, a thorough analysis of wireless networks with directional antennas is necessary. This is the motivation of a major part of this thesis which is discussed in Section 1.1.

Although directional antenna technology is very effective in reducing the interference from other mobiles, it is still not enough to achieve good communication quality in wireless communications. Wireless communications suffer from noise and fading as the signals travel through the wireless channels. Coded modulation and interleaving are techniques widely used in wireless communications to combat noise and fading. To analyze the performance of wireless networks with directional antennas, we must take the effect of coded modulation and interleaving into consideration. This motivates the rest of our work in the thesis, in which we focus on the performance analysis of bit-interleaved coded modulations, bit-interleaved space-time coded systems, and turbo codes. These topics are discussed in Section 1.2-1.4. With these results, we can actually evaluate the performance of wireless networks with directional antennas that use different coded modulation schemes. In the final section of this chapter, we outline the organization of this thesis.

1.1 Wireless Networks with Directional Antennas

The concept of directional antennas is not new. It was applied in military radar systems during World War II. However, not until recent years did people start to consider applying directional antennas in modern wireless communications. There are several reasons for this. One is that the demand of wireless communications did not grow that rapidly until recent years, hence people did not worry about the user capacity problem that much. Another reason is that an advanced directional antenna needs to track the location of the target mobiles and interferers, and adaptively form its beam to achieve near optimal communication quality. This requires a huge amount of signal processing and computation complexity. The task was too demanding for the processors in the past,

which were either too slow or too expensive to be applied. Nowadays we have many fast DSP processors and chips that are reasonably priced. This has led many to reconsider the use of directional antennas in wireless communications during the recent years [2].

By using directional antennas, both transmitting and receiving mobiles have the ability to generate beam patterns with high transmission gain and reception gain in the direction of each other, and low gain elsewhere. This makes the power usage much more efficient, which extends the battery life of the mobile. Moreover, it significantly reduces the interference problem because now only mobiles with receiving antennas pointing directly to the main beam of the transmitting mobile will be interfered by the transmitting mobile. With the interference problem lightened, the system can have a higher user capacity than before.

Although it is promising to apply directional antenna technology to wireless communications, there are still many things that need to be considered to optimize the performance in different applications. For instance, if we apply directional antennas to a wireless network, there are system parameters of the network that need to be optimized to get the best system performance, such as the mobile density of the network or the code rate of the channel coding used. In order to optimally determine system parameters, it is necessary for us to know how a system will perform under different settings of system parameters. This is the major motivation of our work. We want to understand exactly how well does a wireless network with directional antennas perform and how to optimize the system design for such network.

In the literature, a few papers [3–6] have attempted to accomplish our goal. However, the beam patterns of the antennas used in these papers were either omnidirectional or very simplified. These results can not be applied to analyze the system performance when a realistic beam pattern is considered. This motivates us to find an approach to analyze the system performance for an arbitrary beam pattern in a wireless channel. In particular, we are interested in the performance in a realistic channel, thus the channel model we consider includes the effect of path loss, shadowing, and Rayleigh fading. The major goal of our work is to analyze the system performance of wireless

networks with directional antennas for arbitrary beam patterns with realistic channel models. Moreover, we want to find a characteristic value that can characterize the overall system performance. This will be very useful for performance comparison among beam patterns.

Another contribution of our work is to consider the effect of power control when analyzing the performance of wireless networks with directional antennas. In a wireless environment, when there are obstacles between the transmitting and the receiving mobiles, the transmitted signal suffers from the shadowing effect which attenuates the received signal level. Power control is an effective solution to the shadowing problem. Our analysis enables us to evaluate the performance of a wireless network with directional antennas under different power control schemes. Through the numerical experiments, we show that power control can help improve the performance of such wireless networks. We also show how to find the optimal power control scheme by numerical optimization.

Finally, we apply our work to system design optimization problems. In particular, we try to find the optimal mobile density of a wireless network given the transmitting beam pattern used. We also apply the random coding bound and cutoff rate analysis to find the optimal code rate for the network. Our work is shown to be useful for the system design and optimization of wireless networks with directional antennas.

1.2 Bit-Interleaved Coded Modulation (BICM)

Due to the growing demands for high data rates in the modern wireless communications, it is desired to use a larger constellation in modulation. In wireless communications, signals encounter multipath fading which can significantly reduce the received signal level and cause intersymbol interference. The drawback of using a large constellation is that each symbol consists of many coded bits, so one severely faded symbol reception in wireless communication will affect a burst of bits, which significantly increases the probability of decoding error. BICM is effective in mitigating multipath fading by providing time diversity. In a BICM system, codewords are bit-interleaved

before signal mapping. As a result, the bits that are affected by one bad symbol reception are spread out in the received codeword. This significantly reduces the probability of decoding error. Hence, BICM is an effective method to achieve good performance in wireless communications. A union bound on the bit error probability of BICM systems was presented in [7, 8]. The bound was based on the assumption that a symbol error causes a bit error, which is not true in general. To get the correct performance analysis, we derive the union bounds on the packet and bit error probabilities of BICM over additive white Gaussian noise (AWGN) channel and various fading channels including Rayleigh, Rician and Nakagami distributions. Our simulation results show that our bound is tight under all channel models and the result is applied to analyze the performance of wireless networks that use BICM in physical layer.

1.3 Bit-Interleaved Space-Time (BI-ST) Coded Systems

One standard approach to mitigate fading and achieve bandwidth efficiency is transmit diversity in which multiple antennas are used at the transmitter [9]. Using the combination of multiple antennas at the transmitter along with error correction coding is referred to as space-time (ST) coding [10]. A simple and elegant space-time block code (STBC) was proposed by Alamouti [11] to provide diversity at the transmitter. This idea was soon generalized by Tarokh *et al.* [12] to a general number of transmit antennas. As mentioned previously, BICM is efficient in mitigating multipath fading by providing time diversity, hence it is desirable to consider a bit-interleaved space-time coded system which can provide both time and transmit diversity to mitigate fading. Due to the multi-dimensional nature of ST codes, the performance analysis of BI-ST coded systems is much more complicated than BICM systems. However, we are still able to derive the union bounds on the packet and bit error probabilities of a general BI-ST coded system and apply the analysis to two specific examples; namely, the BI space-time coded modulation (BI-STCM) and the BI space-time block codes (BI-STBC). The performance is analyzed extensively under various fading models which include Rayleigh, Rician and Nakagami

fading models. Results show that the analysis curves are tight to the simulation for a wide range of signal-to-noise ratios.

1.4 Error Floor Analysis of Turbo Codes

Turbo codes are known to have extremely good performance close to the Shannon capacity limit and are widely used nowadays. In order to analyze the performance of wireless networks that use turbo codes, it is desirable for us to be able to compute a tight union bound for the performance of a turbo code. However, to compute the union bound, we need to know the weight spectrum of the turbo code. This is actually a very difficult task due to the existence of the interleaver in the turbo encoder structure. Previously in the literature [13–16], the problem was solved by applying the uniform interleaving assumption. It approximates the actual interleaver by a probabilistic interleaver to find the weight spectrum of the turbo code. However the union bound computed from the uniform interleaving assumption is not very tight compared to the actual turbo code performance. This motivates us to find an efficient algorithm for estimating the weight spectrum of a turbo code with any specific interleaver. We find such algorithm and it enables us to compute a very tight union bound for a turbo code with a specific interleaver. The result can be applied to find the performance of wireless networks with directional antennas that use turbo codes in physical layer.

1.5 Thesis Outline

In Chapter 2, we present the performance analysis and various system design optimization problems of wireless networks with directional antennas. In Chapter 3, the performance analysis of BICM under various fading models is presented. In Chapter 4, we analyze the performance of BI-ST coded systems under various fading models. In Chapter 5, we demonstrate our efficient algorithm for analyzing turbo code performance. Finally, conclusions and future research directions are discussed in Chapter 6.

CHAPTER 2

Wireless Networks with Directional Antennas

Interuser interference problem is a major factor that limits the user capacity of a wireless network. Directional antenna technology is regarded as an effective solution for the problem. In this chapter our focus is on the performance of a wireless network with directional antennas under a realistic channel model. The analysis enables us to find the optimal system parameters that optimize the overall system performance, which is the major goal of our work.

2.1 Introduction

In a wireless network, when a mobile transmits signal to another mobile, it causes interference to the other mobiles in the same network. This limits the number of simultaneous transmissions in a wireless network. Many systems use omnidirectional antennas to avoid having to know the location of receiver. An omnidirectional antenna transmits signals to all directions with the same power. Not only does this cause interference to the other mobiles, but also the power usage is very inefficient, because the power is wasted in directions away from the receiving mobile. The interference limits the number of users a system can accommodate. This gives rise to the promising idea of using directional antennas in wireless networks.

By using directional antennas, both transmitting and receiving mobiles have the ability to generate beam patterns with high transmission gain and reception gain in the direction of each other, and low gain elsewhere. The power usage is much more efficient now which extends the battery life of a mobile. The interference problem is also signifi-

cantly reduced because now only mobiles with receiving antennas pointing at the main beam of a transmitting mobile will be significantly interfered by the transmitting mobile. This allows the system to have a larger number of users than with omnidirectional antennas.

To get the best system performance out of such wireless network, there are system parameters of the network that need to be optimized. For instance, the mobile density of the network affects the system performance to a great extent. If the density is large, mobiles experience severe interference from other mobiles which causes poor performance. On the other hand, when the mobile density is small, though the communication quality for each mobile is good, the overall system throughput is low since the network usage is not efficient. There is an optimal choice of mobile density that can maximize the system throughput. Another example is the code rate of the channel coding used in the physical layer of the wireless network. If we use a lower code rate, the probability of successful transmission will be higher, but the amount of information transmitted in each successful transmission will be reduced. On the other hand if we use a higher code rate, the probability of successful transmission will be lower, yet the amount of information transmitted in each successful transmission will be higher. In order to optimally determine system parameters such as the mobile density or the code rate of the wireless network, it is necessary for the system designer to know the relation between system performance and system parameters. In the literature, only a few efforts have been attempted to analyze the performance of wireless networks with directional antennas. In [3, 4], the outage probability of wireless networks with omnidirectional antennas was analyzed. The outage probability of wireless networks using switched beam antennas was analyzed in [5]. However, the antenna beam pattern used in the paper was very simplistic. The result can not be applied to analyze the system performance when a realistic beam pattern is considered. In [6] the outage probability of a receiver using a smart antenna with fixed number of interferers under Rayleigh and Rician fading was analyzed. The medium access control (MAC) protocol was assumed to be slotted ALOHA [17] in [3–5], but it was unspecified in [6]. None of past research efforts considered the performance of a

wireless network using an arbitrary transmitting beam pattern and the effect of specific coding and modulation schemes on the system performance.

In our work, we propose a method with which we can analyze the system performance using an arbitrary beam pattern under a realistic channel model which includes the effects of path loss, shadowing, and Rayleigh fading with slotted ALOHA used for the MAC protocol. We analyze the performance of a targeted link under both slow fading and fast fading which gives us the performance under the two extreme cases of the fading effect. By combining our performance analysis of bit-interleaved coded modulation and turbo codes in later chapters, we can evaluate the performance of a wireless network with specific coding and modulation used in the physical layer.

In the analysis, we initially assume the transmitting and receiving mobiles knows the exact direction of each other. However, this is not usually true in reality due to the MAC protocol or the accuracy of the direction estimation algorithm used. For instance, in the MAC protocol design for IEEE 802.11 with directional antennas, the nodes are often designed with only a finite number of beam directions [18, 19]. Hence the transmitting and receiving mobiles are rarely perfectly aligned. The direction estimation error affects the system performance. We analyze the system performance of a wireless network given the distribution of the direction estimation error. This enables us to compare the performance of different beam patterns given the existence of the direction estimation error between the mobiles.

Besides the direction estimation error, we also look into the effect of power control on the system performance. In wireless communications, signals are often attenuated when there are obstacles between the transmitting and the receiving mobiles, which is called shadowing. Power control is an effective way to compensate the power loss due to shadowing and is often used in wireless communications. Hence, we also analyze the system performance when power control is applied to a wireless network. This enables us to find the optimal power control scheme for a wireless network.

As mentioned earlier, the major motivation of our work is to optimize the system performance for wireless networks with directional antennas. Thus we apply our per-

formance analysis to determine the optimal mobile density that maximizes the system throughput. We also apply the random coding bound and cutoff rate analysis to find the optimal code rate for the link throughput. Our analysis is shown to be very useful in system design optimization.

One thing worth noting is that we find that the system performance and the beam pattern used are related only through one characteristic value, which we call the *antenna interference factor* (AIF), of the beam pattern. The AIF can be computed very easily for any beam pattern and it enables us to do the performance comparison of various beam patterns very easily; any beam pattern with smaller AIF will have better performance than the others.

The remainder of this chapter is organized as follows. In Section 2.2, we give a brief introduction to the system model and the channel model. In Section 2.3, we describe how to compute the outage probability of a slow faded link in a wireless network with a simplified beam pattern. The analysis is then generalized to the case of an arbitrary beam pattern. In Section 2.4, we analyze the performance when the targeted link is fast faded. In Section 2.5, the effect of the direction estimation error on the outage probability is derived. In Section 2.6, we analyze the effect of power control on the system performance. In Section 2.7, our analysis is applied to system design optimization problems to find the optimal mobile density and code rate to maximize the system throughput of the network. Finally, the conclusions are addressed in Section 2.8.

2.2 Model Description

Consider a wireless network as shown in Fig. 2.1. We are interested in the performance of the communication link between two reference mobiles Tx (transmitting mobile) and Rx (receiving mobile). We first assume all mobiles use directional antennas for transmission and omnidirectional antennas for reception. Later we will generalize the analysis to the case where directional antennas are used for both transmission and reception. We assume all mobiles use the same transmitting beam pattern. A typical

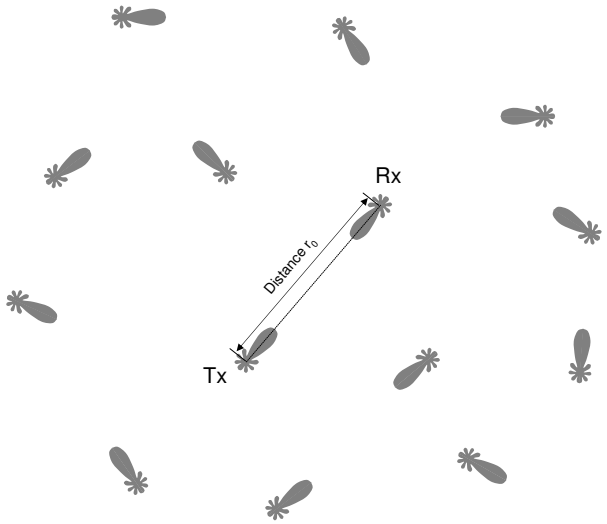

Figure 2.1: Wireless network using directional antennas.

beam pattern $f(\theta)$ is shown in Fig. 2.2, where $f(\theta)$ denotes the gain of the transmitting antenna relative to an omnidirectional antenna in the direction of θ . For an omnidirectional antenna, $f(\theta) = 1$ for any θ. We assume that Tx is always perfectly aligned to Rx, i.e., $\theta = 0$ always points to the direction of Rx. Though the beam pattern considered in this chapter is two dimensional, the result can be generalized to three dimensional beam patterns. Finally it is assumed that all mobiles have the perfect knowledge of their own channels.

We use the same channel model as in [3], shown in Fig. 2.3. Assume that the distance between Tx and Rx is r_0, and Rx is in the direction of θ_0 from Tx. When Tx transmits power P_T, the received power at Rx is then $P_0 = P_T f(\theta_0)\ \zeta_0\ \xi_0^2$, where ζ_0 accounts for path loss and shadowing effect which is constant for at least a packet duration T. It is log-normal distributed with conditional probability density function (pdf)

$$f(\zeta_0 \mid r_0) = \frac{1}{\sqrt{2\pi}\sigma\zeta_0}\ e^{-\frac{1}{2}\frac{\left(\log\zeta_0 - \log(Kr_0^{-\eta})\right)^2}{\sigma^2}}, \tag{2.1}$$

where $Kr_0^{-\eta}$ denotes the average attenuation level due to path loss. The constant K denotes the average attenuation level measured at a reference distance from the transmitting

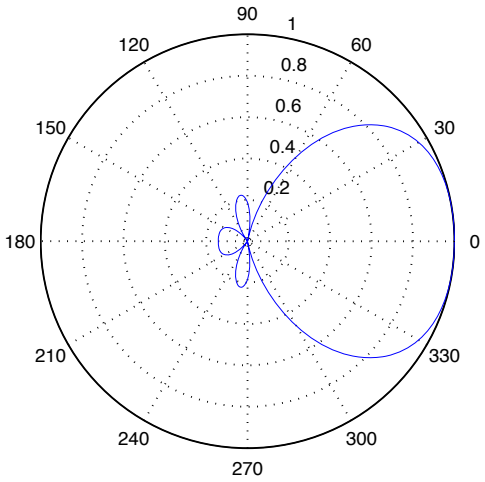

Figure 2.2: Beam pattern $f(\theta)$.

mobile, and η is called path loss exponent which ranges from 2.0 to 6.0 depending on the type of channel [20]. In an urban area, η is around 2.7 to 3.5. In an obstructed environment or in buildings, where signal suffers more path loss, η is around 4.0 to 6.0. Also note that σ is usually denoted in dB. Typical values for σ are 5 to 10 dB.

The fading level ξ_0 is a random variable that accounts for the Rayleigh fading. If ξ_0 is Rayleigh distributed, then ξ_0^2 is exponentially distributed [21]. Hence, the conditional pdf of P_0 given ζ_0 is

$$f_0(P_0 \mid \zeta_0) = \frac{1}{P_T f(\theta_0)\zeta_0}\, e^{-\frac{P_0}{P_T f(\theta_0)\zeta_0}}, \tag{2.2}$$

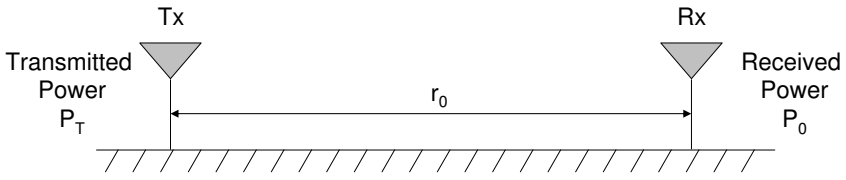

Figure 2.3: Channel between Tx and Rx.

and the conditional cumulative density function (cdf) is

$$F_0(P_0 \mid \zeta_0) = 1 - e^{-\frac{P_0}{P_T f(\theta_0)\zeta_0}}. \tag{2.3}$$

The channel between any interfering mobile and Rx follows the same model described above, except that the distance can be different. Also the signal from each interfering mobile to Rx is independently shadowed and independently Rayleigh faded. We also assume the signal power from an interfering node is constant throughout the packet duration.

The mobiles are assumed to be randomly distributed on the two dimensional plane as a Poisson point process. Let λ_M denote the average mobile density within a circle of radius 1. For any disc of radius r on the plane, the number of mobiles N_r in the disc has a Poisson distribution POI($\lambda_M r^2$), i.e., $Pr\{N_r = k\} = \frac{e^{-\lambda_M r^2}(\lambda_M r^2)^k}{k!}$. We assume slotted ALOHA [17] is used for the MAC protocol. All mobiles are synchronized and every packet is transmitted at the beginning of the time slot right after the packet is generated. Each time slot is of duration T which is the same as the packet duration. Each mobile generates data packets which is modeled by a Bernoulli process of rate p, i.e., packets are generated with probability p in each slot. Hence, given that there are N_r mobiles in the network (excluding Tx and Rx), the number of mobiles that actually interfere with Rx is randomly distributed as BIN(N_r, p). The value of p should not be big, otherwise collisions happen frequently and every mobile suffers performance degradation. Assuming the largest possible distance between Tx and Rx is r_{max}, then the average system load, i.e., the average number of simultaneous transmissions in a disc of radius r_{max}, equals to $\lambda_M r_{max}^2 p$. The system load should be less than 1 to reduce the chance of collision. Hence, p should be less than $\frac{1}{\lambda_M r_{max}^2}$ to avoid poor performance.

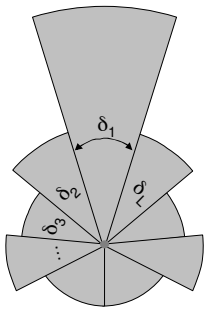

Figure 2.4: Simplified beam pattern.

2.3 Outage Probability of a Slow Faded Link

In this section, we analyze the performance of the link between Tx and Rx by deriving the outage probability of the link under slow fading. By slow fading we mean that the fading level of the targeted link between Tx and Rx is constant for at least a packet duration. This is usually the case when Tx, Rx, and the environment are all of low mobility. We first derive the outage probability for a simplified beam pattern of Tx as shown in Fig. 2.4 in Section 2.3.1. Then the analysis is generalized for any arbitrary shape of beam patterns used by Tx and Rx in Section 2.3.2, and several numerical examples are shown in Section 2.3.3.

2.3.1 Simplified Beam Pattern

First consider the simplified beam pattern shown in Fig. 2.4. The beam pattern has L beams. Beam i, $i = 1, 2, \cdots, L$, has angular beam width δ_i (rad) and gain f_i with respect to the omnidirectional antenna of the same transmitting power. Without loss of generality, beam 1 is always the beam with the largest gain and is always pointing to Rx. The outage probability of the link between Tx and Rx is defined by

$$\phi_{L,r_0}(b) = P\{\text{Outage}\} \triangleq P\left\{\frac{P_0}{P_I + N} < b\right\}, \tag{2.4}$$

where P_0 is the received power, P_I the interference power, and N the noise power at Rx. If we denote the energy per symbol received at Rx (from Tx) by E_s and symbol duration by T_s, it is easy to see that $P_0 = E_s/T_s$ and $N = N_0/T_s$, where N_0 denotes the noise power density. It is assumed that the outage occurs whenever the signal-to-interference-and-noise ratio (SINR) at Rx is less than a certain threshold b which causes the failure of the channel coding and modulation to maintain the small packet error rate (PER) required by the data transmission. Hence, the SINR threshold b depends on the coding and modulation used by Tx. In a slow faded channel, the SINR should remain constant during the whole packet duration. When we determine the value of b for a specific coding and modulation scheme, we should refer to the performance of the coding and modulation scheme in an AWGN channel. The analyses in Chapter 3 and 5 enable us to plot the PER versus signal-to-noise ratio (SNR) for various coded modulation schemes and turbo codes in AWGN and different fading channels. If we model the interference as noise, we can determine the value of b easily from the PER analysis of these Chapters.

The key concept of computing $\phi_{L,r_0}(b)$ is to compute $\phi_{L,r_0}(b,a) = P\left\{\frac{P_0}{P_I(a)+N} < b\right\}$ first, where $P_I(a)$ only includes the interference power from those interferers located within a distance a from Rx. After taking the limit as a goes to infinity, we can obtain the outage probability $\phi_{L,r_0}(b) = \lim_{a\to\infty}\phi_{L,r_0}(b,a)$. Consider mobiles in the disc of radius a centered at Rx (Tx excluded). We classify them into L groups. The mobiles in the i^{th} group all point at Rx with their beam i. Let $\boldsymbol{K_a} = (K_1, K_2, \cdots, K_L)$ denote the number of mobiles in each group. The number of mobiles in a disc of radius a has a Poisson distribution POI($\lambda_M a^2$). If we assume the direction of any mobile to its receiving mobile is uniformly distributed between 0 and 2π, then the probability of a mobile pointing at Rx with beam i is $\frac{\delta_i}{2\pi}$ which is proportional to the angular beam width δ_i. This implies K_i has a Poisson distribution POI($\frac{\lambda_M a^2\delta_i}{2\pi}$). Since K_is' are independent,

$$P(\boldsymbol{K_a}) = \prod_{i=1}^{L} \frac{e^{\frac{-\lambda_M a^2\delta_i}{2\pi}}\left(\frac{\lambda_M a^2\delta_i}{2\pi}\right)^{K_i}}{K_i!}. \tag{2.5}$$

Among the K_i mobiles in the i^{th} group, the number of mobiles that actually trans-

mit packets and thus interfere with Rx, I_i, is of distribution BIN(K_i, p). Define $\boldsymbol{I_a} = (I_1, I_2, \cdots, I_L)$. Then

$$P(\boldsymbol{I_a} \mid \boldsymbol{K_a}) = \prod_{i=1}^{L} \binom{K_i}{I_i} p^{I_i}(1-p)^{K_i - I_i}. \tag{2.6}$$

To analyze the outage probability, number those I_i interferers in the i^{th} group from 1 to I_i. The distance from interferer j in group i to Rx is denoted by $r_{i,j}$. The pdf of $r_{i,j}$ given the interferer is in the disc of radius a centered at Rx is of the form

$$f_a(r_{i,j}) = \frac{2\pi r_{i,j}}{\pi a^2} = \frac{2r_{i,j}}{a^2}. \tag{2.7}$$

For later use, we define vector $\boldsymbol{r_a} \triangleq [\boldsymbol{r_1}, \boldsymbol{r_2}, \cdots, \boldsymbol{r_L}]$, where $\boldsymbol{r_i} = (r_{i,1}, r_{i,2}, \cdots, r_{i,I_i})$, $i = 1, 2, \cdots, L$.

The path loss at Rx experienced by the interference from interferer j in group i is denoted by $\zeta_{i,j}$. From (2.1), we have

$$f(\zeta_{i,j} \mid r_{i,j}) = \frac{1}{\sqrt{2\pi}\sigma\zeta_{i,j}} \; e^{-\frac{1}{2}\frac{\left(\log\zeta_{i,j} - \log(Kr_{i,j}^{-\eta})\right)^2}{\sigma^2}}. \tag{2.8}$$

Define vector $\boldsymbol{\zeta_a} \triangleq [\boldsymbol{\zeta_1}, \boldsymbol{\zeta_2}, \cdots, \boldsymbol{\zeta_L}]$, where $\boldsymbol{\zeta_i} = (\zeta_{i,1}, \zeta_{i,2}, \cdots, \zeta_{i,I_i})$, $i = 1, 2, \cdots, L$.

The received interference power at Rx from interferer j in group i is denoted by $P_{i,j}$. The conditional distribution of $P_{i,j}$ given $\zeta_{i,j}$ is exponentially distributed as described in Section 2.2. The conditional pdf is

$$f(P_{i,j} \mid \zeta_{i,j}) = \frac{1}{P_T f_i \zeta_{i,j}} \; e^{-\frac{P_{i,j}}{P_T f_i \zeta_{i,j}}}. \tag{2.9}$$

Define vector $\boldsymbol{P_a} \triangleq [\boldsymbol{P_1}, \boldsymbol{P_2}, \cdots, \boldsymbol{P_L}]$, where $\boldsymbol{P_i} = (P_{i,1}, p_{i,2}, \cdots, P_{i,I_i})$, $i = 1, 2, \cdots, L$.

Finally recall that r_0, ζ_0, P_0 are the distance, path loss, and received power at Rx from Tx respectively. Since Tx is pointing at Rx with beam 1 which has a gain of f_1, the cdf

of P_0 given ζ_0 in (2.3) becomes

$$F_0(P_0 \mid \zeta_0) = 1 - e^{-\frac{P_0}{P_T f_1 \zeta_0}}. \tag{2.10}$$

Before deriving the outage probability, we first give a high-level description about our derivation process. The probability $P\left\{\frac{P_0}{P_I(a)+N} < b\right\}$ is determined by b, a, and the realization of a random vector $\mathbf{x} \triangleq (\boldsymbol{K_a}, \boldsymbol{I_a}, \boldsymbol{r_a}, \boldsymbol{\zeta_a}, \boldsymbol{P_a}, r_0, \zeta_0, P_0)$. If we denote the pdf of $\boldsymbol{x}$ by $f(\boldsymbol{x})$, then $\phi_{L,r_0}(b,a) = P\left\{\frac{P_0}{P_I(a)+N} < b\right\}$ is simply

$$\phi_{L,r_0}(b,a) = \int_S f(\boldsymbol{x}) d\boldsymbol{x},$$

where $S = \{\boldsymbol{x} : \frac{P_0}{P_I(a)+N} < b\}$. The order of integration (with respect to the elements of $\boldsymbol{x}$) that we take is: P_0, $\boldsymbol{P_a}$, $\boldsymbol{r_a}$, $\boldsymbol{\zeta_a}$, $\boldsymbol{I_a}$, $\boldsymbol{K_a}$, and finally ζ_0. By first taking the integration with respect to P_0 and $\boldsymbol{P_a} = \{P_{i,j}\}$, we can obtain the conditional outage probability given $\boldsymbol{K_a}, \boldsymbol{I_a}, \boldsymbol{r_a}, \boldsymbol{\zeta_a}$, and ζ_0,

$$\begin{aligned}
\phi_{L,r_0}(b,a \mid \boldsymbol{K_a}, \boldsymbol{I_a}, \boldsymbol{r_a}, \boldsymbol{\zeta_a}, \zeta_0) &= P\{P_0 < bP_I(a) + bN \mid \boldsymbol{K_a}, \boldsymbol{I_a}, \boldsymbol{r_a}, \boldsymbol{\zeta_a}, \zeta_0\} \\
&= \int_0^\infty \cdots \int_0^\infty F_0(b\sum_{i=1}^{L}\sum_{j=1}^{I_i} P_{i,j} + bN) \cdot \prod_{i=1}^{L}\prod_{j=1}^{I_i} f(P_{i,j} \mid \zeta_{i,j})\, dP_{i,j} \\
&= 1 - e^{-\frac{bN}{P_T f_1 \zeta_0}} \prod_{i=1}^{L}\prod_{j=1}^{I_i} \left[\frac{1}{1+\frac{bf_i\zeta_{i,j}}{f_1\zeta_0}}\right].
\end{aligned} \tag{2.11}$$

Then by taking the expectation with respect to $\boldsymbol{r_a}$ and $\boldsymbol{\zeta_a}$, we have

$$\begin{aligned}
&\phi_{L,r_0}(b,a \mid \boldsymbol{K_a}, \boldsymbol{I_a}, \zeta_0) \\
&= \int_0^\infty \cdots \int_0^\infty \phi_{L,r_0}(b,a \mid \boldsymbol{K_a}, \boldsymbol{I_a}, \boldsymbol{r_a}, \boldsymbol{\zeta_a}, \zeta_0) \cdot \prod_{i=1}^{L}\prod_{j=1}^{I_i} f(\zeta_{i,j} \mid r_{i,j})\, f_a(r_{i,j}) dr_{i,j}\, d\zeta_{i,j} \\
&= 1 - e^{-\frac{bN}{P_T f_1 \zeta_0}} \prod_{i=1}^{L}\prod_{j=1}^{I_i} \int_0^a \frac{2r_{i,j}\, dr_{i,j}}{a^2} \int_0^\infty \frac{e^{-\frac{1}{2}\frac{\left(\log\zeta_{i,j} - \log(Kr_{i,j}^{-\eta})\right)^2}{\sigma^2}}\, d\zeta_{i,j}}{(1+\frac{bf_i\zeta_{i,j}}{f_1\zeta_0})(\sqrt{2\pi}\sigma\zeta_{i,j})}
\end{aligned}$$

$$
\begin{aligned}
&= 1 - e^{-\frac{bN}{P_T f_1 \zeta_0}} \prod_{i=1}^{L} \prod_{j=1}^{I_i} \frac{1}{\sqrt{2\pi}\sigma} \int_0^a \frac{2r_{i,j}\ dr_{i,j}}{a^2} \int_{-\infty}^{\infty} \frac{e^{-\frac{y^2}{2\sigma^2}}\ dy}{1 + \frac{f_i b}{f_1 \zeta_0}\ e^y \left(\frac{r_0}{r_{i,j}}\right)^\eta} \\
&= 1 - e^{-\frac{bN}{P_T f_1 \zeta_0}} \prod_{i=1}^{L} \prod_{j=1}^{I_i} \frac{1}{\sqrt{2\pi}\sigma a^2} \int_{-\infty}^{\infty} e^{-\frac{y^2}{2\sigma^2}}\ dy \int_0^a \frac{2r_{i,j}\ dr_{i,j}}{1 + \frac{f_i b}{f_1 \zeta_0}\ e^y \left(\frac{r_0}{r_{i,j}}\right)^\eta} \\
&= 1 - e^{-\frac{bN}{P_T f_1 \zeta_0}} \prod_{i=1}^{L} \left[I_a(x, \frac{f_i}{f_1}) \right]^{I_i}, \qquad (2.12)
\end{aligned}
$$

where

$$
I_a(x, \psi) \triangleq \frac{1}{\sqrt{2\pi}\sigma a^2} \int_{-\infty}^{\infty} e^{-\frac{y^2}{2\sigma^2}} dy \int_0^a \frac{2r dr}{1 + \psi\ b\ e^{y-x} \left(\frac{r_0}{r}\right)^\eta)}\ . \qquad (2.13)
$$

Note that y is used to substitute for $\left(\log \zeta_{i,j} - \log\left(K r_{i,j}^{-\eta}\right)\right)$ in the derivation of (2.12). By taking the expectation of (2.12) with respect to ζ_0, we can obtain

$$
\begin{aligned}
\phi_{L,r_0}(b, a \mid \boldsymbol{K_a}, \boldsymbol{I_a}) &= 1 - \int_0^\infty e^{-\frac{bN}{P_T f_1 \zeta_0}} \prod_{i=1}^{L} \left[I_a(x, \frac{f_i}{f_1}) \right]^{I_i} \cdot \frac{1}{\sqrt{2\pi}\sigma\zeta_0}\ e^{-\frac{1}{2}\frac{\left(\log\zeta_0 - \log(K r_0^{-\eta})\right)^2}{\sigma^2}}\ d\zeta_0 \\
&= 1 - \frac{1}{\sqrt{2\pi}\sigma} \int_{-\infty}^{\infty} e^{-\frac{be^{-x}}{\gamma_c} - \frac{x^2}{2\sigma^2}} \cdot \prod_{i=1}^{L} \left[I_a(x, \frac{f_i}{f_1}) \right]^{I_i} dx, \qquad (2.14)
\end{aligned}
$$

where $\gamma_c = \frac{P_T K f_1}{N r_0^\eta} = \frac{E K f_1}{N_0 r_0^\eta}$ is the average received signal-to-noise ratio (SNR) at Rx from Tx, and x is used to substitute for $\left(\log\zeta_0 - \log\left(K r_0^{-\eta}\right)\right)$. Now take the expectation with respect to $\boldsymbol{K_a}$ and $\boldsymbol{I_a}$, we get

$$
\begin{aligned}
\phi_{L,r_0}(b, a) &= \sum_{K_1,\ldots,K_L} P(\boldsymbol{K_a}) \sum_{I_1,\ldots,I_L} \phi_{L,r_0}(b, a \mid \boldsymbol{K_a}, \boldsymbol{I_a})\ P(\boldsymbol{I_a} \mid \boldsymbol{K_a}) \\
&= 1 - \sum_{K_1,\ldots,K_L} \prod_{i=1}^{L} \frac{e^{\frac{-\lambda_M a^2 \delta_i}{2\pi}} (\frac{\lambda_M a^2 \delta_i}{2\pi})^{K_i}}{K_i!} \cdot \frac{1}{\sqrt{2\pi}\sigma} \\
&\qquad \cdot \int_{-\infty}^{\infty} e^{-\frac{be^{-x}}{\gamma_c} - \frac{x^2}{2\sigma^2}} \cdot \prod_{i=1}^{L} \left[1 + p \left(\cdot I_a(x, \frac{f_i}{f_1}) - 1 \right) \right]^{K_i} dx \\
&= 1 - \frac{1}{\sqrt{2\pi}\sigma} \int_{-\infty}^{\infty} \exp\left\{ \sum_{i=1}^{L} \frac{\lambda_M\ a^2\ \delta_i\ p}{2\pi} \cdot \left[I_a(x, \frac{f_i}{f_1}) - 1 \right] - \frac{b\ e^{-x}}{\gamma_c} - \frac{x^2}{2\sigma^2} \right\} dx. \qquad (2.15)
\end{aligned}
$$

To get the outage probability, we need to take the limit of (2.15) as a goes to ∞. The

limit of $a^2(I_a(x,\psi)-1)$ as a goes to ∞ is derived in [3] as

$$\lim_{a\to\infty} a^2(I_a(x,\psi)-1) = r_0^2\, e^{\frac{2\sigma^2}{\eta^2}}\, \frac{2\pi}{\eta}\, \csc\left(\frac{2\pi}{\eta}\right)\, b^{\frac{2}{\eta}}\, \psi^{\frac{2}{\eta}}\, e^{\frac{-2x}{\eta}}. \tag{2.16}$$

After some simplifications from (2.15), we can obtain the final form of the outage probability

$$\phi_{L,r_0}(b) = 1 - \frac{1}{\sqrt{2\pi}\sigma}\int_{-\infty}^{\infty} \exp\left\{-\Lambda(b,x)\cdot r_0^2\cdot\left[\sum_{i=1}^{L}\frac{\delta_i}{2\pi}\left(\frac{f_i}{f_1}\right)^{\frac{2}{\eta}}\right] - \frac{b\, e^{-x}}{\gamma_c} - \frac{x^2}{2\sigma^2}\right\} dx, \tag{2.17}$$

where

$$\Lambda(b,x) \triangleq \lambda_M p\, e^{\frac{2\sigma^2}{\eta^2}}\, \frac{2\pi}{\eta}\, \csc\left(\frac{2\pi}{\eta}\right)\, b^{\frac{2}{\eta}}\, e^{\frac{-2x}{\eta}}. \tag{2.18}$$

Though $\phi_{L,r_0}(b)$ is not in closed-form, the integral can be easily computed through numerical integration.

2.3.2 Arbitrary Beam Pattern and Array Interference Factor

Now consider a more realistic beam pattern such as the one in Fig. 2.2. Note that Fig. 2.4 will converge to Fig. 2.2 when L goes to ∞ and δ_i goes to 0. Taking the limit of (2.17), we have the outage probability $\phi_{r_0}(b)$ of the realistic beam pattern

$$\begin{aligned}\phi_{r_0}(b) &= \lim_{\substack{L\to\infty\\ \delta_i\to 0}} \phi_{L,r_0}(b)\\ &= 1 - \frac{1}{\sqrt{2\pi}\sigma}\int_{-\infty}^{\infty} \exp\left\{-\Lambda(b,x)\cdot r_0^2\cdot\left[\frac{1}{2\pi}\int_0^{2\pi}\left(\frac{f(\theta)}{f(\theta_0)}\right)^{\frac{2}{\eta}} d\theta\right] - \frac{b\, e^{-x}}{\gamma_c} - \frac{x^2}{2\sigma^2}\right\} dx.\end{aligned} \tag{2.19}$$

Notice that $\phi_{r_0}(b)$ depends on the beam pattern only through $\frac{1}{2\pi}\int_0^{2\pi}\left(\frac{f(\theta)}{f(\theta_0)}\right)^{\frac{2}{\eta}} d\theta$. Hence we propose a new parameter, the array interference factor (AIF), for any beam pattern

$$\mathcal{A} \triangleq \frac{1}{2\pi}\int_0^{2\pi}\left(\frac{f(\theta)}{f(\theta_0)}\right)^{\frac{2}{\eta}} d\theta, \tag{2.20}$$

which fully characterizes the performance of the beam pattern in the network. For an omnidirectional antenna, $\mathcal{A} = 1$. It easy to see that when $\mathcal{A}$ becomes large, the integrand of (2.19) becomes small, and thus $\phi_{r_0}(b)$ becomes large. Hence, $\phi_{r_0}(b)$ is an monotonic increasing function of AIF $\mathcal{A}$. This is due to the fact that any beam pattern with smaller AIF value will create (receive) less interference to (from) the system and thus have a better performance. With the introduction of AIF, now we can compare the performance of different beam patterns simply by comparing the AIF of each beam pattern.

For systems that use directional antennas for both transmission and reception, the outage probability can be easily generalized to

$$\phi_{r_0}(b) = 1 - \frac{1}{\sqrt{2\pi}\sigma} \int_{-\infty}^{\infty} \exp\left\{ -\Lambda(b,x) \cdot r_0^2 \cdot [\mathcal{A}_t \cdot \mathcal{A}_r] - \frac{b\, e^{-x}}{\gamma_c} - \frac{x^2}{2\sigma^2} \right\} dx, \tag{2.21}$$

where $\mathcal{A}_t$ and $\mathcal{A}_r$ are the AIF values of the transmitting and receiving beam patterns respectively.

2.3.3 Numerical Examples

In this section, we use the outage probability analysis to evaluate the performance of the wireless networks under slow fading with different coded modulation schemes. Two different coded modulation schemes are considered: BICM (bit-interleaved rate 1/2 (1, 5/7) convolutional coded 64-QAM) and rate 1/3 (1, 33/37, 33/37) turbo code with BPSK. As mentioned earlier, the value of threshold b is determined by the performance of the coded modulation used in an AWGN channel. By applying the performance analyses in Chapter 3 and 5, we can obtain the union bound on the PER of BICM and turbo code in an AWGN channel as shown in Fig. 2.5. If 1 packet error out of every 500 packet transmissions, i.e., a PER of 2×10^{-3}, is considered to be the threshold of acceptable communication quality, then from the figure we can see that the threshold b should be 1.5 dB for the turbo coded system and 13.5 dB for BICM. The BICM system has a 4.5 times higher bandwidth efficiency (1.5 bits/sec/Hz) than the turbo coded system (0.33 bits/sec/Hz). The tradeoff is the higher SNR required for BICM to achieve the PER

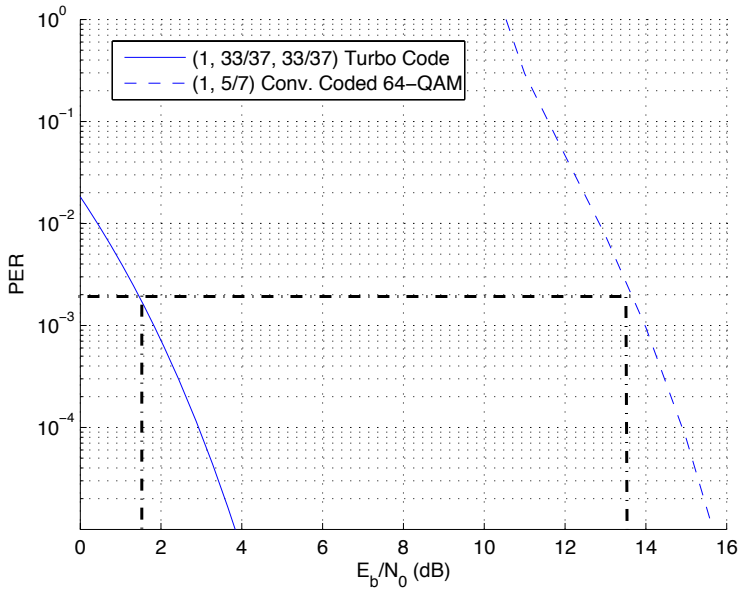

Figure 2.5: PER union bounds of (1, 33/37, 33/37) turbo code and bit-interleaved (1, 5/7) convolutional coded 64-QAM in AWGN channel

threshold 2×10^{-3}. Moreover, turbo code is known to be very energy efficient with near capacity performance. This is why we observe a huge difference of 12 dB between the values of b of the two systems.

For performance comparison, we consider the two different transmitting beam patterns shown in Fig. 2.6−2.7. These beam patterns are generated by end-fire antenna arrays with different number of antenna elements [22]. Beam pattern 1 is generated by 6 antenna elements while beam pattern 2 is generated by 10 antenna elements. The element separation is $\lambda/8$ where λ denotes the wavelength and it equals to 0.15 (m) assuming the operating frequency of the wireless network is 2 GHz. The mainlobe of beam pattern 1 (AIF: 0.6569 at $\eta = 4$ and 0.5699 at $\eta = 2.7$) is wider than beam pattern 2 (AIF: 0.5511 at $\eta = 4$ and 0.4545 at $\eta = 2.7$). The receiving antenna is assumed to be omnidirectional (AIF: 1.0). The variance of shadowing is $\sigma = 6$ dB. In all of the numerical examples in this chapter, $r_0 = 0.1$ (km) and $K = 1$ unless mentioned otherwise. We consider two different path loss exponents in our experiments: $\eta = 4$ for an obstructed environment in building and $\eta = 2.7$ for an urban area [20]. We also consider two different average

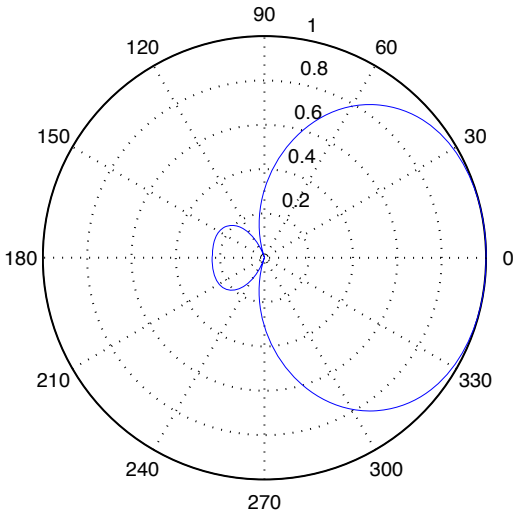

Figure 2.6: Beam pattern 1 (generated by 6 antenna elements, AIF: 0.6569 at $\eta = 4$ and 0.5699 at $\eta = 2.7$).

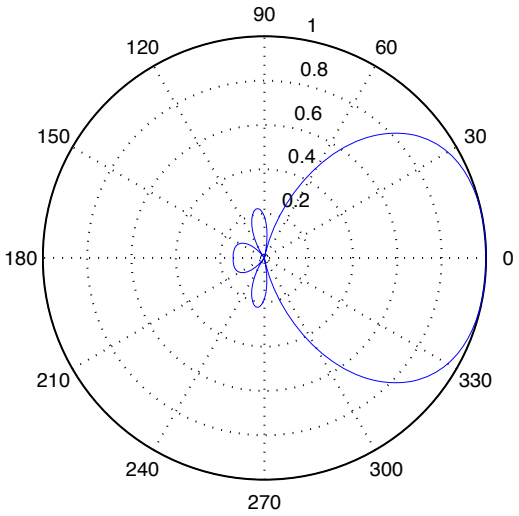

Figure 2.7: Beam pattern 2 (generated by 10 antenna elements, AIF: 0.5511 at $\eta = 4$ and 0.4545 at $\eta = 2.7$).

mobile densities: $\lambda_M = 20.0$ and $\lambda_M = 2.0$ (mobiles/km^2).

In Fig. 2.8 and 2.9 the outage probability is shown for a turbo coded system and a BICM system with $\lambda_M = 20.0$ and $\eta = 4$. The largest value of p is chosen to be 0.045 which is less than $\frac{1}{\lambda_M r_{max}^2}$ for $r_{max} = 1$ km. From the figures we see that beam pattern 2 has lower outage probability than beam patten 1 and omnidirectional antenna has the worst performance at all values of the load p. The interference power is indeed reduced by the narrower mainlobe (smaller AIF) and thus the outage probability is also reduced. We also observe that the outage probability has a nonzero floor as the average received signal SNR γ_c increases beyond 35 dB. When γ_c is large, it indicates that the noise power is small compared to the signal and interference power. Hence the dominating factor of performance degrading now is the interference from other mobiles. Therefore even if we increased the transmission power of all mobiles by the same factor, the SINR is almost the same as is the outage probability. Also note that as p increases, i.e., the mobiles generate packets with higher load, the outage probability also increases since there is more interference in the network.

In Fig. 2.10 we plot the outage probability for a system using BICM with a much lower mobile density $\lambda_M = 2.0$. We see that directional antennas still outperform omnidirectional antenna, but the gap is not as big as the previous cases. The reason for this is because the interference problem is not that serious at a low mobile density. Since the major improvement from using directional antennas is to suppress the interference, we do not get much from directional antennas in the case of low mobile density.

To compare the system performance in different wireless environments, we consider the BICM system in an urban area with a smaller path loss exponent $\eta = 2.7$. The outage probability versus the average received SNR γ_c is plotted in Fig. 2.11. If we compare Fig. 2.11 and 2.10, we can see that the performance in the urban area is worse than that in the obstructed environment at all SNR. This is because path loss is much smaller in the urban area, and thus the interference power from other mobiles is less attenuated than the case in the obstructed area. For the same average received SNR γ_c,

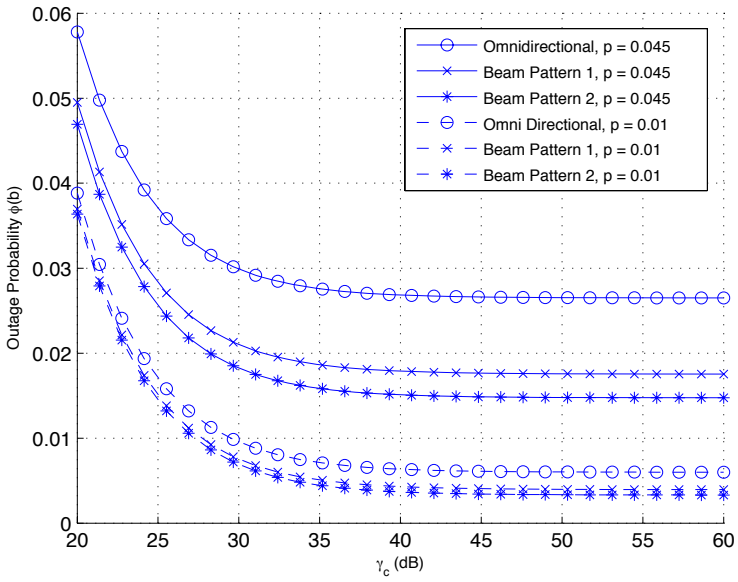

Figure 2.8: Outage probability vs. average received SNR γ_c with (1, 33/37, 33/37) turbo code in an obstructed environment under slow fading, $\lambda_M = 20.0$ mobiles/km^2, $b = 1.5$ dB, $\sigma = 6$ dB, $\eta = 4$, $r_0 = 0.1$ km.

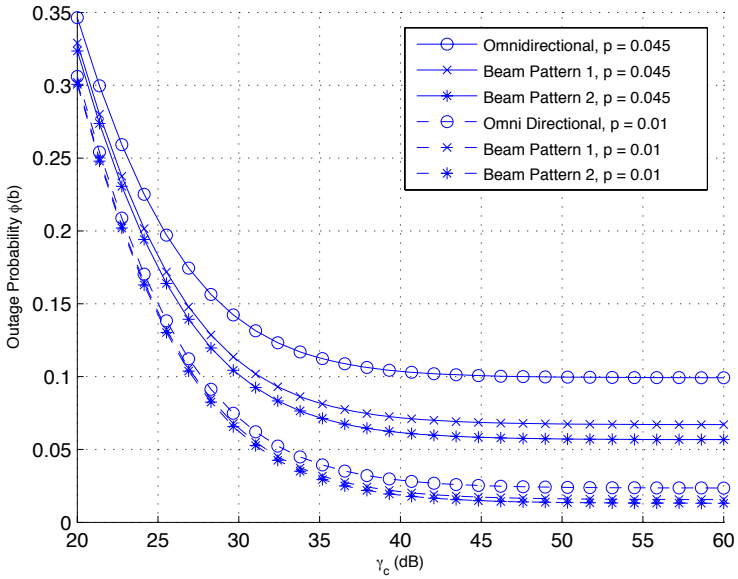

Figure 2.9: Outage probability vs. average received SNR γ_c with (1, 5/7) convolutional coded 64-QAM in an obstructed environment under slow fading, $\lambda_M = 20.0$ mobiles/km^2, $b = 13.5$ dB, $\sigma = 6$ dB, $\eta = 4$, $r_0 = 0.1$ km.

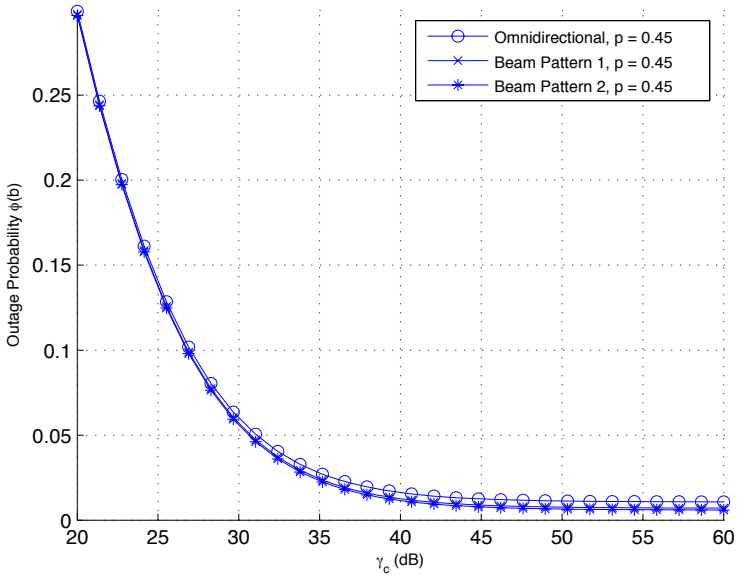

Figure 2.10: Outage probability vs. average received SNR γ_c with (1, 5/7) convolutional coded 64-QAM in an obstructed environment under slow fading with lower mobile density, $\lambda_M = 2.0$ mobiles/km^2, $b = 13.5$ dB, $\sigma = 6$ dB, $\eta = 4$, $r_0 = 0.1$ km.

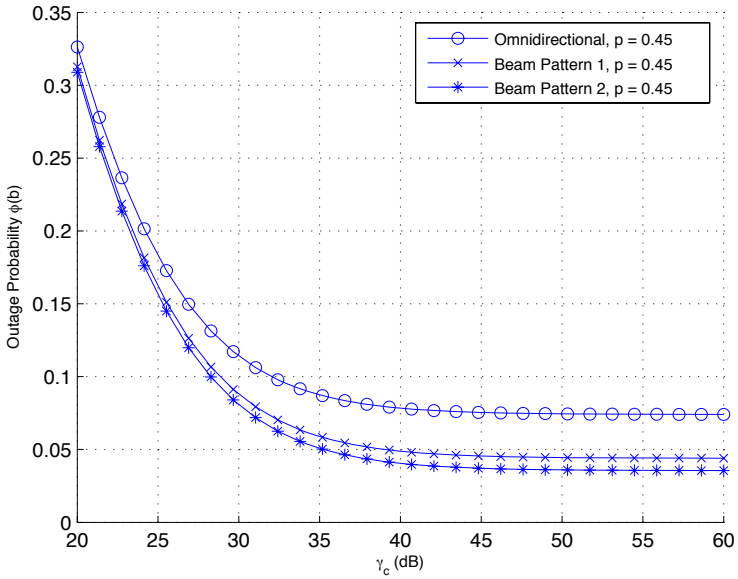

Figure 2.11: Outage probability vs. average received SNR γ_c with (1, 5/7) convolutional coded 64-QAM in an urban area under slow fading, $\lambda_M = 2.0$ mobiles/km^2, $b = 13.5$ dB, $\sigma = 6$ dB, $\eta = 2.7$, $r_0 = 0.1$ km.

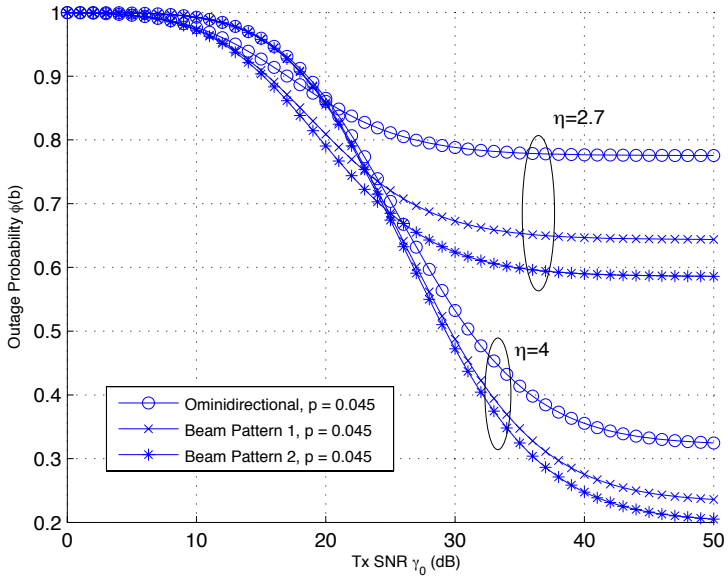

Figure 2.12: Outage probability vs. transmitted SNR γ_0 with (1, 5/7) convolutional coded 64-QAM in an urban area under slow fading, $\lambda_M = 20.0$ mobiles/km^2, $b = 13.5$ dB, $\sigma = 6$ dB, $\eta = 2.7$, $r_0 = 0.2$ km.

the interference problem should be worse in the urban area. Hence we can expect to get a larger improvement by applying directional antennas. This is indeed shown in the figures. We can see that directional antennas yields a larger gain over omnidirectional antenna when $\eta = 2.7$ compared with $\eta = 4$. This shows that the more serious the interference problem is, the more performance gain we can get from using directional antennas (as could be expected).

Finally in Fig. 2.12 we plot the outage probability versus the transmitted SNR $\gamma_0 = \frac{P_T f(\theta_0)}{N} = \frac{E_c f(\theta_0)}{N_0}$ for the turbo coded system in both the urban area and the obstructed environment. The distance between Tx and Rx is 0.2 km. Since we are plotting against the transmitted SNR, the effect of path loss on the signal power now comes to play. At high transmitted SNR, every mobile is transmitting with high power. The SINR is dominated by the interference power and is almost the same as the signal-to-interference ratio (SIR). As discussed earlier, we have higher interference power and thus worse performance in the urban area. However, at low transmitted SNR, it is a different story. The SINR now is dominated by the noise power and it is almost the same as the received SNR.

The received SNR in the urban area is higher than that in the obstructed area due to its smaller path loss exponent. This is why we can see the performance in the urban area to be better at low transmitted SNR. Note that this effect is not seen in Fig. 2.10 and 2.11 because they are both plotted against the received SNR, not the transmitted SNR. Hence the effect of path loss on the signal power from Tx can not be observed in those figures.

2.4 Outage Probability of a Fast Faded Link

In the previous section, the performance of the link between Tx and Rx under slow fading was analyzed. The performance is generally not good because in a slow fading channel, once the channel encounters severe fading, it will be stuck in the bad channel status for a long time and thus severely degrade the system performance. If Tx or Rx has higher mobility, the fading level will change more frequently, which is often regarded as fast fading. For channels that experience fading that is neither fast nor slow, the system performance should be in between the slow and the fast fading cases. This is why it is desirable for us to analyze the performance of the link between Tx and Rx under fast fading.

2.4.1 Outage Probability Analysis

In the fast fading case, the received signal power at Rx from Tx changes frequently during a packet duration. Denote the number of independent realizations in one packet duration by w. The value of w is large when fading changes fast. With channel coding applied, the performance of a communication link is determined by the average received power rather than the instantaneous received power due to the fact that coding can help recover the sporadic badly attenuated receptions of modulated symbols. Hence now it is P_0, the average received power at Rx from Tx in one packet duration, that determines the performance of the link. By the Central Limit Theorem, the average of these realizations P_0 tends to be Gaussian with mean $P_T f(\theta_0)\zeta_0$ and variance $\frac{(P_T f(\theta_0)\zeta_0)^2}{w^2}$. When w goes to infinity, the variance converges to 0 and the Gaussian pdf converges to $\delta(P_0 - P_T f(\theta_0)\zeta_0)$.

Hence if the channel experiences fast fading, we model the cdf of P_0 as

$$F_0(P_0|\zeta_0) = \int_0^\infty \delta(x - P_T f(\theta_0)\zeta_0)\ dx = u(P_0 - P_T f(\theta_0)\zeta_0), \tag{2.22}$$

where $\delta(\cdot)$ and $u(\cdot)$ denote the impulse and the step function respectively. Notice the appearance of the shadowing factor ζ_0 which should be constant for the whole packet.

The choice of the SINR threshold b now is different from the slow fading case. Unlike the slow fading case which has a constant SINR through the whole packet duration, now the SINR changes rapidly. In order to determine the value of b for a specific coded modulation scheme under fast fading, we should examine the performance of the coded modulation under fast fading. Again, we can apply our analyses in Chapter 3 and 5 to help us determine the SINR threshold value for different coded modulation schemes, which is demonstrated in Section 2.4.3.

To get the outage probability, we should substitute $F_0(\cdot)$ in (2.11) with (2.22). However there is a difficulty here. Note that in (2.11), we need to take the expectation of the outage probability with respect to the interference power $P_{i,j}$ from different interferers. Previously in slow fading case, $F_0(\cdot)$ in (2.3) is in exponential form and we can easily rewrite $F_0(\cdot)$ in (2.11) as the product of functions of $P_{i,j}$ only. This enables us to take the expectation with respect of $P_{i,j}$ separately which makes the analysis tractable. Unfortunately this is not the case here. Our $F_0(\cdot)$ now is a step function and we can no longer decompose it into a product of functions directly.

One way to solve this problem is to find a way to represent $F_0(P_0|\zeta_0)$ using exponential functions. This can be done by using the inverse Fourier transform formula

$$F_0(P_0|\zeta_0) = 1 - \text{rect}_{0,P_T f(\theta_0)\zeta_0}(P_0) = 1 - \int_{-\infty}^{\infty} \frac{1 - e^{-j2\pi f P_T f(\theta_0)\zeta_0}}{j2\pi f}\ e^{j2\pi f P_0} df, \tag{2.23}$$

where $\text{rect}_{u,v}(t) = 1$ if $t \in [u, v)$ and 0 otherwise. Substitute $F_0(\cdot)$ in (2.11) with (2.23) and follow the similar steps afterwards, we can obtain the outage probability for a fast

faded link as

$$\begin{aligned}\phi_{r_0}(b) &= 1-\frac{1}{\sqrt{2\pi}\sigma}\int_{-\infty}^{\infty}\frac{df}{j2\pi f} \\ &\quad\cdot\int_{-\infty}^{\infty}\left(1-e^{-j2\pi f P_T f(\theta_0)\ e^x}\right)\exp\left\{-\Lambda(j2\pi f b,x)\cdot r_0^2\cdot[\mathcal{A}_t\cdot\mathcal{A}_r]-\frac{b\ e^{-x}}{\gamma_c}-\frac{x^2}{2\sigma^2}\right\}dx.\end{aligned} \tag{2.24}$$

2.4.2 Numerical Computation Concerns

When we compute the outage probability in (2.24) numerically, the numerical analysis has the form

$$\begin{aligned}\phi_{r_0}(b) &\approx 1-\frac{1}{\sqrt{2\pi}\sigma}\sum_{n=-f_{max}}^{f_{max}}\frac{1}{j2\pi n}\cdot\sum_{m=-x_{max}}^{x_{max}}\left(1-e^{-j2\pi n\Delta f P_T f(\theta_0)e^{m\Delta x}}\right) \\ &\quad\cdot\exp\left\{-\Lambda(j2\pi n\Delta f b,m\Delta x)\cdot r_0^2\cdot[\mathcal{A}_t\cdot\mathcal{A}_r]-\frac{b\ e^{-m\Delta x}}{\gamma_c}-\frac{(m\Delta x)^2}{2\sigma^2}\right\}\Delta x.\end{aligned} \tag{2.25}$$

In (2.25) the inverse Fourier transform of rect$(\cdot)$ actually becomes a Fourier series. In order to get good approximation of rect$(\cdot)$ by the Fourier series, Δf needs to be chosen very small, and f_{max} very large. From our experience, it works well if $\frac{1}{\Delta f}$ is chosen to be twice the maximum possible value of the average received power $P_T f(\theta_0)e^{x_{max}\Delta x}$ (recall that $\zeta_0 = e^x$), and f_{max} chosen to be $\frac{1}{\Delta f}$. To cover a wide range of average received power, Δf has to be very small, and thus f_{max} very large. For instance, $f_{max} = 10^6$ is used for all of our numerical examples in the next section. Thus the numerical computation time of the outage probability under fast fading is 2×10^6 times the computation time of the slow fading case. The long computation time limits the application of our result here. This is the reason why we demonstrate most of our work in the later sections for the slow fading case only.

Another concern raised by the numerical evaluation of (2.24) using (2.25) is that the Fourier series approximation of $\text{rect}_{0,P_T f(\theta_0)\zeta_0}(P_0)$ is not close to 1 in the positive neighborhood of $P_0 = 0$. Basically the outage probability is computed through the

integration of the product of $\text{rect}_{0,P_T f(\theta_0)\zeta_0}(P_0)$ and the pdf of the interference power from 0 to ∞ (see (2.11)). Due to path loss, shadowing and Rayleigh fading, the chance of the interference power close to 0 is not small. Hence the approximation error of $\text{rect}_{0,P_T f(\theta_0)\zeta_0}(P_0)$ at the positive neighborhood of $P_0 = 0$ can introduce a significant error to the outage probability computation. The solution to this problem is to replace $\text{rect}_{0,P_T f(\theta_0)\zeta_0}(P_0)$ we used in (2.23)-(2.24) by $\text{rect}_{\alpha,P_T f(\theta_0)\zeta_0}(P_0)$ for some negative value α so we can ensure the value of the Fourier series approximation is close to 1 at the positive neighborhood of $P_0 = 0$. The numerical computation formula now becomes

$$\begin{aligned}\phi_{r_0}(b) \;\approx\; & 1 - \frac{1}{\sqrt{2\pi}\sigma} \sum_{n=-f_{max}}^{f_{max}} \frac{1}{j2\pi n} \cdot \sum_{m=-x_{max}}^{x_{max}} \left(e^{-j2\pi n \Delta f \alpha} - e^{-j2\pi n \Delta f P_T f(\theta_0) e^{m\Delta x}} \right) \\ & \cdot \exp\left\{ -\Lambda(j2\pi n\Delta f b, m\Delta x) \cdot r_0^2 \cdot [\mathcal{A}_t \cdot \mathcal{A}_r] - \frac{b\, e^{-m\Delta x}}{\gamma_c} - \frac{(m\Delta x)^2}{2\sigma^2} \right\} \Delta x. \end{aligned} \tag{2.26}$$

One last concern is the error introduced by the Fourier series approximation in the numerical calculation of the outage probability. While $\text{rect}_{\alpha,P_T f(\theta_0)\zeta_0}(P_0)$ is an aperiodic function, its Fourier series approximation $\widehat{\text{rect}}_{\alpha,P_T f(\theta_0)\zeta_0}(P_0)$is a periodic function of period $\frac{1}{\Delta f}$. The difference can be bounded by $u(P_0 - \frac{1}{\Delta f} + \alpha)$. From (2.23), we can see the Fourier series approximation error of $F_0(P_0|\zeta_0)$ is also bounded by

$$|F_0(P_0|\zeta_0) - \hat{F}_0(P_0|\zeta_0)| = |\text{rect}_{\alpha,P_T f(\theta_0)\zeta_0}(P_0) - \widehat{\text{rect}}_{\alpha,P_T f(\theta_0)\zeta_0}(P_0)| < u(P_0 - \frac{1}{\Delta f} + \alpha). \tag{2.27}$$

By (2.11), the error of the outage probability computation can then be bounded by

$$|\phi_{r_0}(b) - \hat{\phi}_{r_0}(b)| < E_{\boldsymbol{K_a},\boldsymbol{I_a},\boldsymbol{r_a},\boldsymbol{\zeta_a}} \left\{ \int_0^\infty \cdots \int_0^\infty u(b \sum_{i=1}^{L} \sum_{j=1}^{I_i} P_{i,j} + bN - \frac{1}{\Delta f} + \alpha) \cdot \prod_{i=1}^{L} \prod_{j=1}^{I_i} f(P_{i,j} \mid \zeta_{i,j})\, dP_{i,j} \right\}. \tag{2.28}$$

This bound again consists of a step function $u(\cdot)$ and it involves taking the expectation with respect to $\boldsymbol{K_a}, \boldsymbol{I_a}, \boldsymbol{r_a}, \boldsymbol{\zeta_a}$. The closed-form is untractable (otherwise we would not need the Fourier series approximation to compute the outage probability). By observation, we can see that if interference power $\sum_{i,j} P_{i,j}$ is large, the integral inside the

expectation should be large. Hence we can try to bound the error by considering an extreme realization of $\boldsymbol{K_a}, \boldsymbol{I_a}, \boldsymbol{r_a}, \boldsymbol{\zeta_a}$ which would cause a huge interference to Rx. For instance, if the mobile density $\lambda_M = 20.0$ (mobiles/km^2) and load $p = 0.05$, the probability of having as many as $\kappa = 20$ interference mobiles appear at distance $r_0 = 0.1$ km or less from Rx is 4.06×10^{-59} which can be computed through the pdf of POI($\lambda_M p\ r_0^2$) in Section 2.2. This realization is very unlikely to happen. We can make the case even more extreme by assuming all these κ interfering signals are not shadowed at all. As a result, the integral in (2.28) under this realization should be larger than that of most other realizations. We can use it as an approximate upper bound for (2.28). Note that the sum of κ exponentially distributed random variables is a chi-square random variable β of order 2κ. Assume the noise power N can be neglected under strong interference, we can obtain a closed-form expression for an approximate upper bound

$$|\phi_{r_0}(b) - \hat{\phi}_{r_0}(b)| \lesssim \int_{1/\Delta f}^{\infty} f_\beta(x)dx = e^{\frac{1}{\kappa P_T \Delta f}} \sum_{i=0}^{2\kappa-1} \frac{\left(\frac{1}{\kappa P_T \Delta f}\right)^i}{i!}. \tag{2.29}$$

As mentioned earlier, Δf is usually chosen very small to have good approximation. If we use $\Delta f = 5 \cdot 10^{-7}$ in all of our numerical experiments then the expression above is smaller than 10^{-6} for a wide range of P_T. Hence the numerical error of the outage probability in (2.26) is negligible and should not be an issue.

2.4.3 Numerical Examples

Let us consider the same beam patterns, the same BICM, and the turbo code used in Section 2.3.3. As mentioned earlier, we need to look at the performance of the BICM and the turbo code under fast Rayleigh fading to determine the threshold b. Using our analyses in Chapter 3 and 5, we plot the PER union bound of both coded modulation schemes under fast Rayleigh fading in Fig. 2.13. Again, assume a PER of 2×10^{-3} is the threshold of acceptable communication quality, then from the figure we can see that the threshold b should be 7.5 dB for the turbo coded system and 17 dB for BICM. The

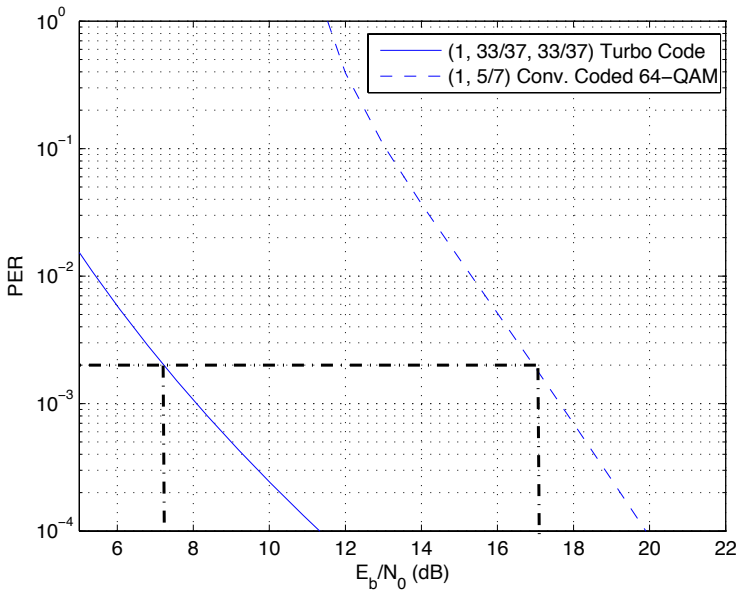

Figure 2.13: PER union bounds of (1, 33/37, 33/37) turbo code and bit-interleaved (1, 5/7) convolutional coded 64-QAM under fast Rayleigh fading

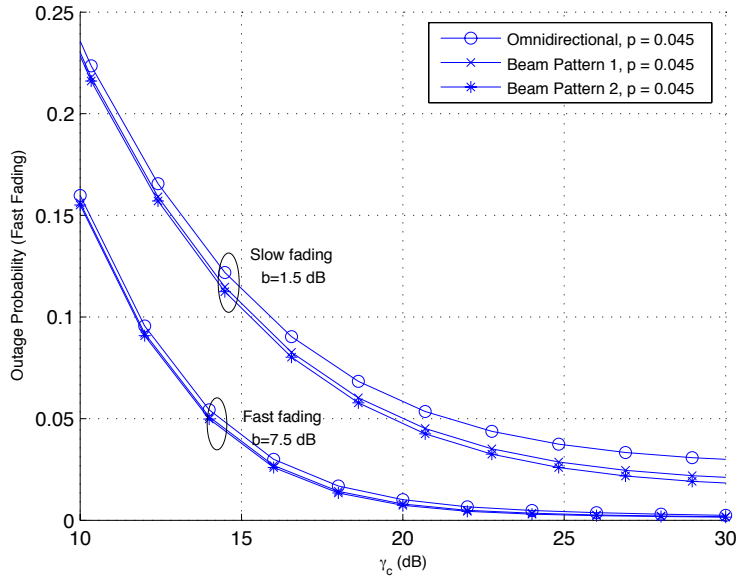

Figure 2.14: Outage probability vs. average received SNR γ_c with (1, 33/37, 33/37) turbo code in an obstructed environment under fast (and slow) fading, $\lambda_M = 20.0$ mobiles/km^2, $\sigma = 6$ dB, $\eta = 4$, $r_0 = 0.1$ km.

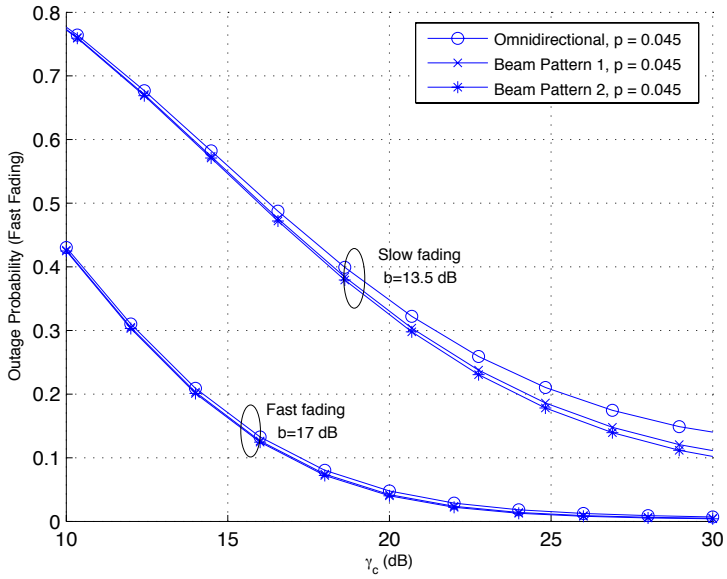

Figure 2.15: Outage probability vs. average received SNR γ_c with (1, 5/7) convolutional coded 64-QAM in an obstructed environment under fast (and slow) fading, $\lambda_M = 20.0$ mobiles/km^2, $\sigma = 6$ dB, $\eta = 4$, $r_0 = 0.1$ km.

outage probability of the two different coded modulation schemes are shown in Fig. 2.14 and 2.15. The slow fading curves from Section 2.3.3 are also plotted for comparison. We see that both the turbo coded system and BICM have much better performance under fast fading than that under slow fading. This is because now the channel does not get stuck in a bad channel status for a long time and thus the system performance is better. This indicates a higher mobile density can be allowed in the fast fading case. We also observe that the performance gain we get from directional antennas is not as big as the slow fading case. This is because the channel is not as critical as the slow fading case; even omnidirectional antennas work well. Thus there is not much room for improvement from directional antennas. One thing to note is the long computation time here. It takes around 5 hours for a Pentium 4 PC running at 2.8 GHz to generate each of the fast fading curves in Fig. 2.14 and 2.15.

2.5 Effect of Direction Estimation Error

In the previous analysis, we assumed Tx is always perfectly aligned to Rx. However, this assumption is not necessarily true in reality. It is always possible to have some amount of estimation error when Tx tries to estimate the direction to Rx. The existence of a direction estimation error has impact on the outage probability. In general the larger the beam width of a Tx beam pattern, the less sensitive the outage probability is to the direction estimation error. However, the less performance improvement is achievable by the directional antenna. To fully understand the effect of the direction estimation error on the system performance, it is desirable to analyze the outage probability given the existence of a direction estimation error. Here we derive the outage probability only for the slow fading case, which can be easily extended to the fast fading case following a similar approach to Section 2.4.

2.5.1 Outage Probability Analysis

In practice, there are many factors that can affect the accuracy of the direction estimation. For instances: the estimation algorithm used, the channel status, noise and interference, the MAC protocol, etc. It is very difficult to characterize the direction estimation error in a deterministic way. Hence, we model it as a random variable δ_t with some given pdf $f_t(\delta_t)$. We define $\phi_{r_0}(b \mid \delta_t)$ as the outage probability given an error of δ_t. From our previous analysis, we can derive the expression of $\phi_{r_0}(b \mid \delta_t)$

$$\phi_{r_0}(b \mid \delta_t) = 1 - \frac{1}{\sqrt{2\pi}\sigma} \int_{-\infty}^{\infty} \exp\left\{ -\Lambda(b,x) \cdot r_0^2 \cdot \mathcal{A}_t(\delta_t) - \frac{b\, e^{-x} f_T(\theta_0)}{\gamma_c f_T(\theta_0 + \delta_t)} - \frac{x^2}{2\sigma^2} \right\} dx, \quad (2.30)$$

where

$$\mathcal{A}_t(\delta_t) \triangleq \frac{1}{2\pi} \int_0^{2\pi} \left(\frac{f_T(\theta)}{f_T(\theta_0 + \delta_t)} \right)^{\frac{2}{\eta}} d\theta \quad (2.31)$$

denotes the AIF of the Tx beam pattern $f_T(\theta)$ given an error of δ_t. By taking the expectation of $\phi_{r_0}(b \mid \delta_t)$ with respect to $f_t(\delta_t)$ and we can obtain the outage probability

$$\phi_{r_0}(b) = 1 - \frac{1}{\sqrt{2\pi}\sigma} \int_0^{2\pi} f_t(\delta_t) d\delta_t \int_{-\infty}^{\infty} \exp\left\{ -\Lambda(b,x) \cdot r_0^2 \cdot \mathcal{A}_t(\delta_t) - \frac{b\ e^{-x} f_T(\theta_0)}{\gamma_c f_T(\theta_0 + \delta_t)} - \frac{x^2}{2\sigma^2} \right\} dx. \tag{2.32}$$

If Rx also has the ability of beam forming, then the direction estimation error δ_r at Rx also needs to be taken into account. Given $f_r(\delta_r)$, the pdf of δ_r, we can obtain the outage probability after some manipulation

$$\begin{aligned} \phi_{r_0}(b) \quad = \quad 1 - \frac{1}{\sqrt{2\pi}\sigma} \int_0^{2\pi} f_t(\delta_t) d\delta_t \int_0^{2\pi} f_r(\delta_r) d\delta_r \int_{-\infty}^{\infty} \exp\left\{ -\Lambda(b,x) \cdot r_0^2 \cdot [\mathcal{A}_t(\delta_t) \cdot \mathcal{A}_r(\delta_r)] - \frac{x^2}{2\sigma^2} \right. \\ \left. - \frac{b\ e^{-x} f_T(\theta_0) f_R(\theta_0)}{\gamma_c f_T(\theta_0 + \delta_r) f_R(\theta_0 + \delta_r)} \right\} dx, \end{aligned} \tag{2.33}$$

where

$$\mathcal{A}_r(\delta_r) = \triangleq \frac{1}{2\pi} \int_0^{2\pi} \left(\frac{f_R(\theta)}{f_R(\theta_0 + \delta_r)} \right)^{\frac{2}{\eta}} d\theta \tag{2.34}$$

denotes the AIF of the Rx beam pattern $f_R(\theta)$ given an error of δ_r.

2.5.2 Numerical Examples

As mentioned earlier, the outage probability of the fast fading case has very high complexity. So we limit ourself in this section only to the slow fading case to explore the effect of the distance estimation error on the system performance. Assume that only Tx has the beam forming ability, and the direction estimation error δ_t is uniformly distributed in the interval $[-\delta_{max}, \delta_{max}]$ as the case in the MAC protocols for IEEE 802.11 with directional antennas [18,19], which has a fixed number B of beam directions. The maximum error δ_{max} would be $\frac{180^o}{B}$.

In Fig. 2.16 and 2.17 we show the outage probability of the two beam patterns (defined in Section 2.3.3) in an obstructed environment for various values of δ_{max}. We see that beam pattern 1 is less sensitive to direction estimation error since it has a wider

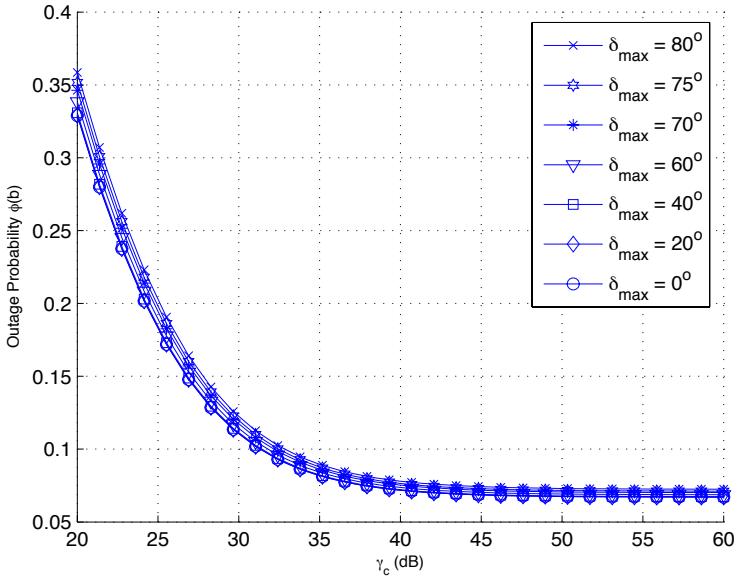

Figure 2.16: Outage probability vs. γ_c with direction estimation error using beam pattern 1 (AIF = 0.6569) and (1, 5/7) convolutional coded 64-QAM in an obstructed environment under slow fading, $\lambda_M = 20.0$ mobiles/km^2, $b = 13.5$ dB, $\sigma = 6$ dB, $\eta = 4$, $p = 0.045$, $r_0 = 0.1$ km.

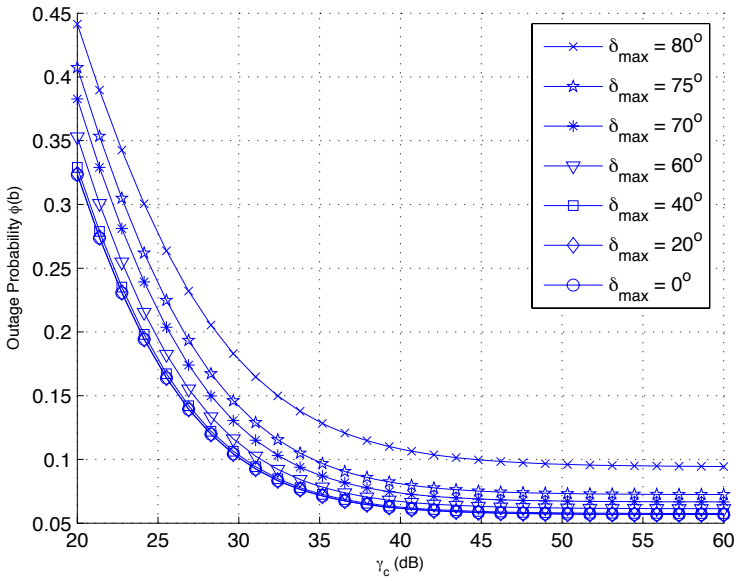

Figure 2.17: Outage probability vs. γ_c with direction estimation error using beam pattern 2 (AIF = 0.5511) and (1, 5/7) convolutional coded 64-QAM in an obstructed environment under slow fading, $\lambda_M = 20.0$ mobiles/km^2, $b = 13.5$ dB, $\sigma = 6$ dB, $\eta = 4$, $p = 0.045$, $r_0 = 0.1$ km.

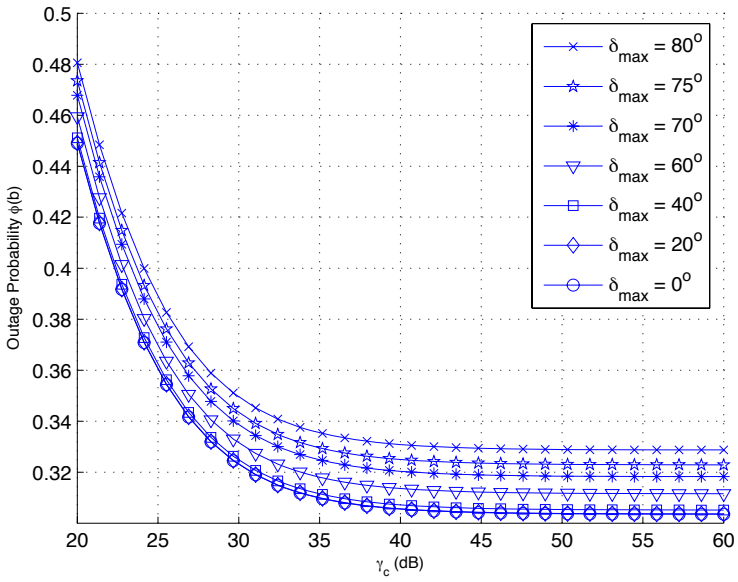

Figure 2.18: Outage probability vs. γ_c with direction estimation error using beam pattern 1 (AIF = 0.5699) and (1, 5/7) convolutional coded 64-QAM in an urban area under slow fading, $\lambda_M = 20.0$ mobiles/km^2, $b = 13.5$ dB, $\sigma = 6$ dB, $\eta = 2.7$, $p = 0.045$, $r_0 = 0.1$ km.

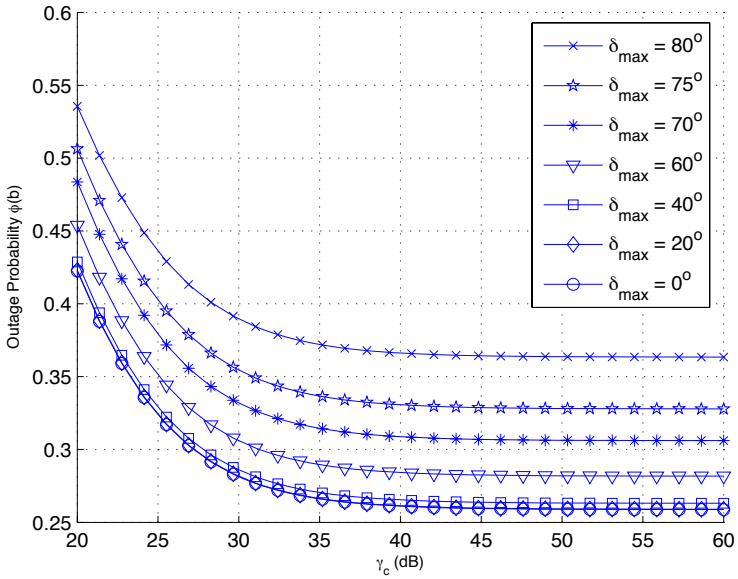

Figure 2.19: Outage probability vs. γ_c with direction estimation error using beam pattern 2 (AIF = 0.4545) and (1, 5/7) convolutional coded 64-QAM in an urban area under slow fading, $\lambda_M = 20.0$ mobiles/km^2, $b = 13.5$ dB, $\sigma = 6$ dB, $\eta = 2.7$, $p = 0.045$, $r_0 = 0.1$ km.

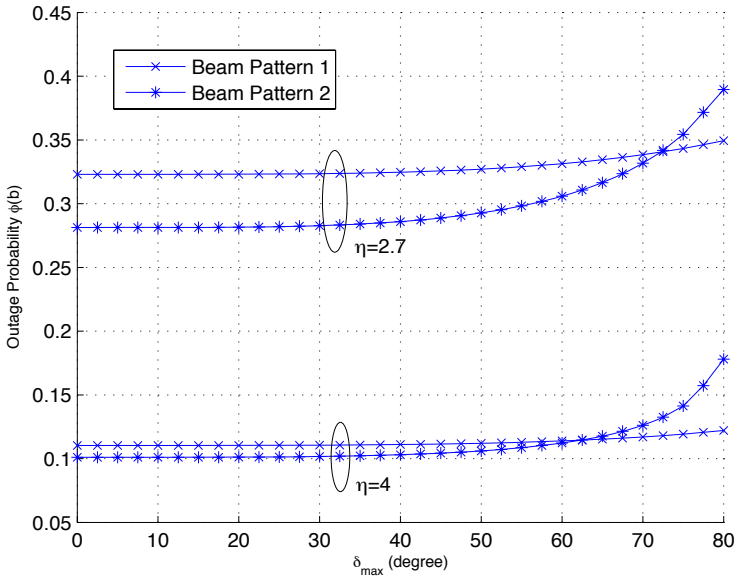

Figure 2.20: Outage probability vs. δ_{max} with fixed γ_c using (1, 5/7) convolutional coded 64-QAM under slow fading, $\gamma_c = 30$ dB, $\lambda_M = 20.0$ mobiles/km^2, $b = 13.5$ dB, $\sigma = 6$ dB, $\eta = 2.7$, $p = 0.045$, $r_0 = 0.1$ km.

mainlobe than beam pattern 2. From Fig. 2.7 we see the mainlobe width of beam pattern 2 is roughly 120^o. When δ_{max} is larger than 60^o, it is possible for Rx to be totally off from the coverage of the mainlobe, which will significantly degrade the system performance. This is why the outage probability of beam pattern 2 starts to increase abruptly after δ_{max} exceeds one half of the mainbeam width (60^o) by some amount of tolerance (15^o). From the figure we can conclude for the MAC protocols in [18,19], beam pattern 2 still works fine if the number of beam directions B is greater than 3, but the performance starts to degrade severely when B goes below 3.

In Fig. 2.18 and 2.19 we show the outage probability of the two beam patterns in an urban area. Since the interference power is less attenuated in the urban area, any direction estimation error that affects the received signal power from Tx can cause the SINR to be attenuated severely. As a result, we can see the outage probability is more sensitive to the direction estimation error for both beam patterns. But still, the wider beam pattern 1 has a better performance than beam pattern 2. We also observe from Fig. 2.19 that the outage probability starts to increase abruptly right before δ_{max} reaches one

half of the mainlobe width of beam pattern 2. The previous tolerance of 15^o no longer exists because the system performance is extremely sensitive to the direction estimation error in the urban area.

In Fig. 2.20 we plot the outage probability versus δ_{max} using both beam patterns with γ_c fixed at 30 dB. We see the outage probability curves of beam pattern 1 and 2 crossover in the figure. At small δ_{max}, beam pattern 2 performs better because of its smaller beam width. However, once δ_{max} exceeds the beam width of beam pattern 2, the outage probability begins to increase rapidly. On the other hand, beam pattern 1 is not that sensitive to δ_{max} due to its wider beam width. As a result, beam pattern 1 outperforms beam pattern 2 at large δ_{max}. Through our analysis, we can determine which beam pattern to use given the largest possible direction estimation error δ_{max}.

2.6 Power Control

From the numerical examples in Section 2.3, we can see that the average received SNR at Rx, γ_c, has to be large to achieve small outage probability. This is mainly because the transmitted signal not only experiences fading, but also power loss due to path loss and shadowing. In order to combat power loss in wireless communications, power control schemes are often used. In this section, we explore the effect of power control on the system performance of wireless networks with directional antennas. While the fading level changes rapidly from packet to packet, the shadowing effect generally lasts longer and does not change frequently. The received power at Rx could be small for a long time if the communication link between Tx and Rx is shadowed by some obstacles. Hence, it is easier to utilize power control to combat shadowing than fading. In this section, we will consider the power control that combats only the shadowing effect. To simplify the analysis, we assume there is no direction estimation error. Again we derive the outage probability only for the slow fading case. The result can be extended to the fast fading case following the steps in Section 2.4. We first look into discrete power control and then continuous power control.

2.6.1 Outage Probability under Discrete Power Control

A discrete power control scheme is characterized by two vectors $\mathbf{V} = (v_0, v_1, \cdots, v_{M-1})$ and $\mathbf{G} = (g_0, g_1, \cdots, g_{M-1})$, where $0 = v_0 < v_1 < \cdots < v_{M-1} < v_M = \infty$ partitions the interval $[0, \infty)$ in to M subintervals. When the shadowing factor ζ_0 between Tx and Rx falls in the subinterval $[v_m, v_{m+1})$, Tx will increase the transmitting power by a gain of g_m to $P_T g_m$. Denote the gain corresponds to ζ_0 by $g(\zeta_0)$, then

$$g(\zeta_0) = g_m, \text{ if } \zeta_0 \in [v_m, v_{m+1}). \tag{2.35}$$

Note that here we assume Rx has the ability to estimate the value of ζ_0 and send the information back to Tx. From the pdf of ζ_0 in (2.1), we can derive $\mu_{r_0}(m)$, the probability of Tx transmitting with power $P_T g_m$, by

$$\mu_{r_0}(m) = \int_{v_m}^{v_{m+1}} \frac{1}{\sqrt{2\pi}\sigma\zeta_0} \, e^{-\frac{1}{2}\frac{\left(\log\zeta_0 - \log(K r_0^{-\eta})\right)^2}{\sigma^2}} \, d\zeta_0, \tag{2.36}$$

which depends on the distance r_0 between Tx and Rx. The distribution of r_0 is determined by the MAC protocol and the network protocol. Assume that it has a pdf $f(r_0)$. Note that $f(r_0)$ here is not necessarily the same as the $f_a(r_{i,j})$ in (2.7), the pdf of the distance $r_{i,j}$ between an interferer and Rx. This is because the distance between an interferer and Rx is generally uncontrolled and thus $f_a(r_{i,j})$ is solely determined by the Poisson point process described in Section 2.2. Given $f(r_0)$, we can obtain the probability of any interferer transmitting with power control gain g_m as

$$\mu_(m) = E_{r_0}\{\mu_{r_0}(m)\} = \int_0^{r_{max}} f(r_0)\mu_{r_0}(m) \, dr_0. \tag{2.37}$$

where r_{max} denotes the largest possible distance between any Tx-Rx pair.

Let us first analyze the outage probability for the simplified beam pattern defined in Section 2.3.1 which has L beams. First consider the interfering mobiles within a disc of radius a centered at Rx. In the case of no power control, all active mobiles transmit with

the same power P_T. Now with power control, we need to classify the mobiles in to M different groups each with different transmitting power. Define $\boldsymbol{K_a^m} = (K_1^m, K_2^m, \cdots, K_L^m)$ where K_i^m denotes the number of interfering mobiles pointing at Rx with beam i with transmitting power $P_T f_i g_m$. Similar to the case in Section 2.3.1, K_i^m is also Poisson distributed with distribution POI($\frac{\lambda_M a^2 \delta_i \mu(m)}{2\pi}$). Also define $\boldsymbol{I_a^m} = (I_1^m, I_2^m, \cdots, I_L^m)$ where I_i^m denotes the number of mobiles among the K_i^m mobiles that actually transmit packets and interfere with Rx, which is of distribution BIN(K_i^m, p). We further define the associated vectors $\boldsymbol{r_a^m}$, $\boldsymbol{\zeta_a^m}$ similarly to $\boldsymbol{r_a}$, $\boldsymbol{\zeta_a}$ of Section 2.3.1. Now (2.11) can be rewritten as

$$\phi_{r_0}(b, a \mid \boldsymbol{K_a^0}, \cdots, \boldsymbol{K_a^{M-1}}, \boldsymbol{I_a^0}, \cdots, \boldsymbol{I_a^{M-1}}, \boldsymbol{r_a^0}, \cdots, \boldsymbol{r_a^{M-1}}, \boldsymbol{\zeta_a^0} \cdots, \boldsymbol{\zeta_a^{M-1}}, \zeta_0)$$

$$= 1 - e^{-\frac{bN}{P_T g(\zeta_0) f_1 \zeta_0}} \prod_{i=1}^{L} \left[\prod_{j_0=1}^{I_i^0} \frac{1}{1 + \frac{b g_0 f_i \zeta_{i,j_0}}{g(\zeta_0) f_1 \zeta_0}} \right] \left[\prod_{j_1=1}^{I_i^1} \frac{1}{1 + \frac{b g_1 f_i \zeta_{i,j_1}}{g(\zeta_0) f_1 \zeta_0}} \right] \cdots \left[\prod_{j_{M-1}=1}^{I_i^{M-1}} \frac{1}{1 + \frac{b g_{M-1} f_i \zeta_{i,j_{M-1}}}{g(\zeta_0) f_1 \zeta_0}} \right]. \tag{2.38}$$

By averaging over $\boldsymbol{r_a^i}, \boldsymbol{\zeta_a^i}, \boldsymbol{K_a^i}, \boldsymbol{I_a^i}$ step by step as we did in Section 2.3.1, we have

$$\phi_{r_0}(b, a \mid \zeta_0) = 1 - \exp\left\{ \sum_{m=0}^{M-1} \sum_{i=1}^{L} \frac{\lambda_M \ a^2 \ \delta_i \ \mu(m) \ p}{2\pi} \cdot \left[I_a(x, \frac{g_m f_i}{g(\zeta_0) f_1}) - 1 \right] - \frac{bK}{g(\zeta_0)\zeta_0 \gamma_c} \right\}. \tag{2.39}$$

Note that we have not taken the average over ζ_0 yet. As a goes to ∞, we obtain

$$\phi_{r_0}(b \mid \zeta_0) = 1 - \exp\left\{ -\Lambda(b, x) \cdot r_0^2 \cdot g(\zeta_0)^{-\frac{2}{\eta}} \cdot \left[\sum_{m=0}^{M-1} \mu(m) g_m^{\frac{2}{\eta}} \right] \cdot \left[\sum_{i=1}^{L} \frac{\delta_i}{2\pi} \left(\frac{f_i}{f_1} \right)^{\frac{2}{\eta}} \right] - \frac{bK}{g(\zeta_0)\zeta_0 \gamma_c} \right\}. \tag{2.40}$$

Now take the limit as L goes to ∞ and then take the expectation with respect to ζ_0, we have the final form of the outage probability with arbitrary beam pattern under the discrete power control $\{\mathbf{V}, \mathbf{G}\}$

$$\phi_{r_0}(b) = 1 - \frac{1}{\sqrt{2\pi}\sigma} \sum_{m=0}^{M-1} \int_{\log v_m - c}^{\log v_{m+1} - c} \exp\left\{ -\Lambda(b, x) \cdot r_0^2 \cdot g_m^{-2/\eta} \cdot \overline{g^{2/\eta}} \cdot [\ \mathcal{A}_t \cdot \mathcal{A}_r] - \frac{\overline{g} \ b \ e^{-x}}{g_m \gamma_c} - \frac{x^2}{2\sigma^2} \right\} dx, \tag{2.41}$$

where $c = \log(Kr_0^{-\eta})$ and

$$\overline{g^\alpha} = \sum_{m'=0}^{M-1} \mu(m') g_{m'}^\alpha. \tag{2.42}$$

2.6.2 Outage Probability under Continuous Power Control

A continuous power control scheme is defined by a continuous function $G(\zeta_0)$, $\zeta_0 \in [0, \infty)$, which is the transmitting power gain given that the communication link is experiencing a shadowing level ζ_0. We can generalize the result of discrete power control to continuous power control case by letting M go to ∞. Define $\Delta_m = \log v_{m+1} - \log v_m$, we have $\lim_{M\to\infty} \Delta_m = 0$ and $\lim_{M\to\infty} g(\zeta_0) = G(\zeta_0)$. As M goes to ∞, we can derive the outage probability under continuous power control from (2.41)

$$\begin{aligned}
&\lim_{M\to\infty} \phi_{r_0}(b) \\
= \;& 1 - \frac{1}{\sqrt{2\pi}\sigma} \sum_{m=0}^{M-1} \exp\left\{ -\Lambda(b, \log v_m - c) \cdot r_0^2 \cdot g_m^{-2/\eta} \cdot \overline{g^{2/\eta}} \cdot [\, \mathcal{A}_t \cdot \mathcal{A}_r] - \frac{\overline{g}\; b\; e^{-(\log v_m - c)}}{g_m \gamma_c} \right. \\
& \qquad \left. - \frac{(\log v_m - c)^2}{2\sigma^2} \right\} \cdot \Delta_m \\
= \;& 1 - \frac{1}{\sqrt{2\pi}\sigma} \int_{-\infty}^{\infty} \exp\left\{ -\Lambda(b, x) \cdot r_0^2 \cdot G(Kr_0^{-\eta} e^x)^{-\frac{2}{\eta}} \cdot \overline{G^{2/\eta}} \cdot [\, \mathcal{A}_t \cdot \mathcal{A}_r] - \frac{\overline{G}\; b\; e^{-x}}{G(Kr_0^{-\eta} e^x)\gamma_c} \right. \\
& \qquad \left. - \frac{x^2}{2\sigma^2} \right\} dx,
\end{aligned} \tag{2.43}$$

where

$$\overline{G^\alpha} \triangleq \int_0^{r_{max}} f(r_0)\; dr_0 \int_0^\infty \frac{[G(\zeta_0)]^\alpha}{\sqrt{2\pi}\sigma\zeta_0}\; e^{-\frac{1}{2}\frac{\left(\log\zeta_0 - \log(Kr_0^{-\eta})\right)^2}{\sigma^2}} d\zeta_0. \tag{2.44}$$

In the case of eliminating the shadowing effect completely, $G(\zeta_0)$ can be chosen as

$$G(\zeta_0) = \zeta_0^{-1}. \tag{2.45}$$

As a result, $\overline{G^\alpha}$ becomes

$$\begin{aligned}
\overline{G^\alpha} &= \int_0^{r_{max}} f(r_0)\ dr_0 \int_0^{\infty} \frac{\zeta_0^{-\alpha}}{\sqrt{2\pi}\sigma\zeta_0}\ e^{-\frac{1}{2}\frac{\left(\log\zeta_0 - \log(Kr_0^{-\eta})\right)^2}{\sigma^2}} d\zeta_0 \\
&= \int_0^{r_{max}} f(r_0)\ dr_0 \int_{-\infty}^{\infty} \frac{(Kr_0^{-\eta}e^x)^{-\alpha}}{\sqrt{2\pi}\sigma}\ e^{-\frac{x^2}{2\sigma^2}} dx \\
&= K^{-\alpha}\ e^{\sigma^2\alpha^2/2} \int_0^{r_{max}} f(r_0)\ r_0^{\eta\alpha}\ dr_0 \\
&= K^{-\alpha}\ \overline{r_0^{\eta\alpha}}\ \ e^{\sigma^2\alpha^2/2},
\end{aligned} \tag{2.46}$$

where

$$\overline{r_0^{\eta\alpha}} = \int_0^{r_{max}} f(r_0)\ r_0^{\eta\alpha}\ dr_0. \tag{2.47}$$

Hence the outage probability under perfect power control is

$$\phi_{r_0}(b) = 1 - \exp\left\{-\lambda_M\ p\ \overline{r_0^2}\ b^{\frac{2}{\eta}}\ e^{\frac{4\sigma^2}{\eta^2}}\ \frac{2\pi}{\eta}\ \csc\frac{2\pi}{\eta}\cdot[\ \mathcal{A}_t\cdot\mathcal{A}_r] - \frac{b\ \overline{r_0^\eta}\ e^{\sigma^2/2}}{r_0^\eta\ \gamma_c} - \frac{x^2}{2\sigma^2}\right\}. \tag{2.48}$$

2.6.3 Numerical Examples

Consider the beam pattern 2 with the same setup as the urban area case in Section 2.3.3. We apply our work to find the optimal discrete power control $\{\mathbf{V}, \mathbf{G}\}$ that minimizes the outage probability of the wireless network. In order to find the global optimum of the outage probability in (2.41), we use the Hide-and-Seek algorithm in [23] which is a type of simulated annealing algorithm. The method of simulated annealing is a technique that is very effective for global optimization problems with a large number of parameters, which is exactly what we need to find the optimal power control $\{\mathbf{V}, \mathbf{G}\}$.

We limit the peak power gain to be less than 10 dB, i.e., $g_m < 10$ for all m. This reduces the size of the feasible region of $\{\mathbf{V}, \mathbf{G}\}$ which can speed up the optimization process. It also reduces the chance of Hide-and Seek getting stuck at a local optimum. As a simple approximation, we assume all Tx-Rx pairs in the network have the same $r_0 = 0.1$ km. The optimal 2, 4 and 8-level power control schemes for each γ_c are searched

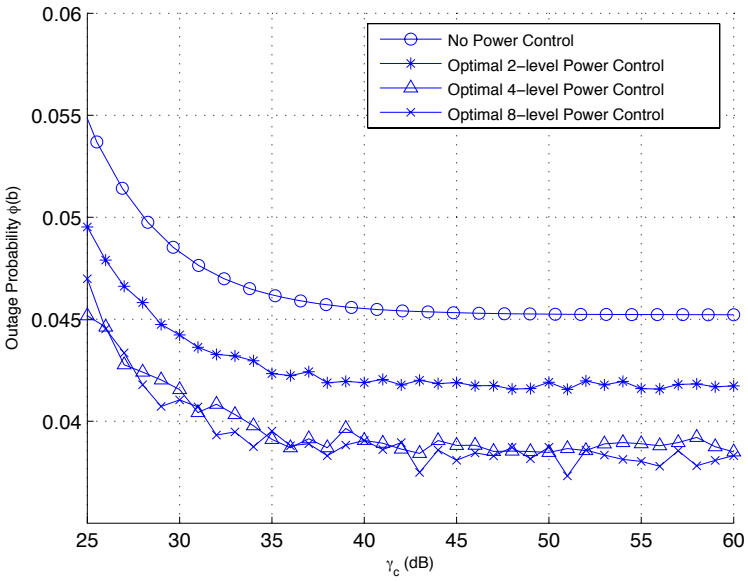

Figure 2.21: Outage probability vs. γ_c using beam pattern 2 (AIF = 0.4545) and (1, 33/37, 33/37) turbo code with optimal power control in an urban area under slow fading, $\lambda_M = 20.0$ mobiles/km^2, $b = 1.5$ dB, $\sigma = 6$ dB, $\eta = 2.7$, $p = 0.045$, $r_0 = 0.1$ km.

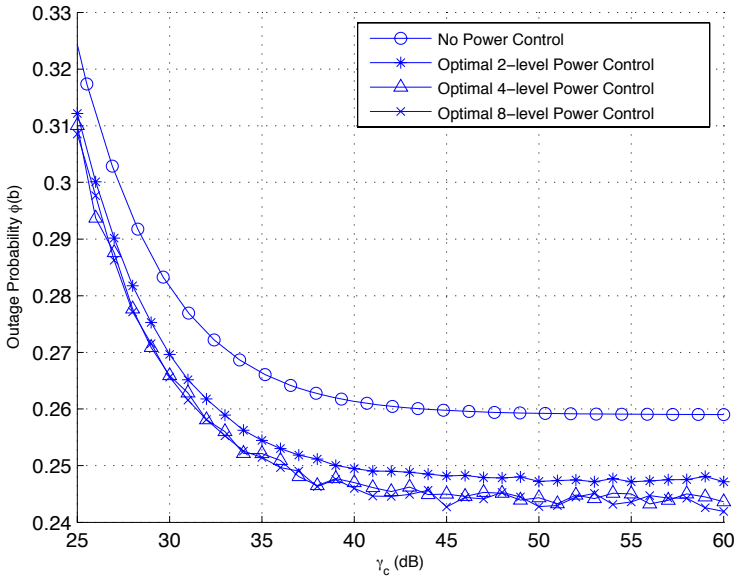

Figure 2.22: Outage probability vs. γ_c using beam pattern 2 (AIF = 0.4545) and (1, 5/7) convolutional coded 64-QAM with optimal power control in an urban area under slow fading, $\lambda_M = 20.0$ mobiles/km^2, $b = 13.5$ dB, $\sigma = 6$ dB, $\eta = 2.7$, $p = 0.045$, $r_0 = 0.1$ km.

though the Hide-and-Seek algorithm and the resulting outage probability is plotted in Fig. 2.21 and 2.22 for turbo coded system and BICM respectively. We see that the power control schemes found by Hide-and-Seek indeed improve the system performance, and the performance converges as the number of power level increases. We also observe that the optimal power control reduces the outage probability by roughly 16% for the turbo coded system while only around 7% for the BICM system. This suggests that power control should be applied when a strong code is used in order to get the most out of the code.

2.7 Application to System Design Optimization

In this section, we want to show the effectiveness of our analysis on the system design optimization. Two problems are considered here. One is to find the optimal mobile density to maximize the system throughput, and the other one is to find the optimal code rate for the channel coding used to optimize the link throughput between Tx and Rx.

2.7.1 Optimal Mobile Density for System Throughput

The system throughput of a wireless network is defined as the average number of successfully transmitted information bits per unit area per symbol duration per dimension (of signal space). It can be approximated by

$$S(b) \approx \frac{\lambda_M p}{\pi} \cdot \left(1 - \int_0^{r_{max}} f(r_0)\ \phi_{r_0}(b)\ dr_0\right) \cdot R \quad \left(\frac{\text{bits}}{\text{unit area} \cdot \text{sec} \cdot \text{Hz}}\right), \tag{2.49}$$

where $\frac{\lambda_M p}{\pi}$ accounts for the average number of simultaneous transmissions per unit area (1/unit area), $\left(1 - \int_0^{r_{max}} f(r_0)\ \phi_{r_0}(b)\ dr_0\right)$ is the probability of successful transmission, and R is the rate of the coded modulation used (bits/sec/Hz). We said (2.49) is an approximation because it assumes the successful transmissions of different mobiles are independent events which is not true in reality since transmitting mobiles interfere with

each other. Also recall that $f(r_0)$ denotes the pdf of the distance r_0 between Tx and Rx which is determined by the MAC protocol and the network protocol. Since the values of r_0 of different Tx-Rx pairs in a network are not necessarily the same, we need to take the expectation of $\phi_{r_0}(b)$ with respect to r_0 when computing the system throughput.

The system throughput of a wireless network is affected by the mobile density of the network. When the density is high, the interference problem becomes more serious and thus the outage probability increases. This will affect the system throughput approximation in (2.49). On the other hand, the outage probability is smaller if the density is low, but since not many mobiles are transmitting, this might cause the network resources (bandwidth) to be wasted without producing much system throughput. Our outage probability analysis can be used to find the optimal mobile density for a wireless network. We consider two different $f(r_0)$. The first case is that all Tx-Rx pairs in the network have the same distance between the two mobiles. Hence, $f(r_0) = \delta(r_0 - c)$ where c is a constant. From 2.49, the system throughput is approximately

$$S_1(b) \approx \frac{\lambda_M p}{\pi} \cdot (1 - \phi_c(b)) \cdot R, \tag{2.50}$$

where $\phi_c(b)$ can be computed through (2.21).

On the other hand, if a mobile is allowed to transmit signals to any mobile within a distance of r_{max}, then $f(r_0) = \frac{2r_0}{r_{max}^2}$. Substitute $\phi_{r_0}(b)$ in (2.49) by (2.21). After some manipulations, we can obtain the system throughput approximation as

$$S_2(b) \approx \frac{\lambda_M p\ R}{\sqrt{2\pi^3}\ \sigma} \int_{-\infty}^{\infty} \frac{1 - \exp\left\{-\Lambda(b,x) \cdot r_{max}^2 \cdot [\mathcal{A}_t \cdot \mathcal{A}_r]\right\}}{-\Lambda(b,x) \cdot [\mathcal{A}_t \cdot \mathcal{A}_r]} \cdot \exp\left\{-\frac{b\ e^{-x}}{\gamma_c} - \frac{x^2}{2\sigma^2}\right\} dx. \tag{2.51}$$

Consider the same setup as in Section 2.3.3. The rate of BICM is $R = 1.5$ (bits/sec/Hz) and that of turbo code is $R = 0.33$ (bits/sec/Hz). We first consider the system throughput $S_1(b)$ for the case that the distance between Tx and Rx is fixed at $r_0 = 0.1$ km for all Tx-Rx pairs. We plot the system throughput approximation $S_1(b)$ versus λ_M for $\eta = 4$ and $\eta = 2.7$ in Fig. 2.23-2.24. In both figures, we see that the system throughput of BICM is

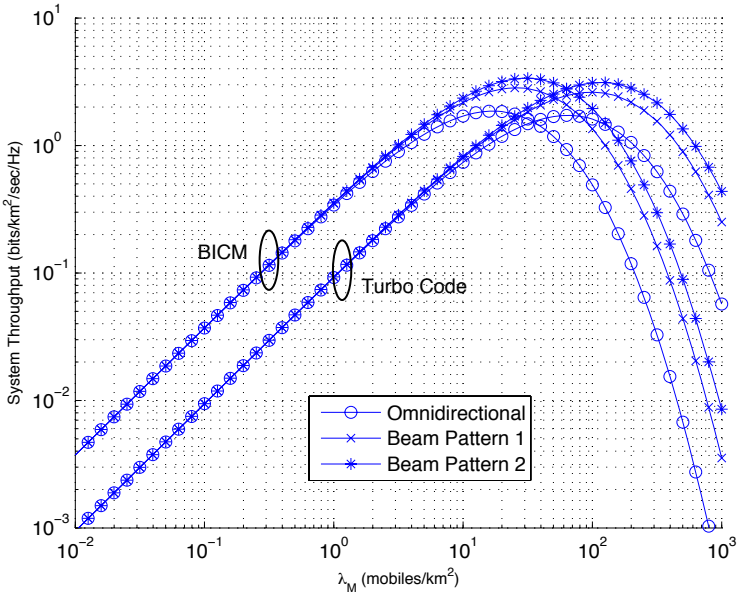

Figure 2.23: System throughput $S_1(b)$ vs. λ_M with $r_0 = c = 0.1$ km in an obstructed environment under slow fading, $\gamma_c = 25$ dB, $\sigma = 6$ dB, $\eta = 4$, $p = 0.9$.

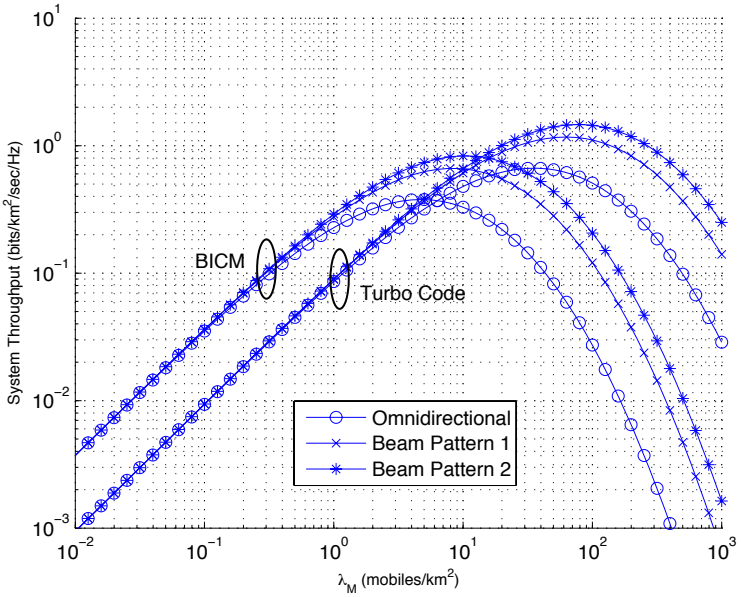

Figure 2.24: System throughput $S_1(b)$ vs. λ_M with $r_0 = c = 0.1$ km in an urban area under slow fading, $\gamma_c = 25$ dB, $\sigma = 6$ dB, $\eta = 2.7$, $p = 0.9$.

higher than the turbo coded system at small λ_M. This is because the interference problem is not large at small λ_M and thus BICM can maintain relative small outage probability. Under such circumstances, the higher bandwidth efficiency of BICM compared to the turbo coded system results in the larger system throughput of BICM. However, when λ_M becomes large, the interference problem causes BICM to have a very large outage probability; it is so large that even the high bandwidth efficiency of BICM can not make up the loss of the system throughput. As a result, the turbo coded system starts to have a higher system throughput than BICM. In any case, we can see that there exists an optimal mobile density for each setup. Beam pattern 2 again has higher optimal throughput than beam pattern 1 and omnidirectional antenna in all cases, and the turbo coded system has higher optimal mobile density than BICM. We also observe that the optimal mobile density in an urban area is smaller than the obstructed environment due to the more serious interference problem.

In Fig. 2.25-2.26 we plot the system throughput approximation $S_2(b)$ versus λ_M where r_0 is no longer fixed and $r_{max} = 1$ km. We see that the system throughput converges as λ_M increases. The asymptotic system throughput when λ_M and γ_c are both large can be derived as

$$\lim_{\substack{\gamma_c \to \infty \\ \lambda_M \to \infty}} S_2(b) = \frac{R}{\frac{2\pi^2}{\eta} \cdot \csc(\frac{2\pi}{\eta}) \cdot b^{2/\eta} \cdot [\mathcal{A}_t \cdot \mathcal{A}_r]}. \tag{2.52}$$

We also observe that the turbo coded system is not guaranteed to have a higher throughput than BICM at large λ_M. It all depends on whether the turbo coded system or BICM has the larger value of $\frac{R}{b^{2/\eta}}$. This is the reason why the turbo coded system fails to beat BICM at all values of λ_M in Fig. 2.25 because it has a smaller $\frac{R}{b^{2/\eta}}$ than that of BICM at $\eta = 4$. On the other hand, for $\eta = 2.7$ in Fig. 2.26, the turbo coded system has a larger $\frac{R}{b^{2/\eta}}$ and thus a higher system throughput than BICM at large λ_M.

In Fig. 2.27, we vary the value of r_{max} according to the value of λ_M. For a smaller λ_M, there are less mobiles in the network and we should allow a larger maximum hop distance r_{max}. Here we plot the system throughput of the turbo coded system in an obstructed environment under slow fading with $r_{max}(\lambda_M) = \min\{100, 1 + 9/\lambda_M\}$ km.

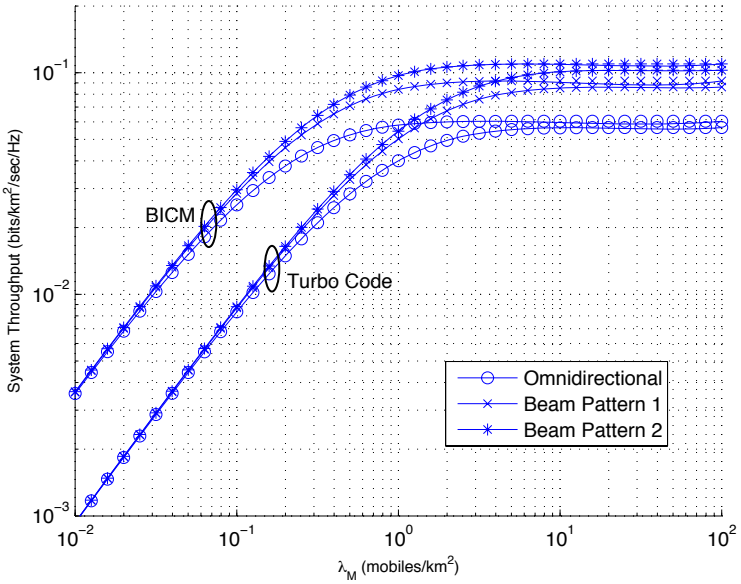

Figure 2.25: System throughput $S_2(b)$ vs. λ_M with $r_{max} = 1$ km in an obstructed environment under slow fading, $\gamma_c = 25$ dB, $\sigma = 6$ dB, $\eta = 4$, $p = 0.9$.

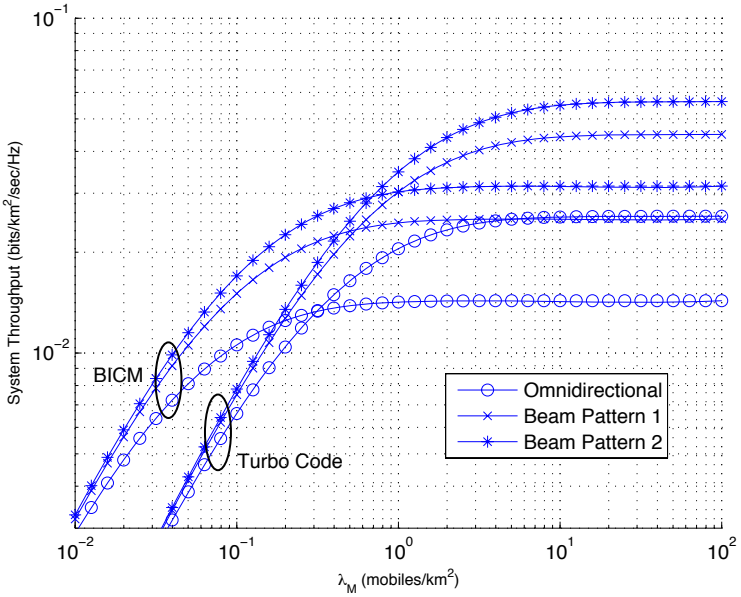

Figure 2.26: System throughput $S_2(b)$ vs. λ_M with $r_{max} = 1$ km in an obstructed environment under slow fading, $\gamma_c = 25$ dB, $\sigma = 6$ dB, $\eta = 2.7$, $p = 0.9$.

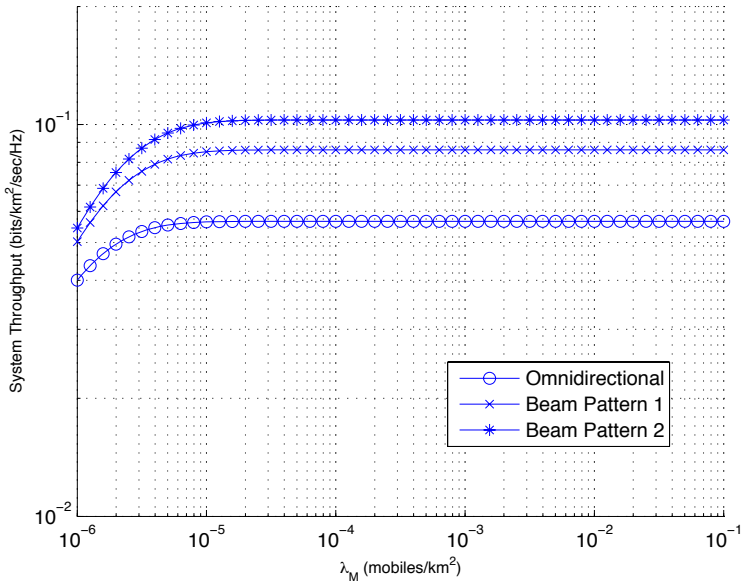

Figure 2.27: System throughput $S_2(b)$ vs. λ_M with $r_{max} = \min\{100, 1 + 9/\lambda_M\}$ km in an obstructed environment under slow fading, $\gamma_c = 25$ dB, $\sigma = 6$ dB, $\eta = 4$, $p = 0.9$.

Compare with Fig. 2.25 and we see that the system throughput at small λ_M is indeed improved. On the other hand, the system throughput at large λ_M remains almost the same, this is because the asymptotic system throughput in (2.52) does not depend on r_{max} and thus changing r_{max} has little affect on the system throughput.

2.7.2 Optimal Code Rate for Link Throughput

The throughput of the link between Tx and Rx is dependent on the code rate of the channel coding used. If the code rate is high, although more information is sent for each channel use, the packet error probability will be higher which might reduce the link throughput. On the other hand, a lower code rate sends out less information for each channel use, but it might be compensated by the low packet error probability. We are interested in finding the optimal code rate to maximize the link throughput.

Using the random coding analysis in [21], $\overline{P_e(\gamma)}$, the packet error probability averaged over all length n codes of code rate R using binary input in an AWGN channel at SNR

γ is bounded by

$$\overline{P_e(\gamma)} < 2^{-n(R_0-R)} = 2^{-n(1-\log_2(1+e^{-\gamma})-R)}, \tag{2.53}$$

where $R_0 = 1-\log_2(1+e^{-\gamma})$ is the cutoff rate of an AWGN channel with binary input. We use this bound as an approximation of the packet error probability of the slow faded link between Tx and Rx when the SINR at Rx equals to γ. The link throughput conditioned on γ is then

$$S_l(\gamma) = R \cdot \left(1 - \cdot 2^{-n(1-\log_2(1+e^{-\gamma})-R)}\right) \quad \left(\frac{\text{bits}}{\text{sec} \cdot \text{Hz}}\right). \tag{2.54}$$

Since the received SINR γ is not deterministic, we need to take the expectation of $S_l(\gamma)$ with respect to the pdf of γ. The cdf of γ is the outage probability $\phi_{r_0}(b) = P\{\gamma < b\}$. The pdf of γ is simply the derivative $\phi'_{r_0}(\gamma)$. The unconditioned link throughput is then

$$S_l = E_\gamma \left\{ R \cdot \left(2^{-n(1-\log_2(1+e^{-\gamma})-R)}\right)\right\} = R \cdot \int_0^\infty \left(1 - 2^{-n(1-\log_2(1+e^{-\gamma})-R)}\right) \ \phi'_{r_0}(\gamma) \ d\gamma. \tag{2.55}$$

In Fig. 2.28 and 2.29 we plot the link throughput versus code rate R for various code lengths under different path loss exponent η. We can see that there are different optimal code rates for different code lengths. In general, when the code length grows larger, the packet error probability decreases. Hence the link throughput also increases. This is why in both figures we observe the optimal code rate grows along with the code length. When the code length is large, the optimal code rate is very close to 1.

2.8 Conclusions

In this chapter, the performance of wireless networks with directional antennas with arbitrary beam patterns was analyzed. By combining our performance analysis of BICM and turbo codes contained in later chapters, we analyzed the performance of wireless networks with directional antennas for various coding and modulation schemes used in the physical layer. The characteristic value that determines the performance of a beam pattern in the network was found, which makes the comparison between beam patterns

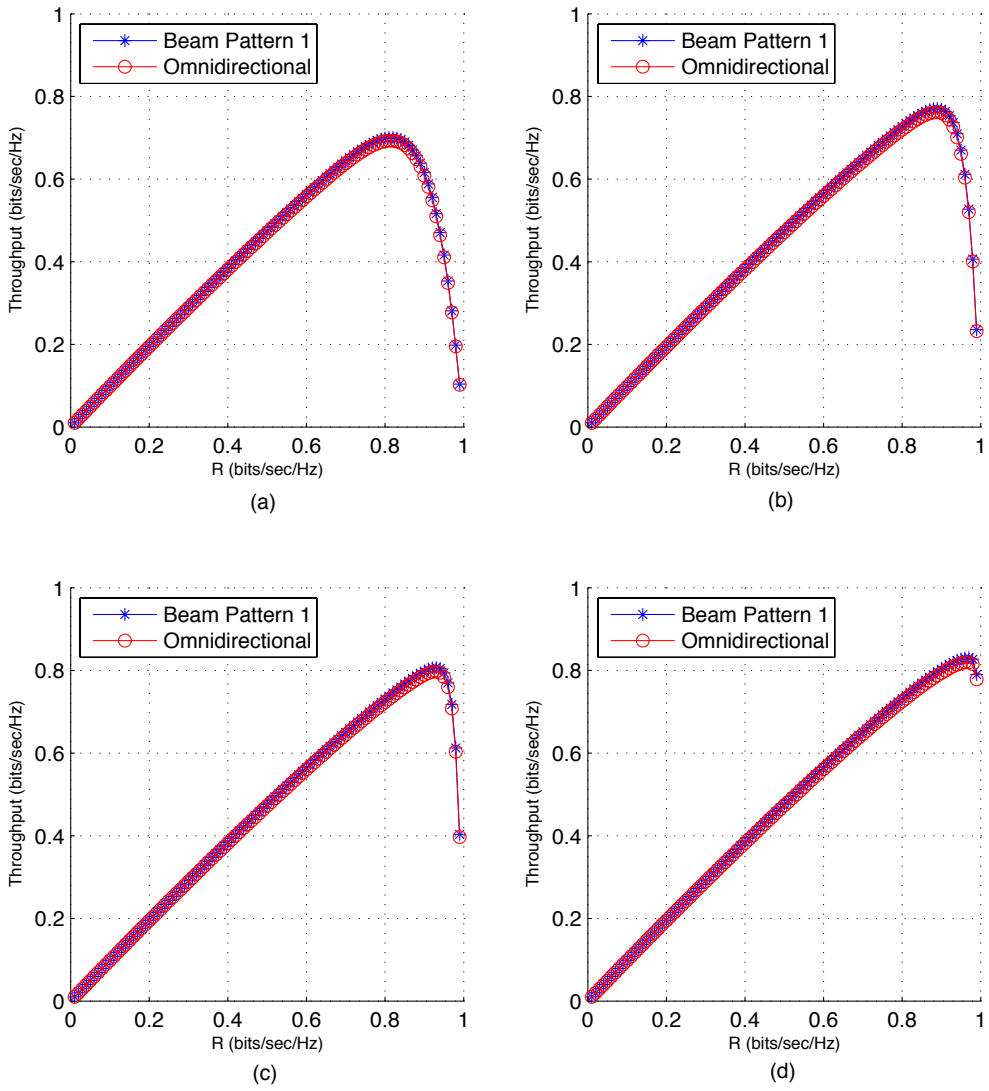

Figure 2.28: Link throughput vs. code rate R under slow fading, $\gamma_c = 18$ dB, $\lambda = 20.0$ mobiles/km^2, $\sigma = 6$ dB, $\eta = 4$, $p = 0.045$, $r_0 = 0.1$ km. (a) $n = 20$, (b) $n = 50$, (c) $n = 100$, (d) $n = 500$

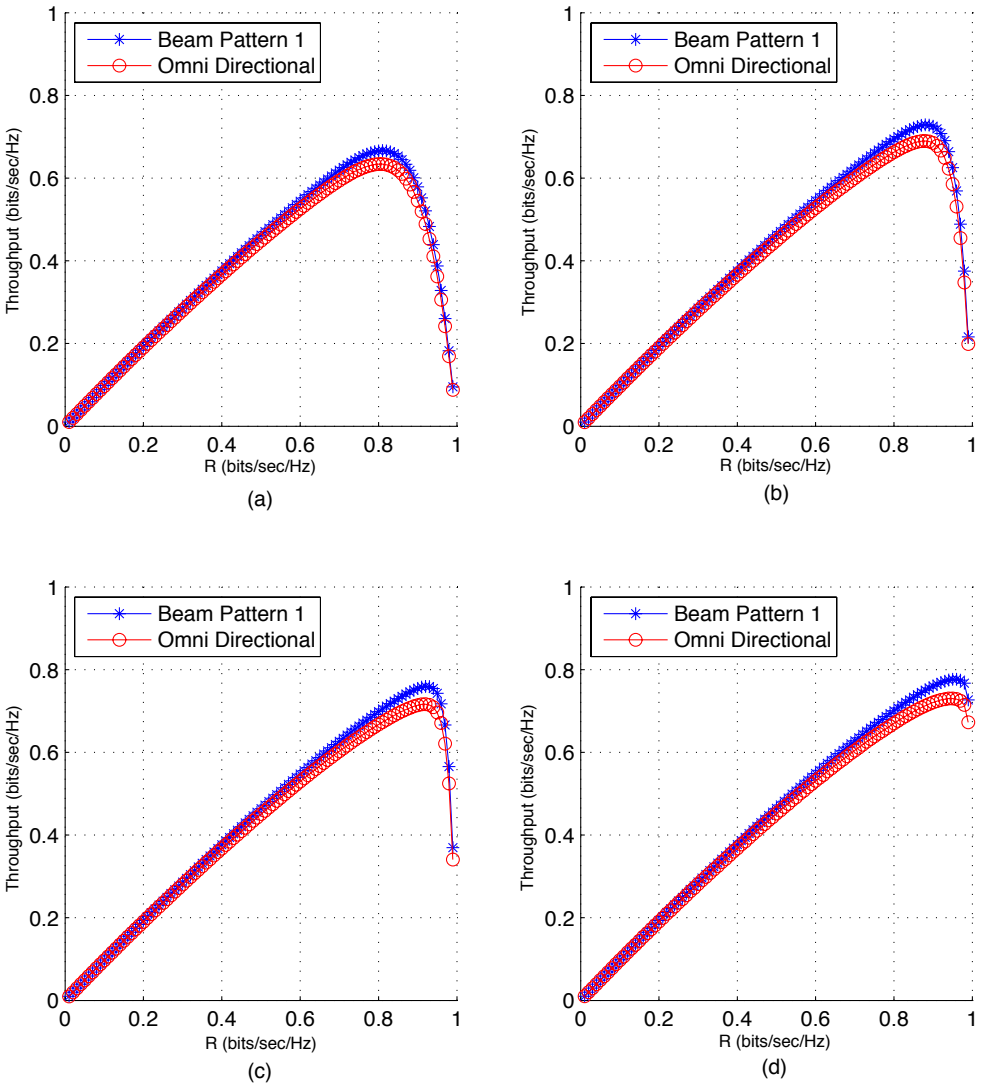

Figure 2.29: Link throughput vs. code rate R under slow fading, $\gamma_c = 18$ dB, $\lambda = 20.0$ mobiles/km^2, $\sigma = 6$ dB, $\eta = 2.7$, $p = 0.045$, $r_0 = 0.1$ km. (a) $n = 20$, (b) $n = 50$, (c) $n = 100$, (d) $n = 500$

very easy. We also analyzed the effects of directional estimation error and power control which enables us to find the optimal power control scheme for the wireless network. Finally we applied our analysis to find the optimal system parameters such as the optimal mobile density and the optimal code rate for maximizing throughput, which shows the usefulness of our work in the system design optimization for wireless networks with directional antennas.

CHAPTER 3

Performance Analysis of Bit-Interleaved Coded Modulation (BICM) in Wireless Environments

In the previous chapter, we analyzed the performance of a wireless network using directional antennas. However in order to accurately evaluate the performance of the wireless network for different coded modulation schemes used in physical layer, we need to set the SINR threshold of the outage probability according to the performance of the coded modulation schemes. Hence it is necessary for us to analyze the performance of coded modulations in wireless environment. That is the goal of this chapter.

3.1 Introduction

The growing demand for high-rate data communications requires bandwidth-efficient transmission techniques. A serious challenge to reliable communication in wireless systems is the time-varying multipath fading environments, which causes the received signal-to-noise ratio to vary randomly. The fading distribution depends on the environment. For example, if a line-of-site (LOS) exists between the transmitter and the receiver in addition to the multipath reception, the fading process can be modeled by a Rician distribution [24]. Another popular fading model is the Nakagami distribution [25], which provides a family of distributions that match measurements in different propagation environments [26].

Coding and diversity techniques are methods that are used to mitigate the effects of multipath fading. Coded modulation [27] jointly considers the error control coding and modulation to achieve high transmission rates at good quality. The basic idea is

to partition the signal space into sets and use coding to maximize a distance measure between the coded signals. For example, Euclidean distance is maximized for additive white Gaussian noise (AWGN) channels whereas the symbol-wise Hamming distance is the appropriate distance measure for Rayleigh fading channels. In fading environments the symbol-wise Hamming distance can be increased by interleaving the coded bits prior to mapping them onto the signal constellation [7,28]. This method is referred to as bit-interleaved coded modulation (BICM).

Because of the interleaver used in the transmitter, each constellation symbol is composed of bits that are located far from each other in the coded sequence (from the decoder point-of-view). Thus a symbol error does not cause consecutive bit errors in the codeword. This improves the performance significantly. However, the random nature of distributing the error bits over different symbols causes the performance analysis to be difficult. A union bound on the bit error probability of BICM systems was presented in [7,8]. The bound was based on the assumption that a symbol error causes a bit error, which is not true in general. The paper used log-sum approximation $\log \sum_j z_j \simeq \max_j \log z_j$ to compute the log likelihood of each encoded bit. The approximation caused the union bound to be a little loose for M-ary constellation with large M. Due to the interleaving used, symbol errors result in bit errors that are randomly distributed in the coded sequence. From another point-of-view, bit errors in a codeword will be randomly distributed among different symbols in the transmission frame.

In this chapter we derive union bounds on the packet and bit error probabilities of BICM over AWGN and fading channels. In the new bound we assume uniform interleaving of the coded bits prior to mapping them onto the signal constellation. The distribution of error bits in a codeword over different symbols is derived and the corresponding pairwise error probability is evaluated. The distribution of error bits was originally analyzed in our past work on the performance analysis of binary codes in a block fading channel [29]. We derived the joint distribution of the number of error bits distributed in each fading block which enabled us to find the squared Euclidean distance distribution of different error patterns. BICM is a little similar to the block fading case in

the sense that several bits are grouped into one symbol, just like several bits are affected by the same fading level in the block fading channel. However, the squared Euclidean distance distribution of BICM is much more complicated than the block fading case because the squared Euclidean distance of one BICM symbol is not proportional to the Hamming weight of the bit errors in that symbol whereas the squared Euclidean distance of one fading block is proportional to the number of the error bits in that fading block. The union bounds given in this chapter can be applied to different modulations and coding schemes with known weight spectrum. We consider AWGN and fading channels including Rayleigh, Rician and Nakagami distributions. Simulation results show that the proposed bound is tight for various signal constellations and channel models.

The remainder of this chapter is organized as follows. The BICM system model is described in the next section. In Section 3.3, the union bound is presented. The pairwise error probabilities corresponding to different channel distributions are derived in Section 3.4. Analytical and simulation results are presented and discussed therein. Conclusions are presented in Section 3.5.

3.2 System Model

The block diagram of a BICM with iterative decoding is shown in Fig. 3.1. The information sequence $\mathbf{U} = \{u_l\}_{l=1}^{K}$ is encoded by a rate-R_c encoder to yield a codeword $\mathbf{C} = \{c_l\}_{l=1}^{N}$ of length N bits. The rate of the code is $R_c = \frac{K}{N}$. The codeword is interleaved using a bit-interleaver. Groups of m bits are mapped onto a signal point in a signal constellation. The mapping rule is an one-to-one mapping $f : \{0,1\}^m \rightarrow \mathcal{S}$, where $\mathcal{S}$ is a signal space of size $M = 2^m$ and dimension D. The signal points in $\mathcal{S}$ are scaled to have the average energy equal to 1. In general, the input to the mapper is a vector $\underline{c} = [c_1, \ldots, c_m]$ and the output is a signal point $s = f(\underline{c})$. The transmission frame consists of $J = \lceil \frac{N}{m} \rceil$ symbols and is denoted by $\mathbf{S} = \{s_l\}_{l=1}^{J}$. Note that the throughput of the system is mR_c/D bits/symbol duration/dimension.

At the receiver the sampled matched filter output corresponding to a transmitted

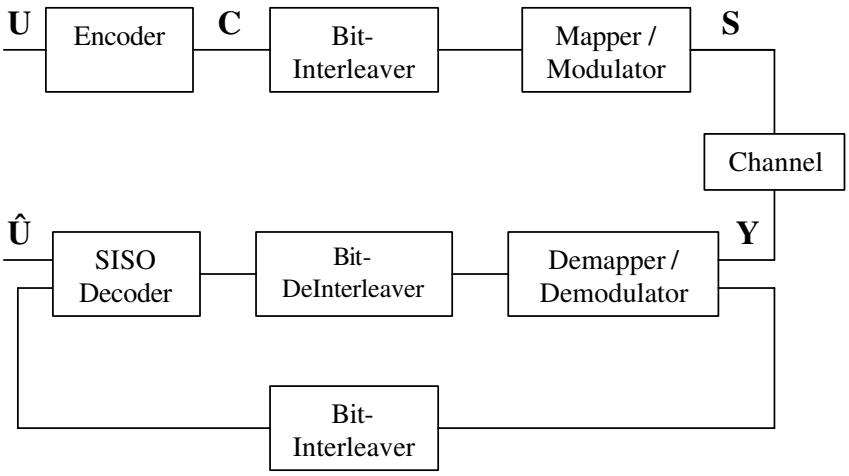

Figure 3.1: Block diagram of a BICM system employing iterative detection and decoding.

symbol in the time interval l is given by

$$y_l = \sqrt{E_s} h_l s_l + z_l, \tag{3.1}$$

where E_s is the average received energy and z_l is noise modeled as a zero-mean complex Gaussian random variable with variance N_0, i.e., $z_l \sim \mathcal{CN}(0, N_0)$. The coefficient h_l is the channel gain affecting the l^{th} transmitted symbol and written as $h_l = |h_l| \exp(j\theta_l)$, where θ_l is an uniformly distributed phase and $|h_l|$ is the channel amplitude. Here we assume that $|h_l|$ is either a constant resulting in an AWGN channel or distributed according to Rayleigh, Rician or Nakagami distributions. Moreover, we assume infinite channel interleaving, which results in each symbol being affected by an independent fading realization from other symbols in the frame. Throughout the chapter the channel side information (amplitude and phase) is assumed to be known at the receiver.

The receiver consists of a demodulator/demapper, deinterleaver and a decoder. The demodulator/demapper computes the log-likelihood ratio (LLR) of the j^{th} coded bit in the l^{th} symbol of the codeword as

$$L(c_j) = \log \left(\frac{\sum_{s_l : c_j = 1} P(y_l |\ s_l)}{\sum_{s_l : c_j = 0} P(y_l |\ s_l)} \right). \tag{3.2}$$

For a fading channel with perfect channel information, $L(c_j)$ has the form

$$L(c_j) = \log \left(\frac{\sum_{s_l:c_j=1} \exp(\lambda(y_l, s_l))}{\sum_{s_l:c_j=0} \exp(\lambda(y_l, s_l))} \right), \tag{3.3}$$

where $\lambda(y_l, s_l)$ is given by

$$\lambda(y_l, s_l) = -|h_l|^2 \frac{E_s}{N_0} ||s_l||^2 + \frac{2\sqrt{E_s}}{N_0} \text{Re}\{h_l \; s_l \; y_l^*\}, \tag{3.4}$$

and $(\cdot)^*$ denotes the conjugate operator. For AWGN channel, $L(c_j)$ is the same as (3.3) except that the h_l in (3.4) should be replaced by 1. The decoder accepts the LLR's of all coded bits and employs a MAP algorithm [30] to compute the LLR's of information bits, which are used for decision. Note that iterative detection and decoding can be applied to improve the performance of BICM [31]. Because the performance gain of the iterative receiver becomes negligible at high SNR [32], we consider in this chapter a non-iterative receiver, which provides maximum likelihood performance at high SNR. The performance analysis of BICM is presented in the following sections.

3.3 The Union Bound

In this section, a union bound on the error probability of BICM is derived. The subscripts c, u and b are used to denote conditional, unconditional and bit error probabilities, respectively. Only BICM systems employing convolutional codes are considered in the derivation. However, the results are general to any code with a known weight spectrum. For convolutional codes with k input bits, the packet error probability is upper bounded [33] by

$$P_p < \sum_{d=d_{min}}^{n} \sum_{j=1}^{K} w_{j,d} \; P_u(d), \tag{3.5}$$

and the bit error probability is bounded [33] by

$$P_b \lesssim \frac{1}{K} \sum_{d=d_{min}}^{n} \sum_{j=1}^{K} j \; w_{j,d} \; P_u(d), \tag{3.6}$$

where d_{min} is the minimum distance of the code, $P_u(d)$ is the unconditional pairwise error probability defined as the probability of decoding a received sequence as a weight-d codeword given that the all-zero codeword is transmitted. In (3.6), $w_{j,d}$ is the number of codewords with input weight j and output weight d, which is obtained from the weight enumerator of the code [33]. One thing to note here is that the channel is not symmetric. For instance, if 16-QAM is used for modulation, it is not necessarily true that any symbol pair with Hamming distance 2 will have the same Euclidean distance as symbol pair 0011 and 0000. Therefore strictly speaking, (3.6) may not be able to characterize the system performance when codewords other than the all-zero codeword are transmitted. Fortunately the problem can be solved later when computing the squared Euclidean distance distribution between symbol pairs. Instead of computing the squared Euclidean distance distribution between a random choice of symbol and the all-zero symbol, we compute it for a pair of two random symbols. By applying the squared Euclidean distance distribution to (3.6), we will be able to characterize the system performance again by (3.6) even when a non-zero codeword is transmitted.

In BICM the unconditional pairwise error probability $P_u(d)$ is a function of the distribution of the d error bits over the J symbols in the frame. This distribution is quantified assuming random interleaving of the coded bits over the symbols. Denote the number of symbols with v error bits by j_v and define $w = \min(m, d)$. Then the symbols are distributed according to the pattern $\mathbf{j} = \{j_v\}_{v=0}^{w}$ where

$$J = \sum_{v=0}^{w} j_v, \qquad d = \sum_{v=1}^{w} v j_v. \tag{3.7}$$

$P_u(d)$ is obtained by averaging over all possible symbol patterns

$$P_u(d) = \sum_{j_w=0}^{L_w} \sum_{j_{w-1}=0}^{L_{w-1}} \cdots \sum_{j_1=0}^{L_1} P_u(d|\mathbf{j}) p(\mathbf{j}|d), \tag{3.8}$$

where

$$L_v = \max\left\{0, \lfloor \frac{d - \sum_{r=v+1}^{w} r j_r}{v} \rfloor \right\}, \quad 1 \le v \le w, \tag{3.9}$$

and $P_u(d|\mathbf{j})$ is the pairwise error probability conditioned on the symbol distribution pattern $\mathbf{j}$. The joint pdf of $\mathbf{j}$ given d is computed using combinatorics as

$$p(\mathbf{j}|d) = \frac{\binom{m}{1}^{j_1}\binom{m}{2}^{j_2}\cdots\binom{m}{w}^{j_w}}{\binom{mJ}{d}} \cdot \frac{J!}{j_1!\ldots j_w!\ (J - \sum_{v=1}^{w} j_w)!}. \tag{3.10}$$

The left factor of $p(\mathbf{j}|d)$ in (3.10) is the probability of distributing d error bits over J symbols with j_v symbols having v bits for possible values of v. The middle term of $p(\mathbf{j}|d)$ is the number of combinations $\mathbf{j} = \{j_v\}_{v=0}^{w}$ among the J symbols. Using (3.8)-(3.10), the union bound on the bit error probability of BICM is found by substituting (3.8) in (3.6).

For fading channels with coherent detection, the conditional pairwise error probability $P_c(d|\mathbf{j})$ conditioned on the symbol pattern $\mathbf{j}$ is given by

$$P_c(d|\ \mathbf{j}, |h_1|, \cdots, |h_J|) = \mathrm{E}_{d_1^2,\cdots,d_J^2}\left[\mathrm{Q}\left(\sqrt{\frac{mR_c\gamma_b}{2} \cdot \sum_{j=1}^{J} |h_i|^2 d_j^2}\right)\right], \tag{3.11}$$

where $\gamma_b = \frac{E_b}{N_0}$ is the SNR per information bit, and d_j^2 is the squared Euclidean distance between the j^{th} symbol of the error codeword and that of the desired codeword. Note that the d error bits are distributed over the J symbols according to the pattern $\mathbf{j}$. The expectation in (3.11) is with respect to the squared Euclidean distances $\{d_j^2\}_{j=1}^{J}$. The unconditional pairwise error probability $P_u(d|\mathbf{j})$ is found by averaging (3.11) over the fading amplitudes $\{|h_j|\}_{j=1}^{J}$. Using the integral expression of the Q-function, $\mathrm{Q}(x) =$

$\frac{1}{\pi}\int_0^{\frac{\pi}{2}} e^{(-x^2/2\sin^2\theta)}d\theta$ [34], $P_u(d|\mathbf{j})$ is expressed as

$$P_u(d|\mathbf{j}) = \frac{1}{\pi}\int_0^{\frac{\pi}{2}} \prod_{j=1}^{J} \mathrm{E}_{|h_j|^2}\left[\mathrm{E}_{d_1^2,\cdots,d_J^2}\left[\exp\left(-\beta(\theta)|h_j|^2 d_j^2\right)\right]\right] d\theta, \tag{3.12}$$

where $\beta(\theta) = \frac{mR_c\gamma_b}{4\sin^2\theta}$ and the product is due to the assumed independence of the fading variables affecting different symbols. The probability in (3.12) is written by grouping symbols with the same number of error bits as

$$P_u(d|\mathbf{j}) = \frac{1}{\pi}\int_0^{\frac{\pi}{2}} \prod_{v=1}^{w} \left\{\mathrm{E}_{|h|^2}\left[\Psi_{d_v^2}(\beta(\theta)|h|^2)\right]\right\}^{j_v} d\theta, \tag{3.13}$$

where $|h|$ is a random variable identically distributed as $|h_j|$'s and $\Psi_{d_v^2}(\zeta) = \mathrm{E}_{d_v^2}\left[e^{-\zeta d_v^2}\right]$ is the characteristic function of the random variable d_v^2, which is the squared Euclidean distance between a pair of symbols with Hamming distance v. It is easy to get the distribution of d_v^2 for a given M-ary signal constellation as follows. Consider all $\binom{M}{2}$ possible distinct symbol pairs, count $\{q_{v,i}\}$ the number of symbol pairs with Hamming distance v and squared Euclidean distance $\xi_{v,i}$, $i = 1, 2, \cdots, k_v$, assuming there exists k_v possible distinct squared Euclidean distances between symbol pairs of Hamming distance v. The probability density function of d_v^2 is then given by

$$f_{d_v^2}(x) = \sum_{i=1}^{k_v} p_{v,i}\ \delta(x - \xi_{v,i}), \tag{3.14}$$

where $p_{v,i} = \frac{q_{v,i}}{\sum_{i=1}^{k_v} q_{v,i}}$. The corresponding characteristic function is given by

$$\Psi_{d_v^2}(z) = \sum_{i=1}^{k_v} p_{v,i}\ e^{-z\xi_{v,i}}. \tag{3.15}$$

Expressions for the pairwise error probability of BICM over AWGN and fading channels are derived in the next section.

3.4 Pairwise Error Probability

In this section we derive the pairwise error probability of BICM over AWGN and fading channels with different fading distributions.

3.4.1 AWGN

Combining (3.13) and (3.15), the pairwise error probability for AWGN channels is given by

$$P_u(d|\mathbf{j}) = \frac{1}{\pi}\int_0^{\frac{\pi}{2}} \prod_{v=1}^{w} \left(\sum_{i=1}^{k_v} p_{v,i} e^{-\xi_{v,i}\beta(\theta)} \right)^{j_v} d\theta. \tag{3.16}$$

Substituting (3.16) in (3.8) results in the union bound on the bit error probability of BICM over an AWGN channel. Throughout the chapter we use as an example a BICM system employing a rate-$\frac{1}{2}$ (1,5/7) convolutional code and M-QAM signal constellations with $M = 64, 256$. The encoded packet length is 2052 bits for the case of $M = 64$ and 2048 bits for the case of $M = 256$. Each BICM uses a specific S-random interleaver with S parameter equals to 15. Fig. 3.2 shows the results for an AWGN channel. We observe that the bound is tight to simulation at medium-to-high SNR values. The random interleaving bound being tight to the simulation of a specific interleaver at high SNR could be an indication that for each of these coded modulations, the minimum Euclidean distances of the error patterns with different interleavers used are very close. Also note that the union bound becomes loose for SNR values lower than the cutoff rate of the system [33].

3.4.2 Rayleigh Fading

The multiplicative amplitude in multipath fading channels is often modeled as a Rayleigh random variable whose normalized distribution is given by

$$f_{|h|}(x) = 2xe^{-x^2}, \qquad x \geq 0. \tag{3.17}$$

If $|h|$ is Rayleigh distributed, than $|h|^2$ is exponentially distributed with pdf

$$f_{|h|^2}(x) = e^{-x}. \tag{3.18}$$

Hence we have characteristic function of $|h|^2$ as

$$\Psi_{|h|^2}(z) = \mathrm{E}_{|h|^2}\left[e^{-z|h|^2}\right] = \int_0^\infty e^{-(1+z)x}\, dx = \frac{1}{1+z}. \tag{3.19}$$

Now consider

$$\begin{aligned}
\mathrm{E}_{|h|^2}\left[\Psi_{d_v^2}(\beta(\theta)|h|^2)\right] &= \mathrm{E}_{|h|^2}\left[\sum_{i=1}^{k_v} p_{v,i}\; e^{-\xi_{v,i}\beta(\theta)|h|^2}\right] \\
&= \sum_{i=1}^{k_v} p_{v,i}\; \mathrm{E}_{|h|^2}\left[e^{-\xi_{v,i}\beta(\theta)|h|^2}\right] \qquad (3.20)\\
&= \sum_{i=1}^{k_v} \frac{p_{v,i}}{1+\xi_{v,i}\beta(\theta)}. \qquad (3.21)
\end{aligned}$$

Substituting (3.21) in (3.13), this results in the pairwise error probability for Rayleigh fading channels with perfect side information

$$P_u(d|\mathbf{j}) = \frac{1}{\pi}\int_0^{\frac{\pi}{2}} \prod_{v=1}^{w}\left(\sum_{i=1}^{k_v}\frac{p_{v,i}}{1+\xi_{v,i}\beta(\theta)}\right)^{j_v} d\theta. \tag{3.22}$$

The union bound on the bit error probability of BICM over a Rayleigh fading channel is obtained by substituting (3.22) in (3.8). Fig. 3.3 shows analytical and simulation results for BICM over a Rayleigh fading channel using a specific S-random interleaver (S=15). The bound is shown to be tight to the simulation results.

3.4.3 Rician Fading

If a LOS exists between the transmitter and the receiver, the amplitude of the channel gain can be modeled as a Rician random variable [24]. In this model the received signal is composed of two signal-dependent components; namely the specular and diffuse com-

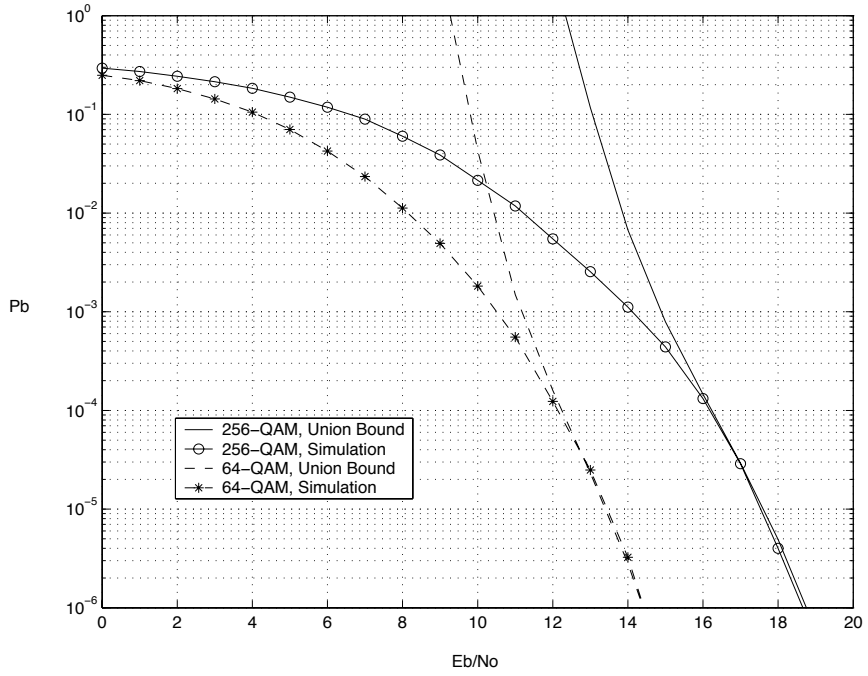

Figure 3.2: Bit error probability of BICM using a rate-$\frac{1}{2}$ (1,5/7) convolutional code and QAM signaling over an AWGN channel.

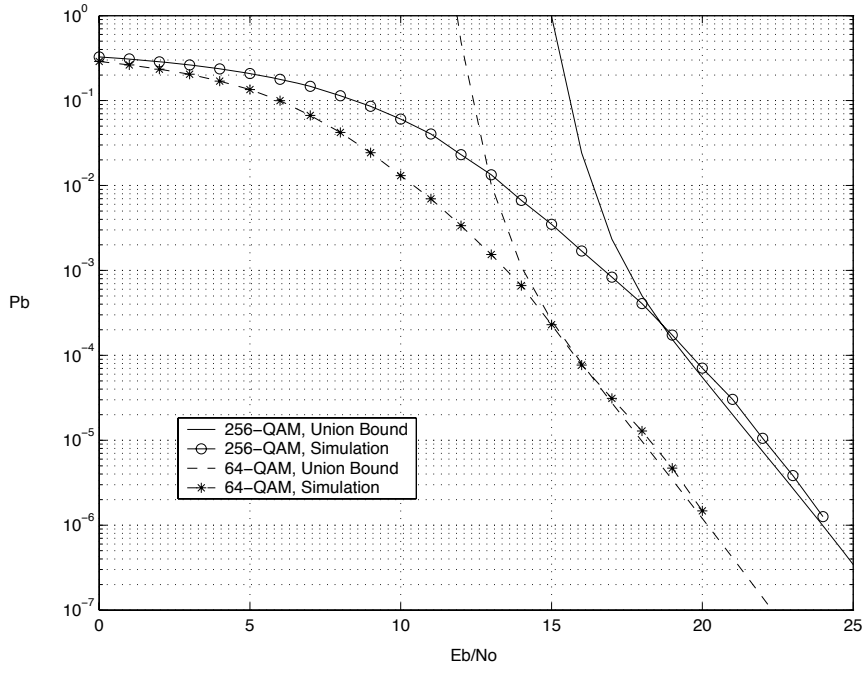

Figure 3.3: Bit error probability of BICM using a rate-$\frac{1}{2}$ (1,5/7) convolutional code and QAM signaling over a Rayleigh fading channel.

ponents. The specular component is due to the LOS reception and the diffuse component results from multipath reception. Let κ denote the ratio of the specular component energy to the diffuse component energy of the channel. In Rician fading, the normalized channel gain h in each fading block is modeled by a complex Gaussian variable with $\mathcal{CN}\left(\sqrt{\frac{\kappa}{1+\kappa}}, \frac{1}{1+\kappa}\right)$ distribution. The pdf of the normalized Rician random variable [35] is given by

$$f_{|h|}(x) = 2x(1+\kappa)\exp\left[-\kappa - x^2(1+\kappa)\right] \cdot \ I_0\left(2x\sqrt{\kappa(1+\kappa)}\right), \qquad x \geq 0, \tag{3.23}$$

where $I_0(\cdot)$ is the zero-order modified Bessel function of the first kind. Setting $\kappa = 0$ results in the Rayleigh distribution while the channel approaches the AWGN case as κ increases toward infinity. Since h is of distribution $\mathcal{CN}\left(\sqrt{\frac{\kappa}{1+\kappa}}, \frac{1}{1+\kappa}\right)$, $|h|^2$ has a noncentral chi-square distribution [21] with noncentrality parameter given by

$$s^2 = \left(\sqrt{\frac{\kappa}{1+\kappa}}\right) + 0^2 = \frac{\kappa}{1+\kappa}, \tag{3.24}$$

and the characteristic function is given by [36]

$$\begin{aligned} \Psi_{|h|^2}(z) = \mathrm{E}_{|h|^2}\left[e^{-z|h|^2}\right] &= \frac{1}{1+z/(1+\kappa)} \cdot \exp\left\{\frac{-\kappa\ z/(1+\kappa)}{1+z/(1+\kappa)}\right\} \\ &= \frac{1+\kappa}{1+\kappa+z} \cdot \exp\left\{\frac{-\kappa\ z}{1+\kappa+z}\right\}. \end{aligned} \tag{3.25}$$

Substitute (3.25) in (3.20) and then (3.13). We can derive the pairwise error probability for BICM over a Rician fading channel with perfect side information as

$$P_u(d|\mathbf{j}) = \frac{1}{\pi}\int_0^{\frac{\pi}{2}} \prod_{v=1}^{w}\left[\sum_{i=1}^{k_v} \frac{p_{v,i}\cdot(1+\kappa)}{1+\kappa+\xi_{v,i}\beta(\theta)} \cdot \exp\left(-\frac{\kappa\xi_{v,i}\beta(\theta)}{1+\kappa+\xi_{v,i}\beta(\theta)}\right)\right]^{j_v} d\theta. \tag{3.26}$$

Substituting (3.26) in (3.8) results in the union bound on the bit error probability of BICM over a Rician fading channel. Analytical and simulation results using a specific S-random interleaver for Rician fading channels with different κ values are shown in Fig. 3.4. From the figure, it is seen that the bound is tight to the simulation results for a

wide range of the specular-to-diffuse energy ratio κ. Note that the curve corresponding to $\kappa = 0$ represents the Rayleigh fading case.

3.4.4 Nakagami Fading

The Nakagami distribution was shown to fit a large variety of channel measurements [26]. Under the Nakagami distribution, the pdf of the normalized received signal envelope [25] is given by

$$f_{|h|}(x) = \frac{2\mu^{\mu}}{\Gamma(\mu)\Omega^{\mu}} x^{2\mu-1} \exp\left(-\frac{\mu x^2}{\Omega}\right), \quad x \geq 0, \mu \geq 0.5, \tag{3.27}$$

where $\Omega = \mathrm{E}[|h|^2] = 1$, $\mu = \frac{\Omega^2}{\mathrm{Var}[|h|]}$ is the fading parameter, and $\Gamma(\cdot)$ is the Gamma function. As the fading parameter μ increases, the fading becomes less severe and reaches the non-fading case when μ goes to ∞. The Nakagami distribution covers a wide range of fading scenarios including the Rayleigh distribution when $\mu = 1$ and the single-sided Gaussian distribution when $\mu = 0.5$. If $|h|$ is Nakagami distributed with integer order μ, then $|h|^2$ is chi-square distributed with order 2μ and characteristic function of the form

$$\Psi_{|h|^2}(z) = \mathrm{E}_{|h|^2}\left[e^{-z|h|^2}\right] = \left(\frac{1}{1 + z/\mu}\right)^{\mu}. \tag{3.28}$$

The pairwise error probability for BICM over a Nakagami fading channel with perfect side information is found by substituting (3.28) in (3.20) and (3.13)

$$P_u(d|\mathbf{j}) = \frac{1}{\pi} \int_0^{\frac{\pi}{2}} \prod_{v=1}^{w} \left[\sum_{i=1}^{q_v} p_{v,i} \cdot \left(\frac{1}{1 + \xi_{v,i}\beta(\theta)/\mu}\right)^{\mu}\right]^{j_v} d\theta. \tag{3.29}$$

Substituting (3.29) in (3.8) results in the union bound on the bit error probability of BICM over a Nakagami fading channel. Fig. 3.5 shows the analytical and simulation results for the BICM using a specific S-random interleaver over Nakagami fading channels with different fading parameters μ. We observe that the union bound provides satisfactory performance evaluation of BICM systems for a wide range of values of the Nakagami

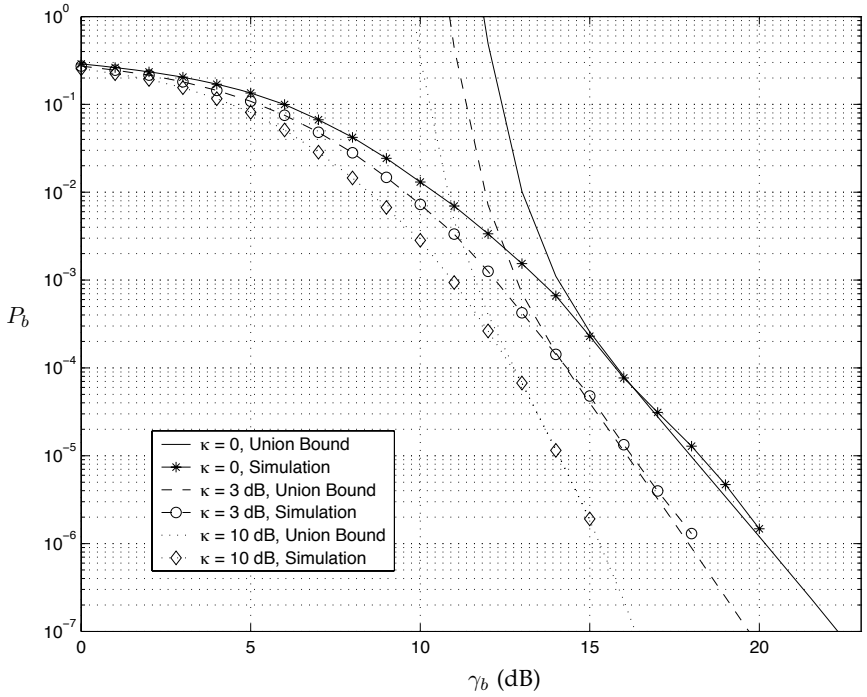

Figure 3.4: Bit error probability of BICM using a rate-$\frac{1}{2}$ (1,5/7) convolutional code and a 64-QAM signaling over Rician fading channels with different κ values.

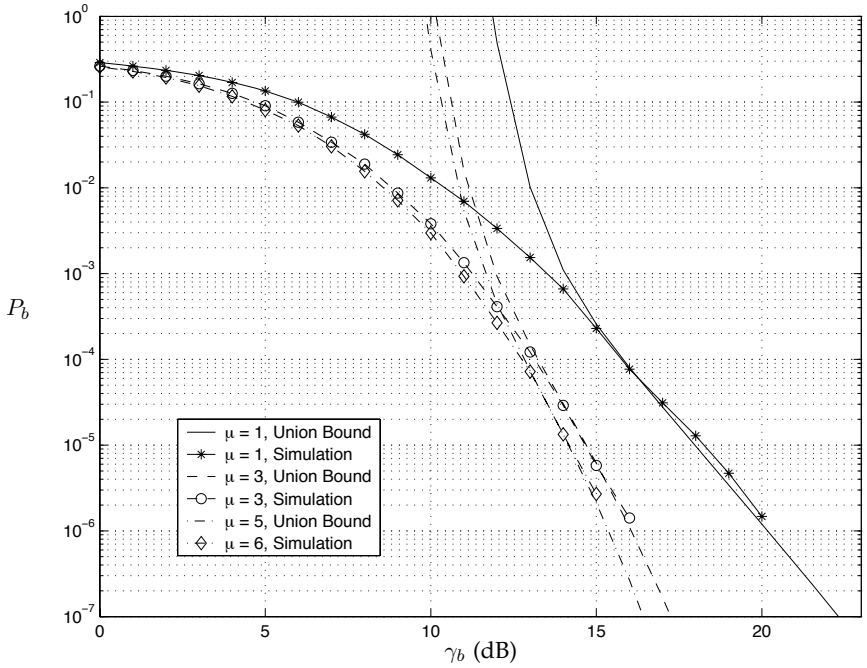

Figure 3.5: Bit error probability of BICM using a rate-$\frac{1}{2}$ (1,5/7) convolutional code and a 64-QAM signaling over Nakagami fading channels with different fading parameters μ.

fading parameter. Note that the $\mu = 1$ case corresponds to the Rayleigh fading.

3.5 Conclusions

In this chapter we derive union bounds on the packet error probability and the bit error probability of BICM over AWGN, Rayleigh, Rician and Nakagami fading channels. The derivation is based on the uniform interleaving of coded bits prior to the mapping to the signal constellation. The bound is a function of the weight spectrum of the channel code and the signal constellation used in the BICM system. Results show that the proposed bound is tight to simulation curves in medium to high SNR regions. This enables us to analyze the performance of the wireless networks in Chapter 2 for specific coding and modulation schemes used in physical layer.

CHAPTER 4

Performance Analysis of Bit-Interleaved Space-Time (BI-ST) Coded Systems in Wireless Environment

In the previous chapter, we analyzed the performance of bit-interleaved coded modulation which is effective in mitigating the fading effect by providing time diversity through bit-interleaving. Space-time codes are known for their ability to provide transmit diversity by using multiple antennas. By combining bit-interleaving and space-time codes, we can have both time diversity and transmit diversity to mitigate the fading even more effectively. Our focus in this chapter is on the performance of a BI-ST coded system in the wireless environment under various fading models.

4.1 Introduction

The demand for high-rate and high-quality wireless communications recently has seen a rapid growth. Achieving reliable communications over a time-varying fading channel resulting from multipath reception is a significant challenge. One standard approach to mitigate fading and achieve bandwidth efficiency is to use transmit diversity in which multiple antennas are used at the transmitter [9]. Using the combination of multiple transmit antennas and error control coding is referred to as space-time (ST) coding [10]. Simple and elegant space-time block codes (STBC) were proposed in [11,12] to provide diversity at the transmitter. In [37,38], BICM was applied to multi-input multi-output (MIMO) systems in which the coded bits are bit-interleaved and each group of bits are mapped onto signals that are transmitted over multiple transmit antennas. Two approaches to mapping the coded bits onto the signals are considered in this chapter;

namely, the BI ST block code (BI-STBC) [39] and the BI ST coded modulation (BI-STCM) [40,41].

The original motivation behind proposing ST coded systems is to provide diversity to systems operating in slow fading environments. However, it is also of interest to study the performance of ST systems over rapidly varying fading channels. For example, multiple antennas can be used at base stations to provide receive diversity to the uplink as well as transmit diversity to the downlink. When the speed of a mobile unit increases, the fading between the base station and the mobile unit becomes rapidly varying and can not be modeled as a quasi-static fading channel. In delay-tolerant applications, interleaving with large depth can be used to imitate the fully-interleaved channels, which results in almost uncorrelated fading attenuations of neighboring symbols within a codeword. Therefore it is of great interest to analyze the performance of ST coded systems over rapidly varying fading channels.

For quasistatic fading environments, union bounds for BI-STBC and BI-STCM were derived in [39] and [40], respectively. In this chapter we derive a union bound on the bit error probability of general BI-ST coded systems over rapid fading channels. Both BI-STBC and BI-STCM systems are considered as specific examples. The new bound is valid when the coded bits are random interleaved prior to mapping them onto modulation symbols that are passed to the transmit antennas. The distribution of the error bits in a received vector is derived and the corresponding pairwise error probability is evaluated. The union bound is valid for any channel coding scheme with a known distance spectrum and any ST coding scheme. Flat multipath fading channels following Rayleigh, Rician and Nakagami distributions are considered. Simulation results show that the proposed bound is tight for various signal constellations, ST coding schemes and channel models.

The remainder of this chapter is organized as follows. The model for a BI-ST coded system is described in Section 4.2. In Section 4.3, the proposed union bound is derived. The characteristic function required to evaluate the union bound is derived for the BI-STCM and BI-STBC systems in Section 4.4 and Section 4.5, respectively. Analytical and simulation results are presented in Section 4.6. Conclusions are discussed in Section 4.7.

4.2 System Model

Consider the BI-ST coded system shown in Figure 4.1. The encoder receives an information block $\mathbf{u}$ of K bits and generates an N-bit codeword $\mathbf{c}$ resulting in a code rate $R_c = \frac{K}{N}$. After encoding, the codeword $\mathbf{c}$ is bit interleaved to generate the interleaved codeword $\pi(\mathbf{c}) = (\mathbf{b}_1, \mathbf{b}_2, \cdots, \mathbf{b}_L)$ that consists of L blocks each of qm bits. Each of the L blocks is referred to as a ST block (STB). Note that $N = qmL$. The STB $\mathbf{b}_l$ is mapped onto q symbols $(s_{l,1}, s_{l,2}, \cdots, s_{l,q})$ by a ST mapper. Each of the q symbols are drawn from an M-ary complex signal constellation that consists of $M = 2^m$ signal points with average symbol energy equal to E_s. Every q symbols are mapped by the ST encoder into p column vectors of length n_T for transmission by n_T transmit antennas.

The ST code is characterized by an $n_T \times p$ transmission matrix, where $p = 1$ or an integer that satisfies $p \geq n_T$. In the case of $p = 1$, the system is called the ST coded modulation (STCM) [10], whereas the case of $p \geq n_T$ results in the well-known ST block code (STBC) [11] as will be clarified in the examples presented below. The rows of the transmission matrix consists of entries that are linear combinations of $s_{l,1}, s_{l,2}, \cdots, s_{l,q}$ and $s^*_{l,1}, s^*_{l,2}, \cdots, s^*_{l,q}$. Denote the transmission matrix by $\mathbf{x}_l = [\ {\mathbf{x}_{l,1}}^T, {\mathbf{x}_{l,2}}^T, \cdots, {\mathbf{x}_{l,p}}^T\ ]$, where $\{{\mathbf{x}_{l,t}}^T\}$ are column vectors of dimension $n_T \times 1$. The ST encoder maps the vector $(s_{l,1}, s_{l,2}, \cdots, s_{l,q})$ onto the column vectors ${\mathbf{x}_{l,1}}^T, {\mathbf{x}_{l,2}}^T, \cdots, {\mathbf{x}_{l,p}}^T$, and the vectors $\{{\mathbf{x}_{l,t}}^T\}$ are transmitted by n_T antennas one at a time over p transmission intervals. The p transmission intervals constitute one STB. The code rate of the ST encoder is $R_s = \frac{qm}{p}$, and the overall rate of the BI-ST coded system is $R = R_s R_c = \frac{qmK}{pN}$. In the case of STBC, i.e., $p \geq n_T$, the rows of transmission matrix are constructed to be orthogonal in order to enable a linear-complexity receiver [11]. Specific examples of ST codes are presented below.

Example 1: When $p = 1$ and $q = n_T$, the resulting system is a STCM system. In STCM, every n_T symbols are transmitted over the n_T transmit antennas during one symbol duration. In this case the fading processes affecting consecutive symbols are assumed to be independent.

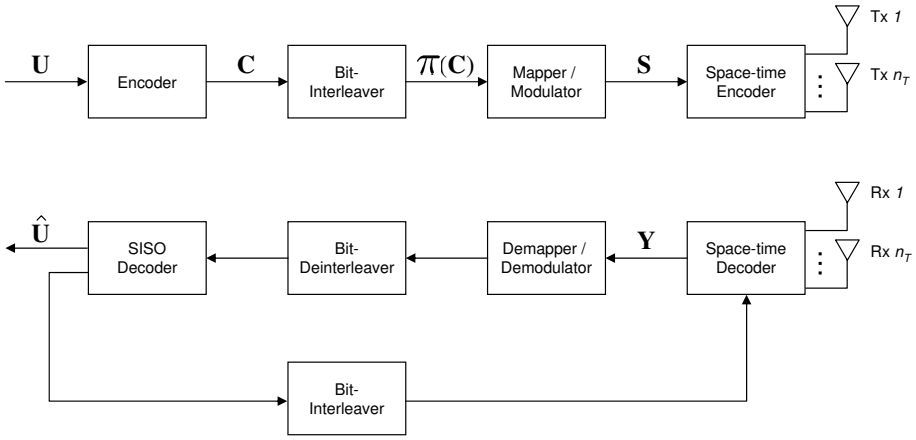

Figure 4.1: Block diagram of the general BI-ST coded system.

Example 2: When $p = q = n_T = 2$, the resulting system is the Alamouti STBC. The Alamouti STBC is characterized by the 2×2 complex matrix $\mathbf{x}_l$ presented in [11]. In this case the fading process should stay constant for at least two symbols to enable simple detection. This is a full-rate STBC.

Example 3: When $n_T > 2$, $q = p > n_T$, the resulting system is a STBC derived from orthogonal designs [12]. In this case the matrix $\mathbf{x}_l$ is one of the $n_T \times p$ complex matrices presented in [12]. This is a STBC with a rate less than unity.

In general, the receiver is assumed to have n_R antennas. However, in order to simplify notation we derive the results for systems with a single receive antenna. Note that all the results are easily generalized to multiple-receive antennas and the result will be summarized separately later. The channel from the n_T transmit antennas to the receive antenna is represented by an $1 \times n_T$ channel vector. The fading channel is assumed to be constant during one STB to enable low-complexity receivers for the STBC case [11]. The channel vector of the t^{th} transmission interval in the l^{th} STB is denoted by $\mathbf{h}_{l,t} = (h_{l,t}^1, h_{l,t}^2, \cdots, h_{l,t}^{n_T})$, where $h_{l,t}^i$ denotes the fading attenuation of the channel from the i^{th} transmit antenna to the receive antenna in the l^{th} STB. The fading channels from different transmit antennas are assumed to be independent and identically distributed (i.i.d.). The magnitudes of the fading random variables are assumed to follow either the

Rayleigh, Rician, or Nakagami distribution.

The received signal vector corresponding to a codeword $\mathbf{c}$ is denoted as $\mathbf{r} = (\mathbf{r}_1, \mathbf{r}_2, \cdots, \mathbf{r}_L)$ where $\mathbf{r}_l = (r_{l,1}, r_{l,2}, \cdots, r_{l,p})$ and

$$r_{l,t} = \mathbf{h}_{l,t}{\mathbf{x}_{l,t}}^T + \mathbf{n}_{l,t}, \tag{4.1}$$

where $\mathbf{n}_{l,t}$ is a length-p AWGN vector at the receiver during the t^{th} transmission period in the l^{th} STB modeled as $\mathcal{CN}(\mathbf{0}_p, N_0\mathbf{I}_p)$, where $\mathbf{I}_p$ denotes the $p \times p$ identity matrix and $\mathbf{0}_p$ is the $1 \times p$ zero matrix. The receiver is assumed to have perfect channel state information (CSI) and the decoding is done by minimizing the decision metric

$$\sum_{l=1}^{L}\sum_{t=1}^{p} ||r_{l,t} - \mathbf{h}_{l,t}{\mathbf{x}_{l,t}}^T||^2, \tag{4.2}$$

which can be closely achieved via iterative ST detection and decoding [42]. For information about the design of iterative detection and decoding, the reader is referred to [42] for further information.

4.3 The Union Bound

In this section, we derive a union bound on the bit error probability the BI-ST coded system described in Section 4.2. In this chapter, only BI-ST coded systems employing convolutional codes are considered. However, the performance analysis applies equally well to any coding scheme with a known distance spectrum such as turbo codes [43], product codes [44] or block codes [21]. For the sake of analysis, we again use the uniform interleaving assumption, i.e., if we feed a codeword $\mathbf{c}$ with a Hamming weight d to the interleaver, then the output could be any weight-d bit sequence of length N with an equal probability given by $\frac{1}{\binom{N}{d}}$. Similar to Chapter 3, the packet error probability for a

convolutional code is upper bounded by

$$P_p < \sum_{d=d_{min}}^{N} \sum_{j=1}^{K} w_{j,d}\ P_u(d), \tag{4.3}$$

and bit error probability by

$$P_b \lesssim \frac{1}{K} \sum_{d=d_{min}}^{N} \sum_{j=1}^{K} j\ w_{j,d}\ P_u(d), \tag{4.4}$$

where again $d_{\min}$ is the minimum Hamming distance of the convolutional code, $w_{j,d}$ denotes the number of convolutional codewords with input Hamming weight j and total weight d, and $P_u(d)$ is the pairwise error probability defined as the probability of decoding a received sequence as a weight-d codeword $\hat{\mathbf{c}}$ given that the codeword $\mathbf{c}$ was transmitted, i.e., the Hamming distance is $d_H(\mathbf{c}, \hat{\mathbf{c}}) = d$. Throughout the chapter, for any variable defined for $\mathbf{c}$, the corresponding variable defined for $\hat{\mathbf{c}}$ is denoted by using " $\hat{}$ ". The subscripts c, u and b are used to denote conditional, unconditional and bit error probabilities, respectively. Clearly $P_u(d)$ depends on the squared Euclidean distance $d_E^2 \triangleq [\ d_E(\mathbf{c}, \hat{\mathbf{c}})\ ]^2$ between the received sequences corresponding to the codewords $\mathbf{c}$ and $\hat{\mathbf{c}}$, which is a function of the distribution of the d nonzero bits over the L STBs in the codeword. Using the integral expression [34] of the Q-function, $Q(x) = \frac{1}{\pi} \int_0^{\frac{\pi}{2}} e^{(-x^2/2\sin^2\theta)} d\theta$, we have

$$P_u(d) = \mathrm{E}_{d_E^2|d} \left[Q\left(\sqrt{\frac{R\gamma_b}{2} \cdot d_E^2} \right) \right] = \frac{1}{\pi} \int_0^{\frac{\pi}{2}} \Psi_{d_E^2|d} \left(\frac{R\gamma_b}{4\sin^2\theta} \right) d\theta, \tag{4.5}$$

where $\gamma_b = \frac{E_b}{N_0}$ is the signal-to-noise ratio (SNR) per information bit and $\Psi_{d_E^2|d}(z) \triangleq \mathrm{E}_{d_E^2|d} \left[e^{-z d_E^2} \right]$ is the characteristic function of the random variable d_E^2 associated with d.

Since the combination of the signal constellation mapping with the ST encoding may not have a symmetric structure for all codewords, the Euclidean distance $d_E(\mathbf{c}, \hat{\mathbf{c}})$ may not be the same for different choices of $\mathbf{c}$ and $\hat{\mathbf{c}}$ even if the Hamming distance $d_H(\mathbf{c}, \hat{\mathbf{c}})$ is fixed at d. Hence we have to take the expectation in (4.5) with respect to the distribution

of d_E^2. Thus the task is to find the distribution of d_E^2 associated with d. Denote the error vector between two codewords $\pi(\mathbf{c})$ and $\pi(\hat{\mathbf{c}})$ by $\mathbf{e}(\mathbf{c},\hat{\mathbf{c}}) = (\mathbf{e}_1, \mathbf{e}_2, \cdots, \mathbf{e}_L)$, where $\mathbf{e}_l = (\mathbf{e}_{l,1}, \mathbf{e}_{l,2}, \cdots, \mathbf{e}_{l,p})$ and $\mathbf{e}_{l,t} = \mathbf{x}_{l,t} - \hat{\mathbf{x}}_{l,t}$. The squared Euclidean distance d_E^2 can be expressed as

$$d_E^2 = \sum_{l=1}^{L}\sum_{t=1}^{p} ||\mathbf{h}_{l,t}\mathbf{e}_{l,t}{}^T||^2 = \sum_{l=1}^{L} d_l^2, \tag{4.6}$$

where $d_l^2 = \sum_{t=1}^{p} ||\mathbf{h}_{l,t}\mathbf{e}_{l,t}{}^T||^2$ is the squared Euclidean distance between the received signal vectors associated with the l^{th} STB, $\mathbf{b}_l$. Since the total number of bit errors in the codeword is d, the distribution of d_l^2 depends on how many bit errors exist in the STB $\mathbf{b}_l$. Thus it is necessary to find the conditional distribution of d_l^2 given f_l, where f_l denotes the number of bit errors in $\mathbf{b}_l$. Due to the uniform interleaving and the independent fading assumptions, the conditional distributions of $\{d_l^2|f_l\}$ are identical and the characteristic function of d_E^2 associated with d can be obtained as

$$\Psi_{d_E^2|d}(z) = \mathrm{E}_{f_1,\cdots,f_L}\left[\prod_{l=1}^{L}\Psi_{d_l^2|f_l}(z)\right] = \mathrm{E}_{j_1,\cdots,j_w}\left[\prod_{v=1}^{w}[\phi_v(z)\,]^{j_v}\right], \tag{4.7}$$

where j_v denotes the number of STB's with v bit errors, $w = \min\{d, qm\}$ and $\phi_v(z)$ is given by

$$\phi_v(z) \triangleq \Psi_{d_l^2|f_l}(z|f_l = v) = \mathrm{E}_{d_l^2|f_l}\left[e^{-zd_l^2}|f_l = v\right], \quad v = 1, \cdots, w. \tag{4.8}$$

Clearly, the form of $\phi_v(z)$ depends on the fading distribution, which will be derived in Section 4.4. Since $d_H(\mathbf{c},\hat{\mathbf{c}}) = d$, the components of the vector $\mathbf{j} = \{j_0, j_1, ..., j_w\}$ are constrained by the conditions

$$L = \sum_{v=0}^{w} j_v, \qquad d = \sum_{v=1}^{w} v j_v. \tag{4.9}$$

The joint pdf of $\mathbf{j}$ given d is similar to what we have in (3.10)

$$p(\mathbf{j}|d) = \frac{\binom{qm}{1}^{j_1}\binom{qm}{2}^{j_2}\cdots\binom{qm}{w}^{j_w}}{\binom{N}{d}} \cdot \frac{L!}{j_1!j_2!\ldots j_w!\,(L - \sum_{v=1}^{w} j_v)!}. \tag{4.10}$$

The left factor of $p(\mathbf{j}|d)$ in (4.10) is the probability of distributing d nonzero bits over L error vectors with j_v error vectors having v bits for possible values of v. The right term of $p(\mathbf{j}|d)$ is the number of combinations of $\mathbf{j} = \{j_v\}_{v=0}^{w}$ among the L error vectors. The expectation in (4.7) is computed as

$$\Psi_{d_E^2|d}(z) = \sum_{j_w=0}^{L_w} \sum_{j_{w-1}=0}^{L_{w-1}} \cdots \sum_{j_1=0}^{L_1} \left(p(\mathbf{j}|d) \prod_{v=1}^{w} [\ \phi_v(z)\ ]^{j_v} \right), \tag{4.11}$$

where

$$L_v = \max\left\{0, \left\lfloor \frac{d - \sum_{r=v+1}^{w} r j_r}{v} \right\rfloor \right\}, \quad 1 \le v \le w. \tag{4.12}$$

Substituting (4.8)-(4.12) into (4.5) results in the final form of the unconditional pairwise error probability. The rest of the chapter is devoted to deriving expressions of the characteristic function $\phi_v(z)$ for BI-STCM ($p = 1$) and BI-STBC ($p \ge n_T$) systems with different fading statistics.

4.4 Characteristic Function

In this section, we derive the characteristic function $\phi_v(z)$ for two bit-interleaved space-time codes, BI-STCM and BI-STBC, under various fading models.

4.4.1 BI-STCM

In BI-STCM systems, $p = 1$ and $q = n_T$, and thus we use the notations $\mathbf{e}_l = \mathbf{e}_{l,1}$ and $\mathbf{h}_l = \mathbf{h}_{l,1}$. In this case, the distance is given by $d_l^2 = |\mathbf{h}_l \mathbf{e}_l{}^T|^2$. Following the derivation in [10], the distance d_l^2 simplifies to

$$d_l^2 = ||\mathbf{e}_l||^2 \cdot |\beta_l(\mathbf{e}_l)|^2, \tag{4.13}$$

where

$$\beta_l(\mathbf{e}) \triangleq \frac{\mathbf{h}_l\ \mathbf{e}^T}{||\mathbf{e}||}, \tag{4.14}$$

is a random variable whose distribution depends on the fading distribution which will be derived later. This implies that $\{\beta_l(\mathbf{e}_l)\}$ are independent random variables. Given a realization of the error vector $\mathbf{e}_l$, the conditional characteristic function of d_l^2 given $\mathbf{e}_l$ becomes

$$\Psi_{d_l^2|\mathbf{e}_l}(z) = \Psi_{|\beta_l(\mathbf{e}_l)|^2}\left(z||\mathbf{e}_l||^2\right). \tag{4.15}$$

To find $\phi_v(z) = \Psi_{d_l^2|f_l}(z)$, we first consider all $\binom{qm}{2}$ possible STB combinations of $\mathbf{b}_l$ and $\hat{\mathbf{b}}_l$. For each pair, we feed them to the STBC encoder to find the corresponding $\mathbf{x}_l, \hat{\mathbf{x}}_l$, and the error vector $\mathbf{e}_l$. Classify these STB pairs into groups according to $d_H(\mathbf{b}_l, \hat{\mathbf{b}}_l)$. Suppose in the group of $d_H(\mathbf{b}_l, \hat{\mathbf{b}}_l) = v$ bits, the STB pairs of the group generates error vectors $\mathbf{e}_{v,1}, \mathbf{e}_{v,2}, \cdots$ each with multiplicity $\mu_{v,1}, \mu_{v,2}, \cdots$, respectively. Then the conditional joint pdf of $\mathbf{e}_l$ given f_l can be written as

$$f_{\mathbf{e}_l|f_l}(\mathbf{e}|v) = \sum_k \chi_{v,k}\ \Delta(\mathbf{e} - \mathbf{e}_{v,k}), \tag{4.16}$$

where $\chi_{v,k} = \frac{\mu_{v,k}}{\sum_k \mu_{v,k}}$ is the probability mass function for $\mathbf{e}_{v,k}$, and $\Delta(\mathbf{e}) \triangleq 1$ if $\mathbf{e} = \mathbf{0}$; and 0 otherwise. By (4.15) and (4.16), we have

$$\phi_v(z) = \Psi_{d_l^2|f_l}(z) = \sum_k \chi_{v,k}\ \Psi_{|\beta_l(\mathbf{e}_{v,k})|^2}\left(z||\mathbf{e}_{v,k}||^2\right). \tag{4.17}$$

Clearly, the form of $\Psi_{|\beta_l(\mathbf{e}_{v,k})|^2}(z)$ is a function of the fading distribution. In the case of Rician fading, $\{h_{l,t}^i\}$ are complex Gaussian random variables with mean $\sqrt{\frac{\kappa}{1+\kappa}}$ and variance $\frac{1}{1+\kappa}$, where κ denotes the ratio of the specular component energy to the diffuse component energy of each fading channel. Therefore $\beta_l(\mathbf{e}_{v,k})$ is a complex Gaussian random variable with mean $\sqrt{\frac{\kappa}{1+\kappa}} \cdot \zeta(\mathbf{e}_{v,k})$ and variance $\frac{1}{1+\kappa}$ per dimension, where $\zeta(\mathbf{e}) \triangleq \sum_i e^i$ is the sum of all elements of the vector $\mathbf{e}$. Hence, $|\beta_l(\mathbf{e}_{v,k})|^2$ is a noncentral chi-square distributed with a characteristic function [36] given by

$$\Psi_{|\beta_l(\mathbf{e}_{v,k})|^2}(z) = \frac{1+\kappa}{1+\kappa+z} \cdot \exp\left(\frac{-z\ \kappa\ |\zeta(\mathbf{e}_{v,k})|^2 \cdot}{1+\kappa+z}\right), \tag{4.18}$$

which yields

$$\phi_v(z) = \Psi_{d_l^2|f_l}(z) = \sum_k \chi_{v,k} \left[\frac{1+\kappa}{1+\kappa+z\ ||\mathbf{e}_{v,k}||^2} \cdot \exp\left(\frac{-z\ \kappa\ |\zeta(\mathbf{e}_{v,k})|^2 \cdot ||\mathbf{e}_{v,k}||^2}{1+\kappa+z\ ||\mathbf{e}_{v,k}||^2} \right) \right]. \tag{4.19}$$

For the special case of Rayleigh fading, $\phi_v(z)$ is given by

$$\phi_v(z) = \Psi_{d_l^2|f_l}(z) = \sum_k \frac{\chi_{v,k}}{1+z||\mathbf{e}_{v,k}||^2}. \tag{4.20}$$

4.4.2 BI-STBC

In BI-STBC systems the fading gain of each channel remains constant during each STB, i.e., $\mathbf{h}_{l,1} = \mathbf{h}_{l,2} = \cdots = \mathbf{h}_{l,p} = \mathbf{h}_l = \{h_l^i\}$. Recall that $\mathbf{e}_{l,t}$ is a vector of dimension $1 \times n_T$ and denoted by $\mathbf{e}_{l,t} = (e_{l,t}^1, e_{l,t}^2, \cdots, e_{l,t}^{n_T})$. Due to the orthogonality of the row vectors of STBC transmission matrix, we have

$$d_l^2 = \sum_{t=1}^{p} ||\mathbf{h}_l\ \mathbf{e}_{l,t}{}^T||^2 = \sum_{i=1}^{n_T} |h^i|^2 \cdot \xi_l^i,$$

where $\xi_l^i = \sum_{t=1}^{p} |e_{l,t}^i|^2$. Since $\{h_l^i\}$ are i.i.d. random variables, the random variables $\{|h_l^i|^2\}$ are also i.i.d. with characteristic function given by $\Psi_{|h|^2}(z)$. Since $\{|h_l^i|^2\}$ are independent, we can obtain the characteristic function of d_l^2 given $\mathbf{e}_l'$ given a realization of $\mathbf{e}_l' = (\xi_l^1, \xi_l^2, \cdots, \xi_l^{n_T})$ as

$$\Psi_{d_l^2|\mathbf{e}_l'}(z) = \prod_{i=1}^{n_T} \Psi_{|h|^2}\left(z\ \xi_l^i\right). \tag{4.21}$$

Again we feed all $\binom{qm}{2}$ possible STB pairs of $\mathbf{b}_l$ and $\hat{\mathbf{b}}_l$ to the ST encoder to get the vector $\mathbf{e}_l'$. Using a similar approach of finding (4.16) in Section 4.4.1, we can obtain the conditional joint pdf of $\mathbf{e}_l'$ given f_l

$$f(\mathbf{e}_l'|f_l = v) = \sum_k \chi_{v,k}'\ \Delta(\mathbf{e} - \mathbf{e}_{v,k}'). \tag{4.22}$$

Denote the i^{th} component of $\mathbf{e}'_{v,k}$ by $\mathbf{e}'_{v,k}(i)$. By (4.21) and (4.22), we have

$$\phi_v(z) = \Psi_{d_l^2|f_l}(z) = \sum_k \chi'_{v,k} \prod_{i=1}^{n_T} \Psi_{|h|^2}\left(z\ \mathbf{e}'_{v,k}(i)\right). \tag{4.23}$$

Clearly, $\Psi_{|h|^2}(z)$ depends on the fading distribution of the channel. In the following, three different fading distributions are considered; namely, Rayleigh, Rician, and Nakagami.

4.4.2.1 Rayleigh Fading

If $|h|$ is a Rayleigh distributed random variable, substitute (3.19) in (4.23) and we have

$$\phi_v(z) = \sum_k \chi'_{v,k} \left[\prod_{i=1}^{n_T} \frac{1}{1 + z\ \mathbf{e}'_{v,k}(i)}\right]. \tag{4.24}$$

4.4.2.2 Rician Fading

If $|h|$ is a Rican random variable, then the characteristic function is given by substituting (3.25) in (4.23)

$$\phi_v(z) = \sum_v \chi'_{v,k} \left[\prod_{i=1}^{n_T} \frac{1+\kappa}{1+\kappa+z\ \mathbf{e}'_{v,k}(i)} \cdot \exp\left(-\frac{z\ \kappa\ \mathbf{e}'_{v,k}(i)}{1+\kappa+z\ \mathbf{e}'_{v,k}(i)}\right)\right]. \tag{4.25}$$

4.4.2.3 Nakagami Fading

If $|h|$ is a Nakagami random variable, then by substituting (3.28) in (4.23), we get

$$\phi_v(z) = \sum_v \chi'_{v,k} \left[\prod_{i=1}^{n_T} \frac{1}{1+\frac{z}{\mu}\ \mathbf{e}'_{v,k}(i)}\right]^{\mu}. \tag{4.26}$$

where μ denotes the Nakagami fading parameter.

4.5 Multiple-Receive Antennas

In the case of multiple receive antennas, $n_R > 1$, the whole analysis remains the same except for (4.17) of BI-STCM system and (4.23) of BI-STBC system. Because the

fading processes at different receive antennas are identical and independent, we have for BI-STCM

$$\phi_v(z) = \Psi_{d_l^2|f_l}(z) = \sum_k \chi_{v,k} \left[\Psi_{|\beta_l(\mathbf{e}_{v,k})|^2}\left(z||\mathbf{e}_{v,k}||^2\right)\right]^{n_R}, \tag{4.27}$$

whereas (4.23) of BI-STBC becomes

$$\phi_v(z) = \Psi_{d_l^2|f_l}(z) = \sum_k \chi'_{v,k} \left[\prod_{i=1}^{n_T} \Psi_{|h|^2}\left(z\ \mathbf{e}'_{v,k}(i)\right)\right]^{n_R}. \tag{4.28}$$

The rest of the derivation for the characteristic function $\phi_v(z)$ under different fading distributions remains the same.

4.6 Numerical Results

As an illustrative example, we use BI-ST coded systems employing a rate-$\frac{1}{2}$ (5,7) convolutional code with two transmit antennas, i.e., $n_T = 2$. Throughout the results, the random interleaver size is set to $N = 1024$ coded bits. It is expected that increasing the interleaver size improves the performance. The modulation techniques used are quadrature-phase shift keying (QPSK) and quadrature-amplitude modulation 16-QAM. The throughputs of the BI-STBC and BI-STCM systems are mR_c and mn_TR_c bits/s/Hz, respectively. The performance of BI-STBC and BI-STCM over Rayleigh fading channels is shown in Figure 4.2. We observe that the bound is tight to simulation curves at medium-to-high SNR values. Note that the union bound becomes loose for SNR values lower than the cutoff rate of the system [45]. We observe that the performance of BI-STBC is better than that of the BI-STCM. This is because the throughput of BI-STCM is n_T times larger than that of BI-STBC. Furthermore, in BI-STBC there are n_T observations available to detect the transmitted n_T signals, whereas there is only one observation in BI-STCM.

Figures 4.3 and 4.4 show the performance of BI-STCM and BI-STBC over Rician fading channels with different Rician parameters κ. Again, the bound is shown to be tight for a wide range of the LOS energy of the channel. As the LOS energy increases the channel becomes more dominated by the LOS component, and hence the performance of the

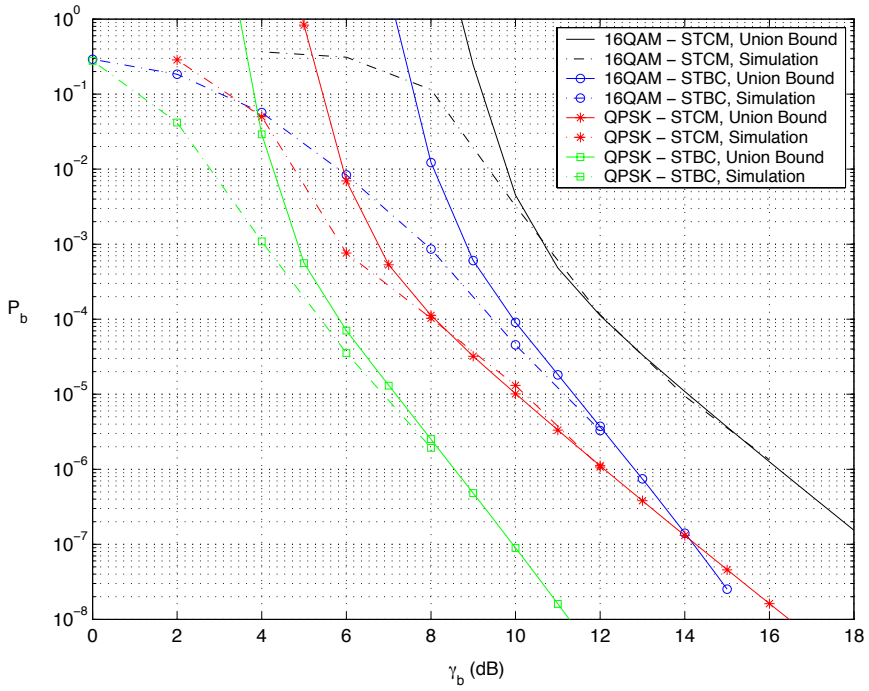

Figure 4.2: Bit error probability of convolutionally encoded BI-ST systems using $n_T = 2$ over a Rayleigh fading channel.

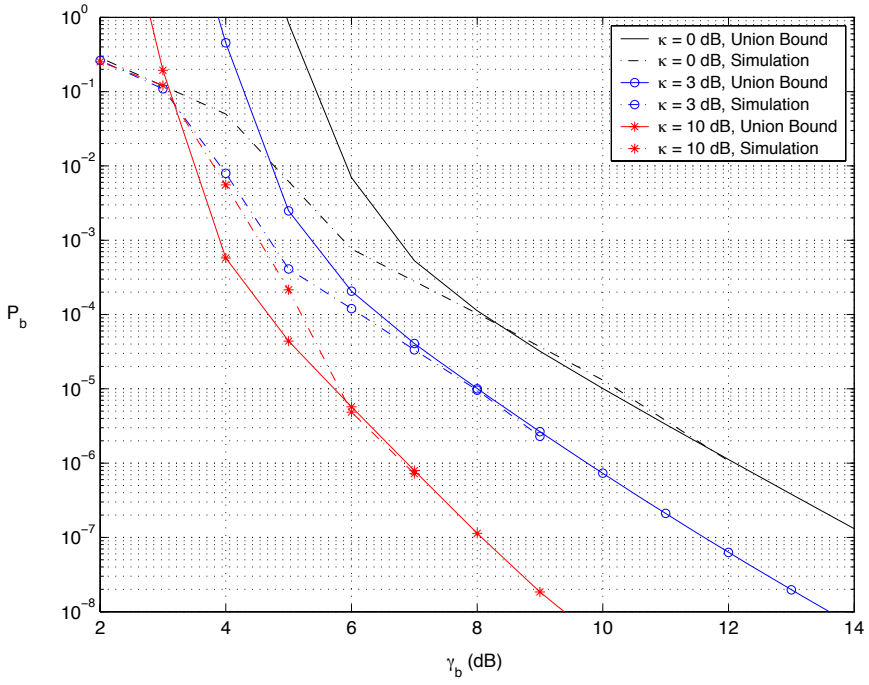

Figure 4.3: Bit error probability of a convolutionally encoded BI-STCM using $n_T = 2$ over Rician fading channels with different κ values.

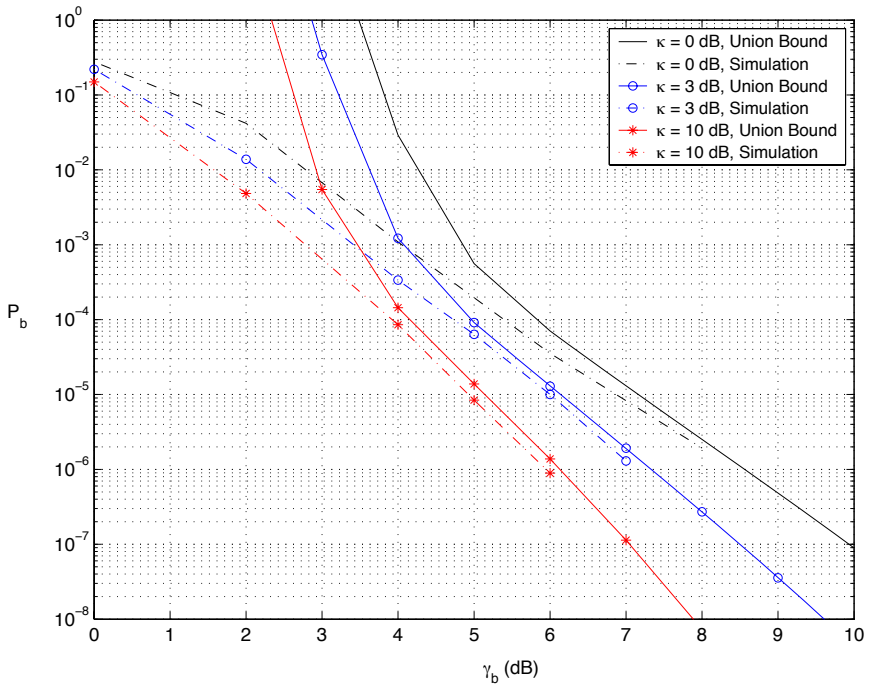

Figure 4.4: Bit error probability of a convolutionally encoded BI-STBC using $n_T = 2$ over Rician fading channels with different κ values.

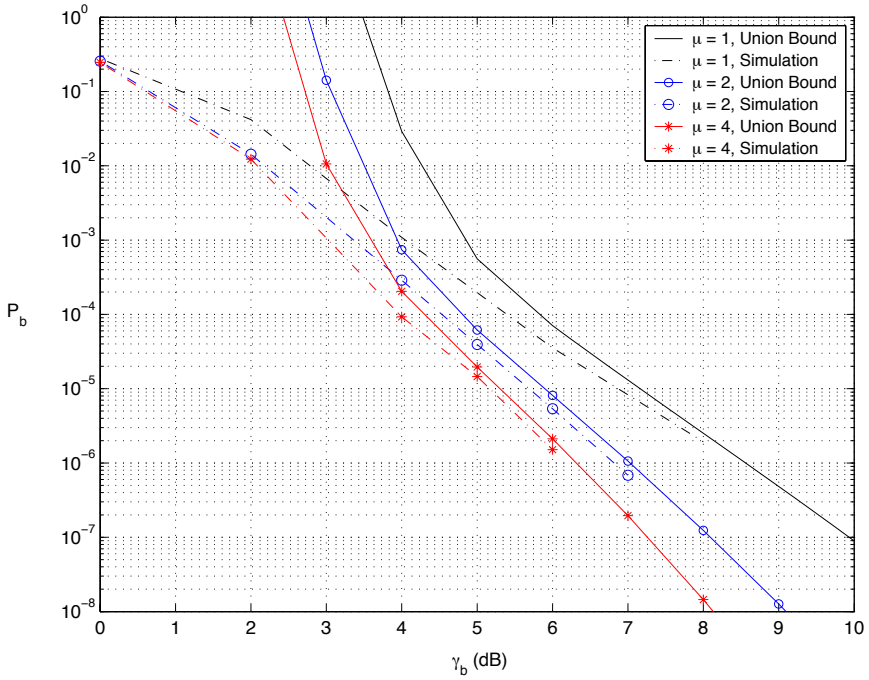

Figure 4.5: Bit error probability of a convolutionally encoded BI-STBC using $n_T = 2$ over Nakagami fading channels with different μ values.

BI-ST coded systems improves. In Figure 4.5 we show the performance of BI-STBC over Nakagami fading channels with different Nakagami parameters μ. As the fading parameter μ of the channel increases, the channel becomes less faded and hence the performance of the BI-STBC system improves accordingly.

4.7 Conclusions

In this chapter we derived union bounds on the packet error probability and the bit error probability of BI-ST coded systems over fast fading channels. The derivation was based on the uniform interleaving of coded bits prior to the ST mapping and encoding. The bound is a function of the distance spectrum of the channel code, the signal constellation, and the ST encoding scheme. The proposed bounds provides an analytical method to evaluate the performance of BI-ST coded systems employing different constellation shapes and sizes as well as different ST encoding schemes. The bound was evaluated for BI-ST coded systems over Rayleigh, Rician and Nakagami fading channels. Results showed that the proposed bound is tight in medium to high SNR regions.

CHAPTER 5

On the Error Floor Analysis of Turbo Codes: Weight Spectrum Estimation (WSE) Scheme

Turbo codes have raised high interest in the past decade due to their great performance close to the Shannon capacity limit. To analyze the outage probability for wireless networks with mobiles that use turbo codes in physical layer, we need to analyze the performance of turbo codes in order to determine the right SINR threshold value for the outage probability computation, just like the case of BICM. In this chapter, our focus is on the performance analysis of turbo codes. In particular, we are interested in finding an efficient algorithm to estimate the weight spectrum of a turbo code, which enables us to obtain an union bound approximation that is very tight to the simulation at high SNR.

5.1 Introduction

Turbo codes have generated much interest in the last decade due to their performance being very close to the channel capacity in Additive White Gaussian Noise (AWGN) channels. Two distinct signal-to-noise ratio (SNR) regions can be identified with respect to the performance of turbo codes: the *waterfall* and the *error floor* regions. The error probability performance in the waterfall region has the characteristic of rapid improvement with a small increase in SNR. The slope of the performance curve is steep in this region. On the other hand, when the SNR is increased past a certain point, the slope is no longer as steep as it is previously. The SNR region beyond this point is called the error floor region although technically the performance is still improving but at a very slow rate.

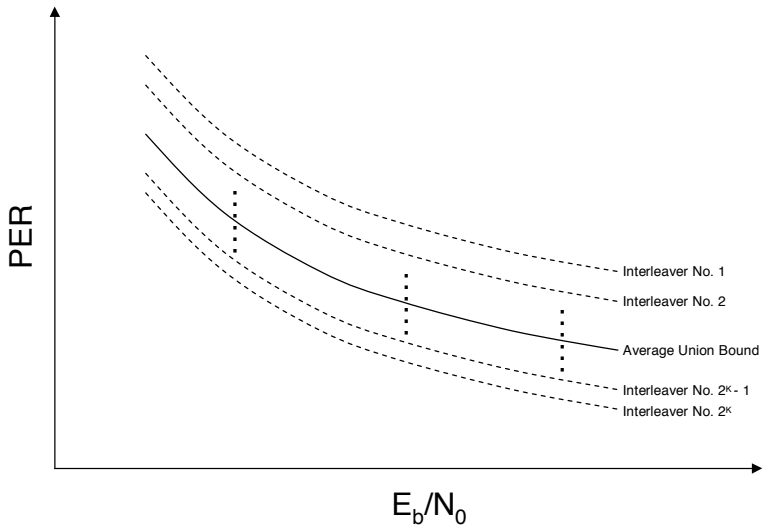

Figure 5.1: Union Bound and the performance of turbo codes with all $K!$ possible interleavers

The performance in the error floor region is not as sensitive to the SNR increment as in the waterfall region. To fully analyze the performance of a turbo code, we need to know the performance in both regions. The performance of a turbo code in the waterfall region has been explored in [46,47]. In this chapter, our main focus is on the error floor analysis of turbo codes.

The performance of a turbo code in the high SNR region is analyzed in [13–16]. All of these papers apply the uniform interleaver assumption to compute the weight spectrum and then the performance is bounded using the weight spectrum. Because a length K uniform interleaver is a probabilistic device that maps a given weight W input word to all possible $\binom{K}{W}$ permutations of the word with equal probability, the weight spectrum computed is actually the average of the weight spectra of the turbo codes with all $K!$ distinct interleavers. The resulting union bound (the solid curve in Fig. 5.1) is the average of the actual union bounds of turbo codes with all $K!$ interleavers (the doted curves). The disadvantage of this type of an average union bound is that it can be very different from the actual performance of the turbo code with a specific interleaver.

In order to accurately analyze the performance of a turbo code with a specific inter-

leaver, one must have a better estimate of the actual weight spectrum rather than the averaged weight spectrum obtained by uniform interleaving. The distance structure of a turbo code was explored in [48] without applying the uniform interleaver assumption, however the focus was only on the minimum distance. In [49, 50], an algorithm was proposed to find the weight spectrum of a turbo code with a specific interleaver. To find the exact weight spectrum for turbo code weights up to d_{max}, the algorithm first searches for all input sequences that produce constituent code weights less than d_{max} on any of the constituent codes. Then it turbo encodes all these input sequences and records the corresponding turbo code weights. The number of input sequences with constituent code weight up to d_{max} is very large since both the input weight and parity weight can go up to d_{max}. This is actually an exhaustive searching algorithm and the computation complexity is of order $F(d_{max}) \cdot K$, where $F(d_{max})$ is a function that grows exponentially with d_{max}. It is mentioned in [50] that $F(d_{max})$ is often much larger than K. Thus the complexity of the algorithm is higher than order K^2, and it often gets worse since we usually choose large d_{max} due to the lack of knowledge about the minimum distance of the turbo code. The high complexity is indeed the major disadvantage of the algorithm. To reduce the complexity, a Viterbi-like algorithm was proposed in [51] and later modified in [52]. For any input sequence, the algorithm uses Viterbi algorithm to check the lower bound of the turbo code weights generated by all input codewords initiated by the input sequence. If the lower bound is larger than a threshold τ, then all those input codewords will be eliminated from the set of input codewords to be searched. The algorithm is more efficient than [50] and performs very well with serially and parallel concatenated schemes. However, the complexity grows exponentially with τ hence an overestimated τ can cause a big problem. Moreover, the algorithm has prohibitive complexity for multilevel turbo codes with more than two constituent encoders. In [53], a different method for estimating the minimum distance was proposed. However, it will not determine the multiplicity nor the remaining lower terms of the weight spectrum.

In this chapter, we propose an efficient method to obtain an accurate estimate of the weight spectrum of a turbo code with a specific interleaver. By going after an estimation

rather than the exact weight spectrum, we are able to significantly reduce the complexity of the search. Since the union bound and thus the performance in the error floor region is dominated by the codewords with small weights, we only focus on the codewords of small code weights. With this weight spectrum estimation of the dominant code weights in the union bound, we can compute the partial sum of the dominant terms (corresponding to those small code weights) in the union bound. This offers an accurate approximation to the actual performance of a turbo code with a specific interleaver. Most important of all, the method is practical and efficient, which is the major merit of this method. The method can also be applied to turbo codes with more than two constituent encoders.

By using the Weight Spectrum Estimation (WSE) method, we see the performance of turbo codes is severely degraded for some interleavers by the existence of small input weight codewords whose all but few 1's are located close to the end of the input block. This degrading effect can be reduced by trellis termination schemes. However, trellis termination schemes introduce more redundancy and yet might not be able to completely eliminate the degrading effect. We develop an interleaver modification algorithm so that the performance of turbo code is not affected negatively by the bits close to the end. Since S-random interleavers are the most popular interleavers used with turbo codes, we propose the modification algorithm for S-random interleavers only. The algorithm can be easily adapted for any other type of interleavers.

The remainder of this chapter is organized as follows. In Section 5.2, we give a brief introduction to the weight spectrum of a turbo code. In Section 5.3, we describe how to approximate the error floor performance using the sum of dominant terms in the union bound. In Section 5.4, we introduce the weight spectrum estimation method for the small code weights of a turbo code with a specific interleaver. In Section 5.5, we introduce our modified S-random interleaver. In Section 5.6, we demonstrate and discuss various numerical examples. Finally, conclusions are addressed in Section 5.7.

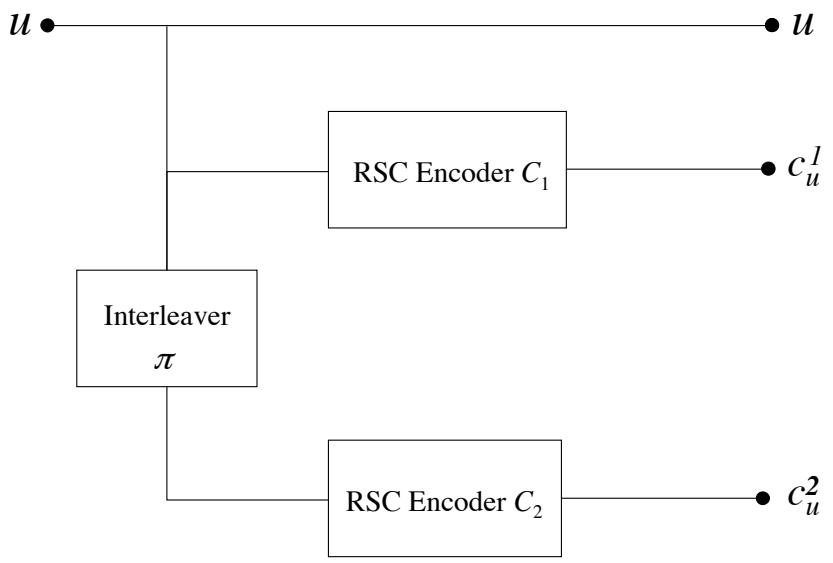

Figure 5.2: A typical turbo encoder with two recursive systematic convolutional (RSC) constituent encoders.

5.2 Weight Spectrum of Turbo Code

We consider a parallel concatenated turbo code with the encoder structure shown in Fig. 5.2. Both constituent encoders C_1 and C_2 are binary Recursive Systematic Convolutional (RSC) encoders, yet they are not necessarily identical to each other. In other words, the turbo codes considered in this chapter can be asymmetric. Though there are only two constituent encoders in the turbo encoder, the results in this chapter can be easily generalized to turbo codes with more than two constituent encoders. Binary Phase Shift Keying (BPSK) is used throughout this chapter, however the work is not restricted to BPSK.

If we fix the input codeword length K of the turbo code, the weight spectrum of the turbo code [13] can be expressed by $A(D, P)$ which has the following form

$$A(D, P) = \sum_{d>0} \sum_{p>0} a_{d,p} D^d P^p, \tag{5.1}$$

where $a_{d,p}$ is the number of codewords with input Hamming weight p and parity Ham-

ming weight d (the term "weight" will refer to Hamming weight hereafter). Due to the existence of the interleaver π before C_2, it is difficult to find the weight spectrum of the turbo code analytically.

5.3 Error Floor Performance of Turbo Code

A turbo decoder consists of multiple constituent decoders that exchange soft information (for example, with BCJR algorithm [54]), as opposed to hard decisions, with one another. This iterative decoding algorithm is actually a suboptimal decoding algorithm. However, it is conjectured in the literature that the suboptimal turbo decoding algorithm performs almost the same as the Maximum Likelihood Bit Decoding (MLBD) at high SNR. Since MLBD and Maximum Likelihood Sequence Decoding (MLSD) behave identically at high enough SNR, the turbo decoder performance should be very close to the MLSD performance at high SNR. Due to the fact that the MLSD performance at high SNR can be upper bounded by the union bound, the union bound should also bound the turbo code performance at high SNR, i.e. in the error floor region.

Given the weight spectrum of a turbo code, the PER in an AWGN channel in the error floor region can be bounded by the union bound [21]

$$\mathrm{PER} \leq \sum_{d>0} \sum_{p>0} a_{d,p}\, Q\left(\sqrt{2R_c(d+p)\frac{E_b}{N_0}}\right), \tag{5.2}$$

where R_c is the turbo code rate and $\frac{E_b}{N_0}$ is the SNR per bit. Due to the fact that $Q(x)$ decreases quite sharply with increasing x, the union bound is dominated only by the terms with small code weights $d+p$. Thus, instead of summing up all of the terms in the union bound, we can approximate the PER in an AWGN channel by just summing up the terms associated with the first several smallest code weights, i.e.

$$\mathrm{PER} \simeq \mathrm{PER}(n) = \sum_{(d,p) \in\, G_n} \sum a_{d,p}\, Q\left(\sqrt{2R_c(d+p)\frac{E_b}{N_0}}\right), \tag{5.3}$$

where G_n is the set of (d, p) whose sum $d + p$ equals to one of the first n smallest code weights of the turbo codes for a sufficiently large n. Similarly we can approximate the BER in an AWGN channel by

$$\mathrm{BER} \simeq \mathrm{BER}(n) = \sum_{(d,p) \in G_n} \sum \frac{d}{K} \; a_{d,p} \; Q\left(\sqrt{2R_c(d+p)\frac{E_b}{N_0}}\right). \tag{5.4}$$

In practice, $\mathrm{PER}(n)$ converges to a curve as n increases. Convergent behavior is observed at relatively small n (typically $n = 10$ is sufficient for our numerical experiments). Because the union bound and the error floor region performance are dominated by the terms corresponding to these first several smallest code weights, we will call these code weights *dominant code weights* hereafter. A very efficient weight spectrum estimation method for these dominant code weights will be introduced in the following section.

To compute the union bounds on the PER and BER for various fast varying fading channels, we should use the integral expression of the Q-function as we did in Chapter 3. For Rayleigh fading case, we only have to replace the Q-function term in (5.3) and (5.4) by $\frac{1}{1+4(d+p)\beta(\theta)}$ where $\beta(\theta) = \frac{R_c Eb}{4N_0 \sin^2\theta}$. For a Rician fading channel of parameter κ, the Q-function should be replaced by $\frac{1+\kappa}{1+\kappa+4(d+p)\beta(\theta)} \cdot \exp\left\{-\frac{4\kappa(d+p)\beta(\theta)}{1+\kappa+4(d+p)\beta(\theta)}\right\}$. Finally for a Nakagami fading channel of parameter μ, we should replace the Q-function by $\left[\frac{1}{1+4(d+p)\beta(\theta)}\right]^{\mu}$.

5.4 Weight Spectrum Estimation

Consider the original turbo code structure in Fig. 5.2. The weight of a turbo codeword $c_u = (u, c_u^1, c_u^2)$, where c_u^i corresponds to the parity sequence from the i^{th} encoder, is defined as

$$w(c_u) = w(u) + w(c_u^1) + w(c_u^2). \tag{5.5}$$

The length of the input sequence u is K. In the case that $w(c_u)$ is small, both $w(u)+w(c_u^1)$ and $w(u) + w(c_u^2)$ should be small. This means that both constituent codes should provide small code weights. In other words, the input sequences that generate small turbo

code weights should very likely be contained in the set of input sequences that generate small code weights with constituent encoders C_1 or C_2 (in Fig. 5.2). Hence we have the following approximation to efficiently estimate the weight spectrum of the turbo code

Approximation: If u generates the n^{th} minimum of $w(u) + w(c_u^1) + w(c_u^2)$, then it is most likely that $u \in H_1 \cup H_2$, where H_i is the set of input sequences that generate the first n smallest constituent code weights of C_i, $i = 1, 2$.

This leads us to the following weight spectrum estimation algorithm:

1. Find H_1 and H_2, the sets of sequences that generate first n smallest code weights of C_1 and C_2 respectively.

2. For each data sequence $u \in H_1 \bigcup H_2$, turbo encode u. Record the input weight d and the resulting turbo parity weight p of each input sequence.

3. Compute the multiplicity of each turbo weight pair (d, p) to get the weight spectrum estimate $a_{d,p}$ of the dominant turbo code weights.

Now the remaining question is how to efficiently obtain H_1 and H_2 for the turbo code. Several paths on a typical trellis diagram of a RSC constituent encoder are shown in Fig. 5.3. We define a *single error event* as the divergence of the constituent encoder from the zero-state and its first convergence back to the zero-state after the divergence such as case (a) and (b). A *tail error event* is defined as the divergence from the zero-state occurred close to the end of the input block, which is shown as case (c). Notice that for a single error event, the constituent encoder has to return to the zero-state, which is not necessary for a tail error event. A *multiple error event* is a collection, or concatenation, of several single error events or tail error events shown as in case (d). Note that a recursive encoder which does not return to the zero-state continues to produce nonzero parity bits even though its current input bits are all 0's[1]. Unless the error events of an input

[1]This statement is true unless there exists a loop with zero-input and zero-output in the state diagram

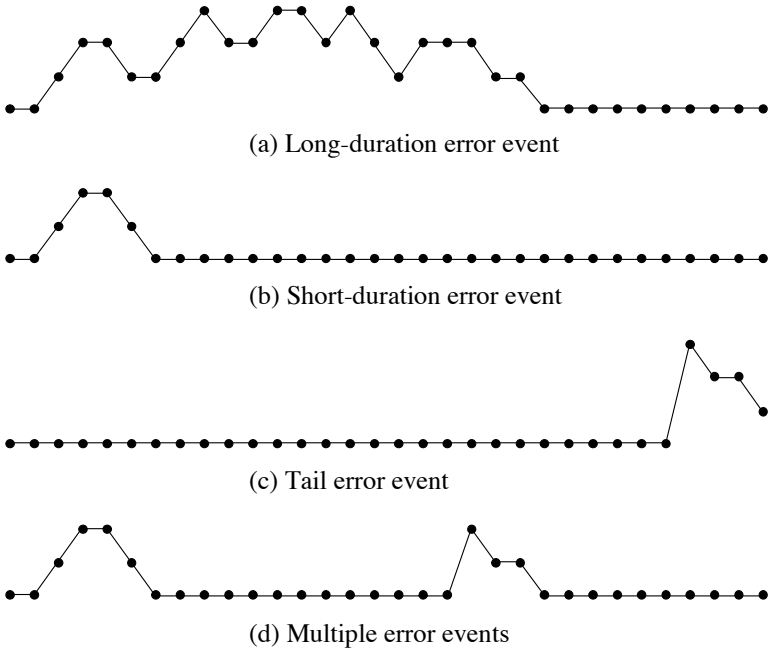

Figure 5.3: Typical trellis diagrams generated by the RSC constituent encoder.

sequence are all of short durations, the weight of the constituent codeword is large. Case (a) in Fig. 5.3 has an error event of long duration which should generate a large constituent code weight. On the contrary for (b), (c) and (d), which all consist of error events of short durations, the corresponding constituent codewords should have small weights. Since we are only interested in the input sequences that generate small weights on each constituent encoder, we should ignore (a) and focus only on (b), (c), and (d). H_i is then the set of input sequences that generate such short-duration error events for C_i.

The search for H_1 and H_2 is separated into two phases. Phase I searches for input sequences that generate single error events or tail error events like (b) and (c), while Phase II searches for multiple-error-event input sequences like (d). Consider an input sequence that generates multiple error events from C_1 and each error event is of short

of the recursive code. This sort of recursive code should be avoided in practice since it brings out small weight codewords. Such a code can be easily detected by the state transition matrix of the code. When raised to the L^{th} power, this matrix is the L-step transition matrix with polynomial elements. If any of its diagonal elements (other than the one corresponding to the zero-state) contains a nonzero constant term, there exists such a loop. The code should be avoided and thus ignored here.

duration. The parity weight generated by C_1 could be small since each error event is short. However, since the weight of the input sequence is at least two times the number of error events, there must be many 1's in the input sequence. After interleaving, these 1's are distributed over the input block to C_2. Since only specific bit sequences can force the RSC encoder C_2 back to the zero-state, it is very unlikely for the error events generated by $\pi(u)$ from C_2 to be all of short durations. The parity weight generated by C_2 is thus very large and results in a large turbo code weight. A good discussion of this issue is given in [55]. Hence for most cases, the error performance is dominated by single-error-event input sequences and thus Phase I search is enough which is only of complexity K. The weight spectrum estimation and the PER and BER approximations can be obtained very efficiently. However, for a turbo code with very large minimum distance, the code weight of a multiple-error-event input sequence might not be that large compared to the minimum distance. Therefore we have to proceed to Phase II search to obtain an accurate weight spectrum estimation. The WSE algorithm as a whole is illustrated by the flow chart in Fig. 5.4. The various testing criterions shown in the flow chart will be addressed later in the following sections.

5.4.1 Phase I: Single Error Event and Tail Error Event Search

In this phase, we want to search for input sequences that generate a single error event or tail error event for either C_1 or C_2. The Single error event case will be considered first. For each error event, define an *error fragment* as the portion of the input sequence that corresponds to the error event. For instance, if the input sequence associated with case (b) in Fig. 5.3 is $u = [01001010000\cdots0]$, then the error fragment is $[100101]$. Let j_s and j_e be the bit indices of the first and the last 1's in a single-error-event input sequence u, we define the span of u as

$$\mathrm{span}(u) = j_s - j_e + 1. \tag{5.6}$$

For instance, for the previously defined u, we have $j_s = 2$, $j_e = 7$. Hence $\mathrm{span}(u) = 7 - 2 + 1 = 6$. Note that $\mathrm{span}(u)$ is the duration of the error event generated by u on

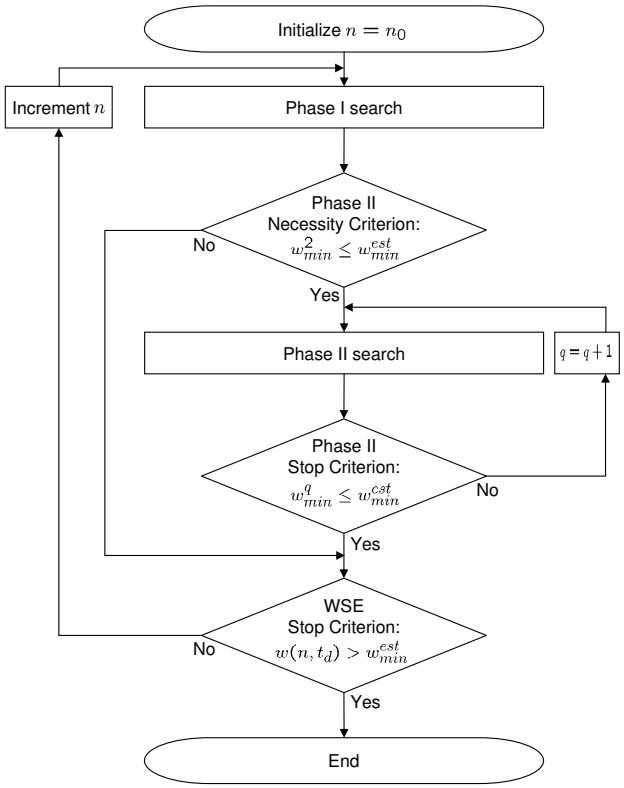

Figure 5.4: Flow chart of WSE algorithm.

the constituent encoder considered, which also equals to the number of bits contained in the associated error fragment.

Define the shift of an input sequence as any circular shift of the input sequence (with respect to period K) that still keeps all of the error fragments of the input sequence intact after the circular shift. Since shifting an input sequence does not change the bit content of any error fragment and thus the corresponding error event, the resultant constituent codeword weight will still remain the same. Hence, we will consider only the single-error-event input sequences that start with 1. We call these sequences *basic input sequences* hereafter.

Now define set S_1^m as the set of basic input sequences with span less than or equal to m that achieves the $1^{st}, 2^{nd}, \ldots, n^{th}$ smallest constituent code weights of C_1, and all of the shifts of these basic input sequences. It has the following form

$$S_1^m = \bigcup_{i=1}^{n} \arg_u^m \min_i \{w(u) + w(c_u^1)\}, \tag{5.7}$$

where

$$\arg_u^m \min_i \{f(x)\} \triangleq \{u \mid \text{span}(u) \leq m, f(u) \text{ is the } i^{th} \text{ minimum of } f(x)\}. \tag{5.8}$$

Similarly, all the arguments hold for the constituent encoder C_2 and the set of basic input sequences associated with C_2 is of the following form

$$S_2^m = \bigcup_{i=1}^{n} \arg_u^m \min_i \{w(u) + w(c_u^2)\}. \tag{5.9}$$

Note that it is $\text{span}(\pi(u))$ now upper bounded by m, not $\text{span}(u)$. In practice, n and m need not be chosen very big. S_1^m and S_2^m contain most of the input sequences that generate single error events with small code weights on either one of the constituent codes. The input sequences that generate small turbo code weights would be most likely contained in these two sets. However, there is another type of sequence which is also very likely to have a small constituent code weight: tail-error-event input sequences. That is, if $w(u)$ is small and all the 1's in u happen to be located very close to the end, the weight of (u, c_u^1) is small and upper bounded by $(K - \mathcal{I}_u + 1)/R_{C_1}$, where $\mathcal{I}_u$ is the bit index of the first 1 in u and R_{C_1} is the rate of the first constituent code. Similar thing also happens to the second constituent code if all 1's are distributed close to the end of $\pi(u)$. In order to take this effect into consideration we will also define the following input sequence sets for C_1 and C_2 respectively

$$T_1^{t_1} \triangleq \{u \mid \mathcal{I}_u > K - t_1\}, \tag{5.10}$$

$$T_2^{t_2} \triangleq \{u \mid \mathcal{I}_{\pi(u)} > K - t_2\}, \tag{5.11}$$

with some thresholds t_1 and t_2.

As mentioned earlier, for input sequence u with large $w(u)$, it is very unlikely for

both u and $\pi(u)$ to generate small parity weight with the associated constituent codes. We can reduce the size of each set by setting a small upper limit t_d for $w(u)$, which is generally set to be no larger than 4. The complexity reduction in our proposed method compared to other methods in the literature comes with this realization. The set of input sequences we are searching for in Phase I would then be

$$S_1^{m\prime} \cup T_1^{t_1\prime} \cup S_2^{m\prime} \cup T_2^{t_2\prime}, \tag{5.12}$$

where

$$S_i^{m\prime} = S_i^m \cap \{u \mid w(u) < t_d\}, i \in \{1, 2\}, \tag{5.13}$$

$$T_i^{t_i\prime} = T_i^{t_i} \cap \{u \mid w(u) < t_d\}, i \in \{1, 2\}. \tag{5.14}$$

Note that if we only perform Phase I search, then $H_1 = S_1^{m\prime} \cup T_1^{t_1\prime}$ and $H_2 = S_2^{m\prime} \cup T_2^{t_2\prime}$. Since thresholds t_1 and t_2 are generally small and t_d no larger than 4 in practical applications, we can obtain $T_i^{t_i\prime}$ efficiently even through exhaustive search over all $\binom{t_1}{t_d} + \binom{t_2}{t_d}$ codewords. Sets $S_i^{m\prime}$ can be obtained very easily by applying Viterbi algorithm on the trellis of C_i. The cost function is defined as the constituent code weight generated by C_i, $w(u) + w(c_u^i)$. Assuming that we want to obtain $S_1^{m\prime}$, we should work on the trellis of C_1. Since we only focus on single-error-event input sequences that start with 1, all paths must begin with input bit equals to 1 and the cost of the branch that departs from the zero-state should be infinity at all stages except the 1^{st} stage. At each stage of the Viterbi algorithm, we compute the code weight of each surviving path should we terminate it right away (i.e. append bits to the input sequence to force it going back to the zero-state right after the current stage). Only the paths with input weight less than t_d that generate the first n smallest code weights get to survive. Since no path can depart once it enters the zero-state, the algorithm will stop once the surviving paths all rest in the zero-state. $S_1^{m\prime}$ is then the resulting set of the surviving sequences. We can obtain $S_2^{m\prime}$ using a similar approach.

5.4.2 Phase II: Multiple Error Event Search

When the minimum distance of the turbo code is large (which often happens for large interleaver sizes), the contribution of multiple-error-event input sequences of each constituent encoder to the weight spectrum of small turbo code weights could be significant and thus can not be ignored. It is stated in a lemma in [55] that when the interleaver size is large, only multiple-error-event input sequences of each constituent encoder whose error fragments are all of weight 2 have significant contribution to the weight spectrum of the turbo code. Hence in Phase II, we only examine such multiple-error-event input sequences. This significantly reduces the set of the multiple-error-event input sequences to be examined for weight spectrum estimation. To further reduce the set of sequences, we set a limit on the weight of each single error event. The weight of each single error event must not exceed the r^{th} smallest (constituent) code weight generated by the weight 2 basic input sequences of C_i. In other words, we consider only input sequences that are concatenations of error fragments from B_i where

$$B_i \triangleq \{u \mid u \text{ is the error fragment of } v, \text{ where } v \text{ is a weight 2 basic input sequence of } C_i \text{ that produces one of the first } r \text{ smallest parity weights among all weight 2 basic input sequences of } C_i\}.$$

Note that B_i can be easily obtained after the basic input sequence search in Phase I algorithm by eliminating basic input sequences of weights greater than 2 from set H_i.

Define $p^2_{min,i}$ as the minimum parity weight generated by C_i using input sequences of weight 2. $p^2_{min,i}$ can be obtained directly from the transfer function of C_i. The lower bound of the turbo code weight generated by a multiple-error-event input sequence which consists of q weight 2 error fragments is then

$$w^q_{min} = q \cdot (2 + p^2_{min,1} + p^2_{min,2}). \tag{5.15}$$

This gives us the testing criterion for the necessity to performing Phase II.

Necessity criterion of Phase II: Let w_{phase_I} be the minimum turbo code weight found in a Phase I search. If $w_{min}^2 = 2 \cdot (2 + p_{min,1}^2 + p_{min,2}^2) \leq w_{phase\_I}$, then it is necessary to proceed on Phase II.

The Phase II algorithm can be decomposed to stages $2, 3, 4,$ and so on. In stage q, we consider all possible length K concatenations of q error fragments from B_i, $i = 1, 2$. The number of input sequences examined in stage q is of order $|B_i|^q \binom{K}{q}$, where $|B_i|$ denotes the size of B_i. The number could be large if K is large and $q \neq 1$. Similar to the *necessity criterion*, we can obtain the *stop criterion* of Phase II by comparing the minimum turbo code weight obtained up to stage $q-1$ with w_{min}^q. The Phase II algorithm is described as follows.

1. Initialize q to 2. Let $w_{min}^{est} = w_{phase\_I}$.
2. Generate set H_i^q by first choosing any q error fragments from B_i (repeated choice allowable). Concatenate these q error fragments and pad 0's between each of them to make the overall sequence length K. Generate sequences with all possible zero-padding combinations and include all of the shifts of the sequences into the set.
3. For each $u \in H_1^q$, turbo encode u. For each $v \in H_2^q$, turbo encode $\pi^{-1}(v)$. Record d the input weight and p the resulting turbo parity weight of each input sequence. If $\exists\ (d, p)$ s.t. $d + p < w_{min}^{est}$, set $w_{min}^{est} = d + p$.
4. Compute the multiplicity of each turbo weight pair (d, p) to update the weight spectrum estimation $a_{d,p}$.
5. *Stop criterion of Phase II*: If $w_{min}^{est} < w_{min}^{q+1}$, stop. Else set $q = q + 1$, goto Step 2.

Note that when K is large, it takes a long time to run Phase II. However, we can significantly reduce the amount of time in step 3. Keep in mind that we are considering the concatenations of error events of C_i with C_i resting in the zero-state in between. When C_i is in the zero-state, it is not necessary to do the encoding at all since the output

is always 0. This can save us considerable computation time because most of the time C_i is in the zero state. We can also save some computation time by keeping track of the current total code weight when we encode on each constituent encoders. Once the current total code weight is significantly larger than w_{min}^{est}, we can stop turbo encoding right away without having to finish it. After applying these two approaches, Phase II can be done much more efficiently.

5.4.3 Accuracy Analysis and Stopping Criterion of WSE

In this section, we want to analyze the accuracy of the WSE algorithm by deriving a lower bound for the minimum undetected turbo code weight for any given n and t_d used in the algorithm. Denote the free distance of the i^{th} constituent code by $d_{free,i}$. It is clear that all sequences checked by our methods satisfy $w(u) + w(c_u^i) \leq d_{free,i} + (n-1)$. Recall that input sequences with $w(u) \geq t_d$ are unlikely to cause small code weights [55]. Disregarding such input sequences, if a sequence u' is not checked by our method, we have

$$w(u') + w(c_{u'}^1) \geq d_{free,1} + (n-1) + 1 = d_{free,1} + n, \tag{5.16}$$

$$w(u') + w(c_{u'}^2) \geq d_{free,2} + (n-1) + 1 = d_{free,2} + n, \tag{5.17}$$

which implies the turbo code weight of u' satisfies

$$w(u') + w(c_{u'}^1) + w(c_{u'}^2) \geq d_{free,1} + d_{free,2} + 2n - w(u'). \tag{5.18}$$

Since for u' with large $w(u')$, the turbo code weight is generally large and u' will not be of our interest. So we also assume $w(u') \leq t_d$, and thus we have

$$w(u') + w(c_{u'}^1) + w(c_{u'}^2) \geq w(n, t_d) \triangleq d_{free,1} + d_{free,2} + 2n - t_d. \tag{5.19}$$

What this bound implies is that if WSE ignores a sequence u', the turbo code weight generated by u' should be larger or equal to $w(n, t_d)$. In other words, $w(n, t_d)$ is the lower bound of the undetected turbo code weights. Conversely this means that WSE can find all of the turbo code weights up to $w(n, t_d) - 1$. Not only this bound tells us how good WSE works for any given n and t_d, but it also provides a stop criterion for WSE. As we mentioned, WSE can find all turbo code weights up to $w(n, t_d) - 1$. So if w_{min}^{est}, the minimum turbo code weight among the sequences checked by WSE so far, satisfies $w_{min}^{est} \geq w(n, t_d)$, this means $w(n, t_d)$ might be smaller than the d_{min} of the turbo code and WSE is not guaranteed to have captured d_{min}. We should increment n and return to Phase I search again. On the other hand, if $w_{min}^{est} < w(n, t_d)$, this implies that our method has captured d_{min} and we can stop there since we only care for the turbo code weights close to d_{min}. This gives us the *stopping criterion* of WSE.

5.5 Modified S-random Interleaver

In Section 5.4.1, we mentioned that input sequences with small weights and all 1's distributed close to the end of the sequences will generate constituent codewords with small weights. If $w(u)$ is small, for some sequence u with tail 1's, there is some possibility that the interleaved $\pi(u)$ might have all of its 1's again distributed at the tail part. Hence, both C_1 and C_2 generate small constituent parity weights and the overall turbo code weight is small. We call such kind of codeword *heavy tail codeword*. In our turbo code simulations with various interleavers, we found that this phenomenon occurred quite frequently and degraded the error floor performance of turbo codes significantly. The degrading effect from the heavy tail codewords can be reduced by trellis termination schemes. However, trellis termination schemes introduce more redundancy and yet might not be able to completely eliminate the degrading effect from all heavy tail codewords. Consider a sequence with one nonzero bit which is located close to the end of a data block both before and after interleaving. The weight of each constituent code's parity is larger than the unterminated case by at most twice the memory size of the

constituent encoder. The resultant turbo codeword can still have a small weight if both constituent codes have small memory sizes. In order to overcome this problem, we propose an interleaver modification algorithm so that we can fix any existing interleaver and never have to suffer from the heavy tail codewords. No trellis termination is needed and thus the rate and the energy efficiency will not be sacrificed. The key idea is to modify the interleaver so that any bit close to the end of an input sequence will be interleaved to another bit position that is far away from the end of the sequence. This ensures that heavy tail problem will not occur simultaneously on both constituent encoders. Since S-random interleavers are the most popular interleavers used in turbo encoders, we will describe our modification algorithm based on S-random interleavers. The algorithm can be easily modified to apply to any other type of interleavers. Assume that the interleaver size is K, the S-parameter equals to S, and we use π_i to denote the new bit index of the i^{th} bit after interleaving ($i = 1, 2, \ldots, K$). The algorithm is described as follows.

1. Initialize t to $K - T$ for some threshold T.
2. Randomly pick an integer i from $\{1, 2, \ldots, K - T - 1\}$.
3. If $\pi_i \geq K - T$, go to step 2.
4. For $j = max\{1, i - S\}$: $min\{K, i + S\}$, check if $|\pi_t - \pi_j| > S$. If not, go to step 2.
5. For $j = max\{1, t - S\}$: $min\{K, t + S\}$, check if $|\pi_i - \pi_j| > S$. If not, go to step 2.
6. Swap the value of π_t and π_i. Set $t = t + 1$.
7. If $t \leq K$ goto step 2, otherwise stop.

The larger the threshold T is, the larger the guarantee it is to completely eliminate the heavy tail problem. Typically we choose T to be about twice the minimum weight of the turbo code.

5.6 Numerical Examples

In this section, we demonstrate the comparison of the simulation results of various turbo codes in an AWGN channel with the uniform interleaving bounds (UIB) and our performance approximations. All of the weight spectrum estimates are obtained from Phase I with parameters $n = 10$, $m = 100$, $t_d = 4$, and $t_1 = t_2 = 60$. This is the typical setting of the parameters. They are set large enough to give accurate performance approximation yet small enough to obtain the performance approximation efficiently in a short amount of time. We first ran simulations for the symmetric turbo code $(1, 33/37, 33/37)$ with two different S-random interleavers with $S = 12$, input length $K = 1000$, and code rate $R_c = 1/3$. From Fig. 5.5−5.6, we can see that $\mathrm{PER}(n)$ is very accurate. While UIB is off the simulated PER by 0.5 to 0.8 dB, $\mathrm{PER}(10)$ is only off within 0.1 to 0.2 dB. As we mentioned earlier, this is because UIB uses the weight spectrum derived from the uniform interleaving assumption, which can in no way account for the use of a specific interleaver. This is why UIB fails to capture the performance of a turbo code with a specific interleaver. This also shows the merit of the proposed weight spectrum estimation method. Notice that when n is large, $\mathrm{PER}(n)$ converges to a curve. Usually $n = 10$ is large enough to observe the convergence.

In Fig. 5.7 we show the simulation results of an asymmetric turbo code $(1, 5/7, 33/23)$ with S-random interleaver. Although we can not observe the occurrence of the error floor in simulation, the trend of the simulation curve indicates that $\mathrm{PER}(n)$ should be very close to the error floor performance. On the other hand, it can be seen that UIB is off by around 0.75 dB.

In Fig. 5.8, we consider a punctured turbo code $(1, 5/7, 33/23)$ with S-random interleaver. The figures show that our performance approximation method works very well. The UIB works well too, but not as accurately as $\mathrm{PER}(10)$ in Fig.5.8. One reason why the UIB works pretty well with punctured turbo codes is because the inaccuracy of the weight spectrum approximation from the uniform interleaver assumption is reduced. When the constituent parity bits are punctured, the proportion of the parity weight among the

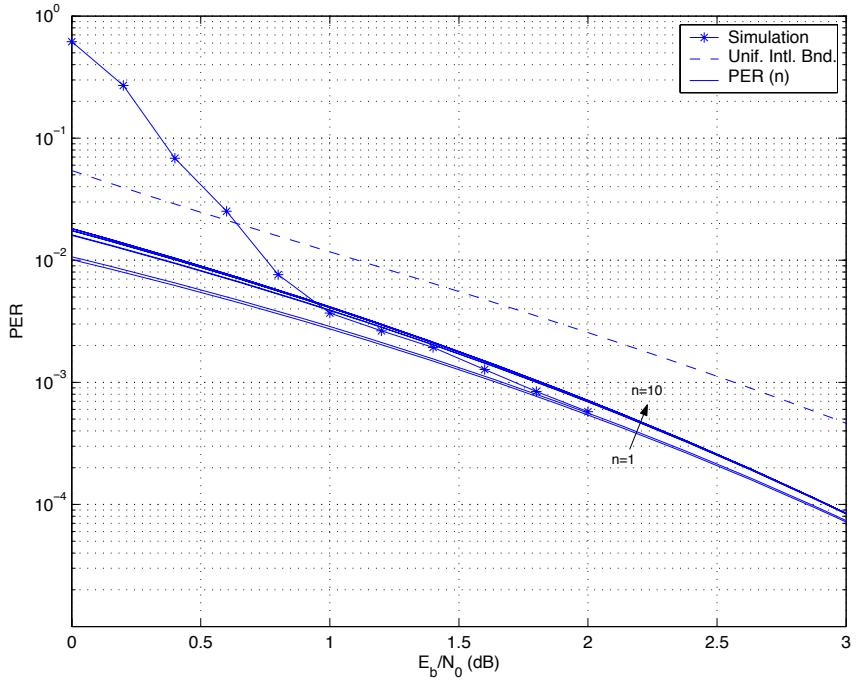

Figure 5.5: $(1, 33/37, 33/37)$ turbo code with interleaver #0, $S = 12$, $K = 1000$, and $R_c = 1/3$.

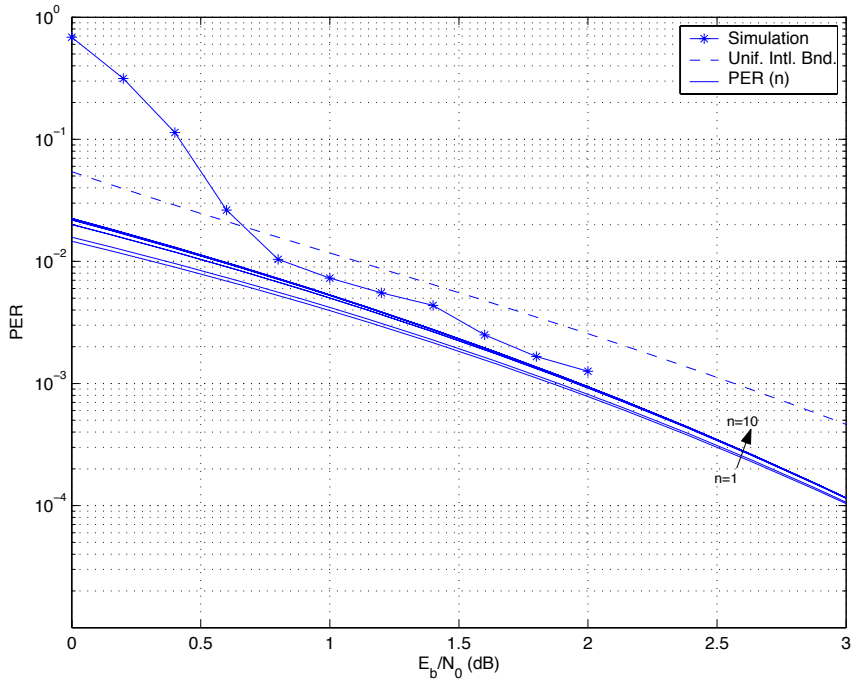

Figure 5.6: $(1, 33/37, 33/37)$ turbo code with interleaver #1, $S = 12$, $K = 1000$, and $R_c = 1/3$.

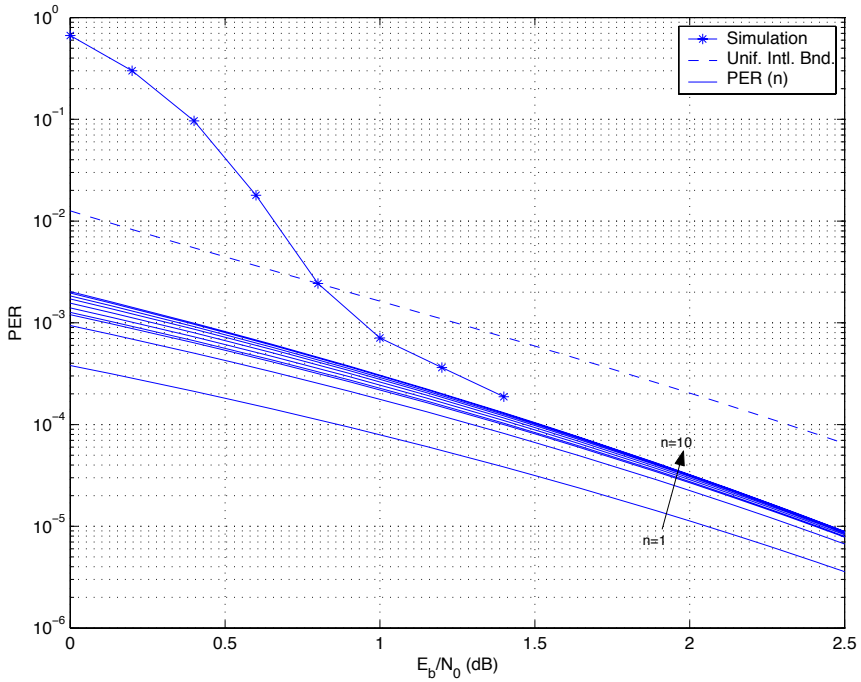

Figure 5.7: $(1, 5/7, 33/23)$ turbo code with interleaver #1, $S = 12$, $K = 1000$, and $R_c = 1/3$.

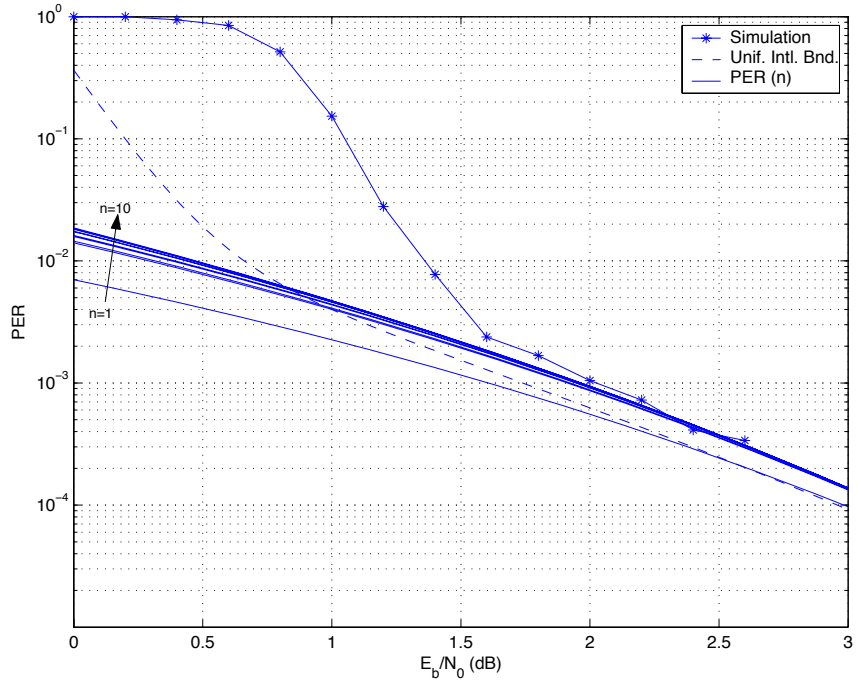

Figure 5.8: $(1, 5/7, 33/23)$ punctured turbo code with interleaver #1, $S = 12$, $K = 1000$, and $R_c = 1/2$.

whole turbo code weight is reduced. Since the inaccuracy of the weight spectrum from the uniform interleaver assumption originates from the second constituent parity generated after interleaving, the weight spectrum inaccuracy is reduced when the proportion of the parity weight is reduced by the puncturing. Therefore, the UIB works pretty well in this case. In other words, the UIB works well when the code rate is higher (since the proportion of the parity weight is small, the inaccuracy is also small) and bad when the code rate is low. However, in either cases, the proposed weight spectrum estimation method still gives better performance approximation than UIB.

In Fig. 5.9, we compare the accuracy of $\mathrm{PER}(10)$ obtained from Phase I for a $(1, 5/7, 5/7)$ turbo code and a $(1, 33/37, 33/37)$ turbo code. As we can see, $\mathrm{PER}(10)$ is very accurate for the $(1, 33/37, 33/37)$ turbo code, but not very well for the $(1, 5/7, 5/7)$ turbo code. The reason is because the Necessity Criterion for Phase II is false for the $(1, 33/37, 33/37)$ turbo code ($w^2_{min} = 20$, $w_{phase\_1} = 16$) and true for the $(1, 5/7, 5/7)$ turbo code ($w^2_{min} = 20$, $w_{phase\_1} = 20$). After we performed Phase II for the $(1, 5/7, 5/7)$ turbo code, the resulting $\mathrm{PER}(10)$ becomes much more accurate.

The merit of this WSE scheme compared to other Viterbi-like searching methods is the linear complexity of the algorithm with the number of encoders. The number of sequences that should be considered stays the same while they are fed to more constituent encoders only. Fig. 5.10 shows the simulation results and error rate approximation based on the proposed algorithm for a multilevel turbo code. The multilevel turbo code is obtained by adding a third encoder with an interleaver to the original turbo coding scheme. Three identical 4-state codes were concatenated to obtain the code. Two S-random interleavers were utilized for concatenation. The extended serial decoding [56] is used as the decoding algorithm of the multilevel code. The error floor is quite low as seen in the plot. The proposed method is able to obtain a very good error rate approximation in a time-efficient manner.

Finally in Fig. 5.11, we show the performance comparison between an S-random interleaver and the modified S-random interleaver. From the figure we can see that the performance gain is about 0.25 to 0.5 dB at high SNR. We successfully improve the

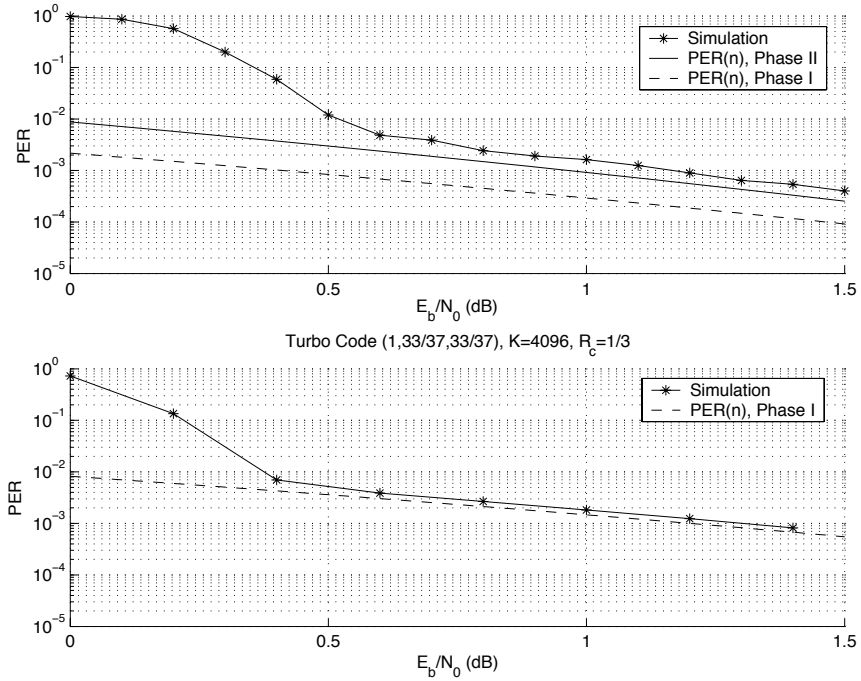

Figure 5.9: $(1, 5/7, 5/7)$ and $(1, 33/37, 33/37)$ turbo codes with $K = 4096$ and $R_c = 1/3$.

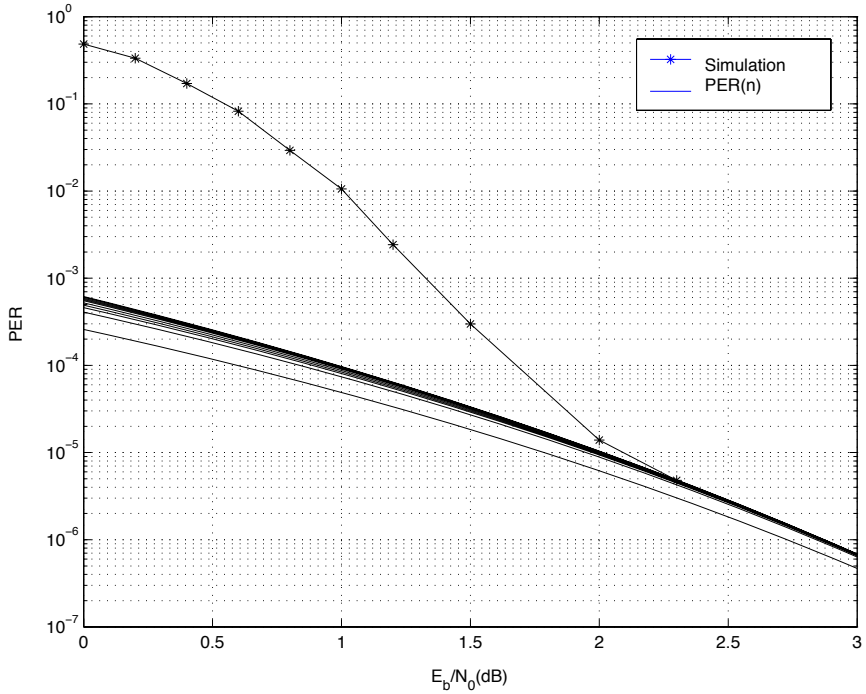

Figure 5.10: $(1, 5/7, 5/7, 5/7)$ multilevel turbo code with $K = 256$ and $R_c = 1/4$.

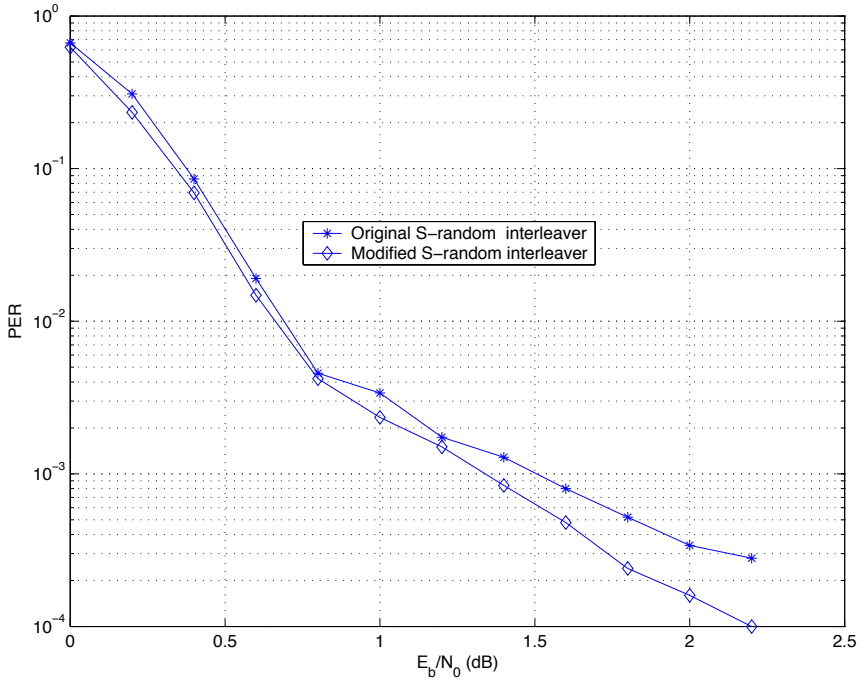

Figure 5.11: Performance comparison of (1,33/37,33/37) turbo code with the original and the modified S-random interleaver (with $T = 60$), $S = 15$, $K = 1024$, and $R_c = 1/3$.

performance without applying any trellis termination. Note that this does not mean the modified interleaver can always outperform the original interleaver to a great extent. The modified interleaver can improve the performance significantly only when the original interleaver suffers a lot from the heavy tail problem described in Section 5.5. Otherwise the original and the modified interleavers would perform almost the same.

5.7 Conclusions

In this chapter, we proposed a weight spectrum estimation method to approximate the turbo code performance in the error floor region. Numerical results showed the proposed method provides good approximation to the error rate. We also showed that the method can be applied to multilevel turbo codes with more than two constituent encoders. This offers a very efficient way to analyze the turbo code performance with a specific interleaver, which is not possible by the conventional method with the uniform

interleaver assumption. The analysis in this chapter enables us to analyze the outage probability of wireless networks with directional antennas that use turbo codes in physical layer. We also found that for some bad interleavers, codewords with only a few 1's at the tail of the input sequence would severely degrade the code performance. Without using the trellis termination scheme which introduces redundancy, we proposed an interleaver modification algorithm that can fix the problem at no cost. Simulation results showed that the algorithm can improve the performance significantly if the original interleaver suffers a lot from the heavy tail problem.

CHAPTER 6

Conclusions and Future Research

In this chapter, we conclude the thesis by summarizing our contributions in each chapter and discussing possible future research directions.

6.1 Summary of Contributions

The major goal of the thesis is to analyze the performance of wireless networks with directional antennas and apply the work to optimize the system performance. In Chapter 2, we analyzed the performance of a wireless network with arbitrary beam pattern under a realistic channel model which includes the effects of path loss, shadowing, and Rayleigh fading. The outage probability of a targeted link in the network was derived for both slow fading and fast fading cases. We also showed that we can apply our BICM analysis and turbo code analysis presented in later chapters to evaluate the performance of the wireless network when BICM or turbo code is used in the physical layer. The effects of the direction estimation error and power control on the system performance were also analyzed in the chapter. Finally we applied the performance analysis to find the optimal mobile density for system throughput. We also used the random coding bound to find the optimal code rate to optimize the link throughput. The results showed that our goal of optimizing the system design for wireless networks with directional antennas was achieved through our performance analysis.

In order to fully characterize the system performance of a wireless network using a specific coded modulation scheme, we need to set the SINR threshold for the outage probability computation accordingly. BICM is often used in wireless communications to

mitigate the fading effect by providing time diversity. In order to analyze the performance of wireless networks using BICM, we need to analyze the performance of BICM in AWGN and fast Rayleigh fading channels. This is the goal of Chapter 3. In Chapter 3, we derived the union bounds on the packet and bit error probabilities for BICM under AWGN and various fading models including Rayleigh, Rician, and Nakagami. The analysis works for various modulation schemes and channel codes with known weight spectrum. Numerical examples showed that our union bound is really tight to the simulation at high SNR. The analysis was applied in Chapter 2 to help us determine the SINR threshold for wireless networks using BICM in the physical layer.

Space-time code is another technique that is effective in mitigating the effect of fading by providing transmit diversity. If bit-interleaving can be combined with space-time codes, then we have both time diversity and transmit diversity which enable us to mitigate the effect of fading even more effectively. This is why we extended our BICM analysis to BI-ST systems in Chapter 4. The extension is not just a trivial extension. The multi-dimensional nature of space-time codes makes the analysis much more complicated than BICM analysis. We focused on the performance of two BI-ST coded systems: BI-STBC and BI-STCM. The union bounds of the two systems under fast Rayleigh, Rician, and Nakagami fading were derived respectively. Numerical experiments again showed that our union bounds are very tight to the actual system performance.

Finally in Chapter 5, we focused on the performance analysis of turbo codes, which are widely used nowadays due to their great performance close to the Shannon capacity limit. We proposed an efficient algorithm that can estimate the weight spectrum of small code weights of a turbo code. This enables us to compute the partial sum of the union bound for the turbo code. Simulation showed that the analysis result is very close to the actual error floor performance of the turbo code. We applied the result to help us determine the SINR threshold in Chapter 2 in order to evaluate wireless network performance when a turbo code is used in physical layer. Other than weight spectrum estimation, we also proposed a technique that can improve the performance of S-random interleavers at no cost. Numerical experiments showed that the algorithm works well

especially when a turbo code suffers from small weight codewords with 1's clustered near the end of the blocks which can severely degrade the performance of the turbo code.

6.2 Future Research

There are several possible future research directions regarding wireless networks using directional antennas. Currently we assume all mobiles are using the same transmitting beam pattern, but this is not necessarily true in reality. A possible future research is to consider the case when mobiles are allowed to use different beam patterns. The analysis should be tractable by first classifying interfering mobiles in to different categories according to their beam patterns and then following the similar techniques in Chapter 2 to find the outage probability.

Another research problem worth considering is to extend the outage probability analysis to three dimensional beam patterns so that our work can be applied to wireless networks with mobiles located at different altitudes, such as buildings or special battlefields. The analysis in Chapter 2 should be possible to be generalized to the three dimensional case, though the derivation likely would be a lot more tedious.

Additional future research topic of interest is to consider the case when mobiles can adaptively choose the coded modulation to use according to the channel condition. When the channel is suffering from a long term shadowing, the mobile can use a stronger code with lower rate such as turbo code. As the channel condition becomes better, the mobile can switch to BICM that provides higher rate and thus higher throughput. We can extend our current outage probability analysis to analyze the performance of such adaptive networks. Through the analysis we want to find the optimal switching strategy for the mobiles in an adaptive network.

BIBLIOGRAPHY

BIBLIOGRAPHY

[1] J. C. Liberti and T. S. Rappaport, *Smart Antennas for Wireless Communications: IS-95 and Third Generation CDMA Applications*, Prentice-Hall, 1999.

[2] P. H. Lehne and M. Pettersen, "An overview of smart antenna technology for mobile communications systems," *IEEE Communications Surveys*, vol. 2, no. 4, pp. 2–13, 1999.

[3] M. Zorzi and S. Pupolin, "Outage probability in multiple access packet radio networks in the presence of fading," *IEEE Transactions on Vehicular Technology*, vol. 43, pp. 604 – 610, August 1994.

[4] M. Zorzi and R.R. Rao, "Capture and retransmission control in mobile radio," *IEEE Journal on Selected Areas in Communications*, vol. 12, pp. 1289 – 1298, October 1994.

[5] W.K. Fung, M. Hamdi, and R.D. Murch, "Performance evaluation of mobile radio slotted aloha with smart antennas," *IEEE Wireless Communications and Networking Conference*, vol. 1, pp. 271 – 275, 1999.

[6] M. Kang, M. Alouini, and L. Yang, "Outage probability and specturm efficiency of cellular mobile radio systems with smart antennas," *IEEE Transactions on Communications*, vol. 50, pp. 1871 – 1877, December 2002.

[7] G. Caire, G. Taricco, and E. Biglieri, "Bit-Interleaved Coded Modulation," *IEEE Transactions on Information Theory*, vol. 44, pp. 927–946, May 1998.

[8] A. Chindapol and J. Ritcey, "Design, Analysis, and Performance Evaluation for BICM-ID with Square QAM Constellations in Rayleigh Fading Channels," *IEEE Journal on Selected Areas in Communications*, vol. 19, pp. 944–957, May 2001.

[9] B. Vucetic and J. Yuan, *Space-Time Coding*, John Wiley & Sons, 2003.

[10] V. Tarokh, N. Seshadri, and A. Calderbank, "Space-Time Codes for High Data Rate Wireless Communication: Performance Criterion and Code Construction," *IEEE Transactions on Information Theory*, vol. 44, pp. 744–765, March 1998.

[11] S. Alamouti, "A Simple Transmit Diversity Technique for Wireless Communications," *IEEE Journal on Selected Areas in Communications*, vol. 16, pp. 1451–1458, October 1998.

[12] V. Tarokh, H. Jafarkhani, and A. Calderbank, "Space-Time Block Codes from Orthogonal Designs," *IEEE Transactions on Information Theory*, vol. 45, pp. 1456–1467, July 1999.

[13] D. Divsalar, S. Dolinar, R. J. McEliece, and F. Pollara, "Performance analysis of turbo codes," *IEEE Military Communications Conference*, vol. 1, pp. 91 – 96, November 1995.

[14] S. Benedetto and G. Montorsi, "Unveiling turbo codes: some results on parallel concatenated coding schemes," *IEEE Transactions on Information Theory*, vol. IT-42, pp. 409 – 428, March 1996.

[15] T. M. Duman and M. Salehi, "New performance bounds for turbo codes," *IEEE Transactions on Communications*, vol. 46, no. 6, pp. 717 – 723, June 1998.

[16] O. Y. Takeshita, M. P. C. Fossorier, and D.J. Costello, "A new technique for computing the weight spectrum of turbo-codes," *IEEE Communications Letters*, vol. 3, pp. 251 – 253, August 1999.

[17] D. Bertsekas and R. Gallager, *Data Networks*, Prentice-Hall, 1992.

[18] A. Nasipuri, Kai L., and U.R. Sappidi, "Power consumption and throughput in mobile ad hoc networks using directional antennas," *International Conference on Computer Communications and Networks*, pp. 620–626, Oct 2002.

[19] T. Korakis, G. Jakllari, and L. Tassiulas, "A mac protocol for full exploitation of directional antennas in ad-hoc wireless networks," *ACM MobiHoc*, pp. 98–107, Jun 2003.

[20] T. S. Rappaport, *Wireless Communications*, IEEE Press, 1996.

[21] J. G. Proakis, *Digital Communications*, McGraw-Hill, 4^{th} edition, 2000.

[22] C. A. Balanis, *Antenna Theory*, John Wiley & Sons, 1997.

[23] H. E. Romeijn and R. L. Smith, "Simulated annealing for constrained global optimization," *Journal of Global Optimization*, vol. 5, pp. 101 – 126, 1994.

[24] S. Rice, "Statistical Properties of a Sine Wave Plus Random Noise," *Bell Systems Technical Journal*, vol. 27, pp. 109–157, January 1948.

[25] M. Nakagami, *"The m-Distribution- A General Formula of Intensity Distribution of Fading"*, in Statistical Methods in Radio Wave Propagation. Pergamon Press, London, 1960.

[26] E. Al-Hussaini and A. Al-Bassiouni, "Performance of MRC Diversity Systems for the Detection of Signals with Nakagami Fading," *IEEE Transactions on Communications*, vol. COM-33, pp. 1315–1319, December 1985.

[27] G. Ungerboeck, "Effect of Spatial Fading Correlation on Performance of Space-Time Codes," *IEEE Transactions on Information Theory*, vol. 28, pp. 55–67, January 1982.

[28] E. Zehavi, "8-PSK Trellis Codes for A Rayleigh Channel," *IEEE Transactions on Communications*, vol. 40, pp. 873–884, May 1992.

[29] S. Zummo, P. C. Yeh, and W. Stark, "A Union Bound on the Error Probability of Coded Multi-Antenna Systems in Block Fading Environments," *IEEE Transactions on Wireless Communications*, accepted 2005.

[30] L. Bahl, J. Cocke, F. Jelinek, and J. Raviv, "Optimal Decoding of Linear Codes for Minimizing Symbol Error Rate," *IEEE Transactions on Information Theory*, vol. IT-20, pp. 284–287, March 1974.

[31] X. Li and J. Ritcey, "Trellis-Coded Modulation with Bit Interleaving and Iterative Decoding," *IEEE Journal on Selected Areas in Communications*, vol. 17, pp. 715–724, April 1999.

[32] S. Benedetto, D. Divsalar, G. Montorsi, and F. Pollara, "Serial Concatenation of Interleaved Codes: Performance Analysis, Design, and Iterative Decoding," *IEEE Transactions on Information Theory*, vol. 44, pp. 909–926, May 1998.

[33] A. Viterbi, "Convolutional Codes and Their Performance in Communication Systems," *IEEE Transactions on Communications*, vol. COM-19, pp. 751–772, October 1971.

[34] M. Simon and D. Divsalar, "Some New Twists to Problems Involving the Gaussian Probability Integral," *IEEE Transactions on Communications*, vol. 46, pp. 200–210, February 1998.

[35] G. L. Stuber, *Principles of Mobil Communicatino*, Kluwer Academic Publisher, 2nd edition, 2001.

[36] A. Papoulis and S. U. Pilai, *Probability, Random Variables, and Stochastic Processes*, McGraw-Hill, 4^{th} edition, 2001.

[37] A. Tonello, "Space-Time Bit-Interleaved Coded Modulation with Iterative Decoding Strategy," *IEEE Vehicular Technology Conference, VTC/Fall*, pp. 473–478, 2000.

[38] L. Lampe and R. Schober, "Bit-Interleaved Coded Differential Space-Time Modulation," *IEEE Transactions on Communications*, vol. 50, pp. 1429–1439, September 2002.

[39] Y. Huang and J. Ritcey, "Tight BER Bound for Iteratively Decoded Bit-Interleaved Space-Time Coded Modulation," *IEEE Communications Letters*, vol. 8, pp. 153–155, March 2004.

[40] H. Koo and B. Lee, "Performance Analysis for ST-BICM System With an Arbitrary Constellation," *IEEE International Conference on Communication, ICC*, pp. 3016–3020, 2003.

[41] A. Tonello, "Performance of Space-Time Bit-Interleaved Codes in Fading Channels with Simplified Iterative Decoding," *IEEE International Conference on Communication, ICC*, pp. 1357–1361, 2001.

[42] X. Li and J. Ritcey, "Bit-Interleaved Coded Modulation with Iterative Decoding," *IEEE Communications Letters*, vol. 1, pp. 169–171, November 1997.

[43] C. Berrou and A. Glavieux, "Near Optimum Error Correcting Coding and Decoding: Turbo Codes," *IEEE Transactions on Communications*, vol. 44, pp. 1261–1271, October 1996.

[44] Y. Du, "Enhanced Space-Time Block Coded Systems by Concatenating Turbo Product Codes," *IEEE Communications Letters*, vol. 8, pp. 388–390, June 2004.

[45] A. Viterbi and J. Omura, *Principles of Digital Communication and Coding*, McGraw-Hill, 1979.

[46] S. ten Brink, "Convergence behavior of iteratively decoded parallel concatenated codes," *IEEE Transactions on Communications*, vol. 49, no. 10, pp. 1727–1737, October 2001.

[47] A. Özgür Yılmaz and W. E. Stark, "Application of Gaussian approximation to iterative decoding with finite blocklengths," *IEEE Transactions on Information Theory*, submitted.

[48] W. Blackert, E. Hall, and S. Wilson, "An upper bound on turbo code free distance," *IEEE International Conference on Communications*, vol. 3, pp. 957–961, 1996.

[49] F. Daneshgaran and M. Mondin, "An efficient algorithm for obtaining the distance spectrum of turbo codes," *International Syposimum on Turbo Codes*, pp. 251 – 254, September 1997.

[50] F. Daneshgaran and M. Mondin, "Permutation fixed points with application to estimation of minimum distance of turbo codes," *IEEE Transactions on Information Theory*, vol. 46, no. 7, pp. 2336 – 2349, November 2000.

[51] R. Garello, P. Pierleoni, and S. Benedetto, "Computing the free distance of turbo codes and serially concatenated codes with interleavers: Algorithms and applications," *IEEE Journal on Selected Areas in Communication*, vol. 19, no. 5, pp. 800 – 812, May 2001.

[52] E. Rosnes and O. Ytrechus, "On algorithms for determination of turbo code weight distribution," *IEEE International Symposium on Information Theory*, p. 82, July 2002.

[53] C. Berrou and S. Vaton, "Computing the minimum distances of linear codes by the error impulse method," *IEEE International Symposium on Information Theory*, p. 5, July 2002.

[54] L. R. Bahl, J. Cocke, F. Jelinek, and J. Raviv, "Optimal decoding of linear codes for minimizing symbol error rate," *IEEE Transactions on Information Theory*, vol. IT-20, pp. 248 – 287, March 1974.

[55] L. C. Perez, J. Seghers, and D. J. Costello, "A distance spectrum interpretation of turbo codes," *IEEE Transactions on Information Theory*, vol. 42, no. 6, pp. 1698 – 1709, November 1996.

[56] J. Han and O. Takeshita, "On the decoding structure for multiple turbo codes," *IEEE International Symposium on Information Theory*, p. 98, June 2001.